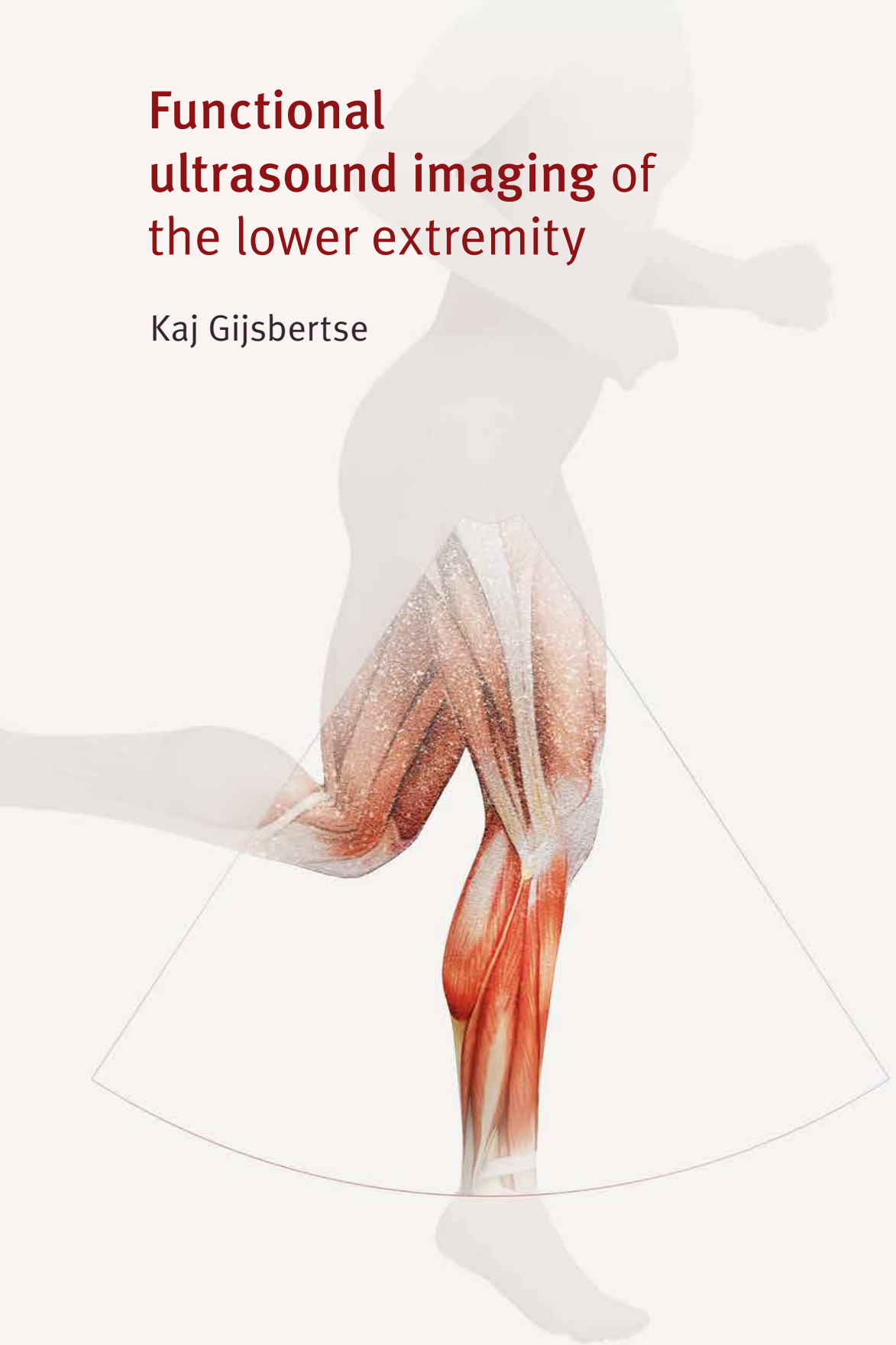


Functional ultrasound imaging of the lower extremity

Kaj Gijsbertse



The work in this thesis was carried out within the Radboud Institute for Health Sciences.
Financial support for the research described in this thesis was provided by European Research Council under the European Union's Seventh Framework Programme (FP/2007-2013) / ERC Grant Agreement n. 323091 awarded to N. Verdonchot.

ISBN

978-94-92896-86-5

Design/lay-out

Promotie In Zicht, Arnhem

Print

Ipskamp Drukkers, Enschede

© K. Gijsbertse, 2018

All rights are reserved. No part of this book may be reproduced, distributed, stored in a retrieval system, or transmitted in any form or by any means, without prior written permission of the author.

Functional ultrasound imaging of the lower extremity

Proefschrift

ter verkrijging van de graad van doctor
aan de Radboud Universiteit Nijmegen
op gezag van de rector magnificus prof. dr. J.H.J.M. van Krieken,
volgens besluit van het college van decanen
in het openbaar te verdedigen op donderdag 20 december 2018
om 12.30 uur precies

door

Kaj Gijsbertse

geboren op 20 juni 1986
te Wageningen

Promotoren

Prof. dr. ir. N. Verdonshot

Prof. dr. ir. C.L. de Korte

Copromotoren

Dr. A.M.J. Sprengers

Dr. M.M. Nillesen

Manuscriptcommissie

Prof. dr. B.G.M. van Engelen

Prof. dr. ir. D.F. Stegeman

Prof. dr. J. D'hooge (KU Leuven, België)

Table of contents

Chapter 1	General introduction and thesis outline	7
Chapter 2	Strain imaging of the lateral collateral ligament using high frequency and conventional ultrasound imaging: An ex-vivo comparison	19
Chapter 3	Ultrasound imaging of muscle contraction of the tibialis anterior in patients with facioscapulohumeral dystrophy	31
Chapter 4	Continuous analysis of skeletal muscle strain with respect to fascicle orientation using ultrasound	49
Chapter 5	Three-dimensional ultrasound strain imaging of skeletal muscles	65
Chapter 6	Computer aided detection of fasciculations and other movements in muscle with ultrasound: development and clinical application	85
Chapter 7	Summary and general discussion	107
Chapter 8	Samenvatting	121
Appendices	List of publications	131
	List of conference presentations	133
	PhD portfolio	135
	Dankwoord	137
	Curriculum Vitae	143

1

General introduction and thesis outline

Parts of this chapter were published as a book chapter:

Introduction to speckle tracking in ultrasound video, Handbook of Speckle Filtering and Tracking in Cardiovascular Ultrasound Imaging and Video (p. 241-257); IET 2018; 10.1049/PBHE013E

Authors

Gijs A.G.M. Hendriks, Stein Fekkes, Kaj Gijsbertse and Chris L. de Korte

1.1 Musculoskeletal disorders

Our musculoskeletal system is composed of muscles, tendons, ligaments, bones and cartilage that support our body and allow movement. Musculoskeletal disorders is the collective term to describe clinical problems that affect any part of the musculoskeletal system. These disorders often result in pain, injury, illness and poor quality of life. They are the most common cause of severe long term pain and disability, and are currently reported to be affecting hundreds of millions of people around the world [1]. In the United States, musculoskeletal disorders affect more than one out of every two persons aged 18 and over, and nearly three out of four aged 65 and over [2]. In addition to the considerable decrease in quality of life induced by musculoskeletal disorders, there are consequences for society, economy and industry in terms of lost working time, medical treatment and hospitalization, and decreased productivity [3].

To improve the diagnosis of musculoskeletal disorders, as well as methodologies to guide treatments and rehabilitations, a fundamental and comprehensive understanding of functioning of muscle and other tissues such as ligaments and tendons is important. Skeletal muscle imaging is increasingly used as a complementary tool to clinical and electrophysiological examination and has been applied to directly assess muscles *in vivo* to provide detailed information about muscle functioning. Ultrasound and Magnetic Resonance Imaging (MRI) techniques have been developed as the modalities of choice and can reveal abnormalities in tissue composition, architecture and movement that point to neuromuscular pathology, and both allow monitoring of disease progression tracking such changes over time [4, 5]. Computed Tomography (CT) imaging is less suitable because of its low soft tissue contrast and use of ionizing radiation.

This thesis focuses on the development and use of ultrasound imaging techniques to obtain functional information of the human lower extremities. The work is part of the BioMechTools project that aims to generate biomechanical models of the lower extremities that can be used to optimize surgery and functional outcome of the patient. Therefore, it is important to acquire geometrical and mechanical information of ligaments, tendons and muscles, and the dynamic deformation of these structures. Moreover, these parameters can be used in diagnosis, characterization and follow-up of musculoskeletal disorders.

1.2 Ultrasound basics in muscle imaging

The principle of medical ultrasound imaging is based on the reflection and backscattering of emitted sound waves, by piezo-electric elements, with a frequency over 20 kHz. Sound propagating through tissue is reflected due to differences in acoustic properties at the transition of different tissue types. When applied to the musculoskeletal system, this results in clearly visible fascicles (bundles of muscle fibers) in muscles or collagen fibers in tendons

and ligaments (**Figure 1.1A**). Additionally, scattering and interference of sound waves result in a characteristic speckle pattern that is unique for the underlying tissue. Tracking these ultrasound signatures is the fundament of many quantitative techniques for tissue motion estimation.

In the early period of ultrasound imaging, 2D images were formed by mechanically sweeping a single element. Presently, advanced ultrasound transducers consist of multiple elements that are activated with varying time-delays to obtain 2D or 3D images without moving the transducer itself. Ultrasound transducers are characterized by their type and operating frequency, which is typically in the range of 3 to 20 MHz for clinical applications. Each application requires an appropriately selected transducer which is best suited for the particular investigation. There is a trade-off between penetration depth and image resolution depending on the frequency of the ultrasound waves. The axial resolution (along the beam direction, **Figure 1.1B**) is depending on the pulse length, which is typically in the order of two wavelengths. With increasing frequency, the wavelength decreases resulting in shorter pulse lengths and an increased axial resolution. Also, the lateral resolution (perpendicular to the axial direction) increases for higher frequencies as a result of a smaller beam width. In general, the highest frequency transducer that can reach the required image depth should be employed to optimize the image quality. For instance, deep muscles, such as the vastus intermedius require a low frequency transducer to obtain a sufficient penetration depth, while superficial structures such as the collateral ligaments should be imaged with higher frequency transducers. Another trade-off with penetration depth exist, namely the temporal resolution *i.e.* the frame rate. The frame rate depends on image depth and on the number of scan lines. Consequently, 3D imaging, which requires many scan lines, has a lower frame rate compared to 2D acquisitions. Sufficient temporal resolution is required when studying dynamic events such as (fast) contracting muscles.

1.3 Dynamic ultrasound measurements

The dynamic nature of examination (*i.e.* high temporal resolution) makes ultrasound uniquely suited for the assessment of musculoskeletal tissue during natural movement tasks. Ultrasound-based quantitative measures of muscle morphology and architecture, such as muscle thickness, length, cross sectional area (CSA), and pennation angle have been widely used and studied with respect to muscle force output or motion during dynamic tasks. [6-8]. In cardiology, the dynamic function of the heart muscle has been evaluated using ultrasound strain imaging or Doppler techniques to measure tissue velocities and deformation [9], but these techniques are not yet fully exploited in the musculoskeletal field.

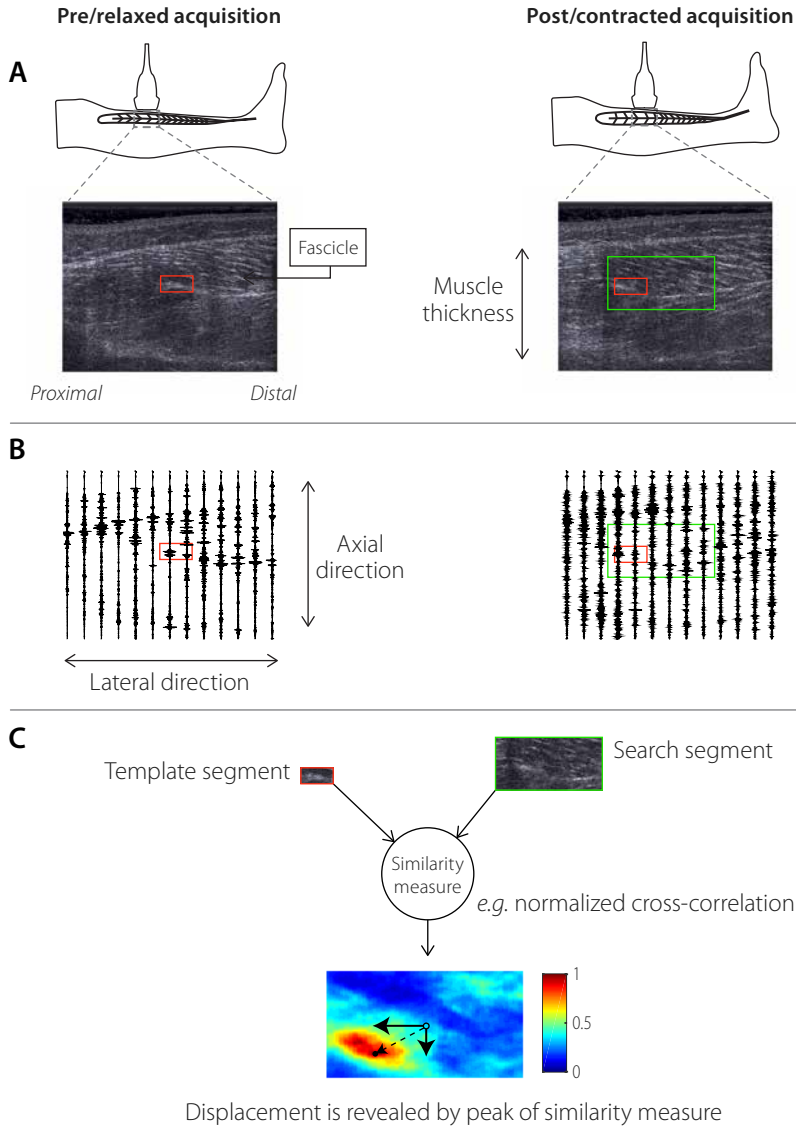


Figure 1.1 Basic principle of ultrasound imaging and displacement estimation. Multiple sound waves (scan lines) are emitted from an ultrasound transducer. Sound that propagates through the tissue is reflected or scattered due to the variance in acoustic properties. These reflections are detected by the transducer and forms the ultrasound image A). With B) the underlying received RF-data. Tissue displacement is often estimated by finding the location of the best matching location of segments (*i.e.* blocks) of the ultrasound data in the consecutive image, for example, by calculating the normalized cross-correlation of the segments C).

Assessment of local muscle contraction velocity may provide evidence about muscle heterogeneity, which has not been extensively examined *in vivo*. In particular, muscle deformation may be useful to directly assess differences in muscle functioning of healthy and pathologic muscles and their role in muscular disorders such as knee instability or muscular dystrophies. Direct measurements of muscle and tendon kinematics using ultrasound imaging may lead to improved understanding of musculoskeletal function and the way forces are transferred. Also, it enhances our understanding of the complexity of the musculoskeletal system that involves different muscle shapes and architecture *e.g.* biarticular muscles or pennate muscles. Pennate muscles offer a force advantage over muscles with parallel orientated fibers since there are more fibers in a muscle of a given volume. Dynamic ultrasound imaging enables to quantitatively characterize the relationship between muscle deformation and the underlying architecture *in vivo*. Additionally, the high temporal resolution of ultrasound allows to visualize spontaneous muscle movement seen in neuromuscular diseases, such as fasciculations, which are caused by diseased motor neurons that evoke these involuntary contractions. These involuntary contractions are biomarkers for neuromuscular diseases and play an important role in the diagnosis and monitoring of disease progression [10].

Besides direct impact on the diagnosis, ultrasound imaging techniques can provide valuable outcome parameters to verify, validate and optimize biomechanical computer models of the musculoskeletal system [11]. These simulation models enable researchers and clinicians to study the complex dynamics underlying human movement and may predict the effect of an intervention such as total hip or knee replacements [12, 13]. Especially, intrinsic parameters that cannot be measured directly in experiments, such as individual muscle force and joint load, have been estimated from biomechanical analysis of musculoskeletal models based on *in vivo* measurements [14]. However, these models frequently rely on input data derived from cadaver measurements and therefore are not patient specific. A patient-specific model requires: 1) geometrical information of the involved structures, 2) information how the knee or hip dynamically deforms and 3) information about the mechanical properties of the tissues involved. Ultrasound imaging can reveal the dynamic behavior of the tissues and deliver *in vivo* data in the musculoskeletal modeling pipeline.

1.3.1 Ultrasound strain imaging

A number of ultrasound based techniques have been used to study the dynamic behavior of soft tissue within the musculoskeletal system [14]. A technique that has been extensively used to quantify tissue deformation is called strain imaging. Strain is defined as the relative shortening/compression or elongation/expansion of tissue. This method is based on tracking the speckle of the underlying tissue over time using block-matching techniques. Tissue displacement is estimated by finding the location of the best matching location of segments (*i.e.* blocks) of the ultrasound data in the consecutive image. The best match is

computed via a similarity measure between both segments, for instance, the normalized cross-correlation or the sum of squared differences (**Figure 1.1C**). The spatial coordinate of the maximum similarity value with respect to the center point of the search segment in the consecutive frame is determined. The distance between these coordinates is a measure for the displacement [15].

Subsequently, the spatial derivative of the displacement estimations can be calculated to determine the strain, as was first introduced by Ophir et al. [16]. The used data for the block matching techniques can vary in both dimensionality (*e.g.* 1D, 2D, 3D) and in type. In short, the input data type includes the DICOM data *i.e.* the brightness-mode (B-mode) ultrasound image sequence, or the underlying raw radio frequency data (RF-data) which is the beam-formed data from the received signals of the transducer elements. The presence of phase information in the axial direction of the RF-data (**Figure 1.1B**) is an important feature for displacement estimation, as it allows for high-precision displacement estimations that are particularly relevant for situations with only small displacements or strain. DICOM data has lower spatial resolution and precision but is more robust. However, access to the RF-data requires dedicated equipment and sequences, which are not typically available on ultrasound machines used in clinical practice. Several groups have worked on methods that combine the robustness of DICOM displacement estimation with the high precision provided by RF-data in an iterative process, where in the first iteration the envelope of the RF-signal (similar to DICOM data) is used to find the coarse displacement and subsequently the RF-signal is used for higher accuracy [17]. Additionally, the performance of displacement estimation is depending on the chosen ultrasound data segment sizes. Segments of ultrasound data acquired from an initial state of tissue (templates) are compared to larger segments in the consecutive frame (*i.e.* search window). The dimensions of the search window is depending on the amount of tissue displacement between the consecutive frames. This search area can be the entire frame, but this may lead to erroneous matches also known as “peak hopping” and additionally increases computational time of the similarity values. Therefore, the search area is usually limited and based on the expected tissue motion. The size of the template segments depends on the expected strain. A larger window will result in a more robust and well defined cross-correlation function but will only work for low strain values, as described by a theoretical framework called “strain filter” [18]. Furthermore, the similarity score is influenced by the amount of de-correlation of the data segments as a result of tissue deformation and subsequently change in speckle appearance, or tissue simply moving out of the image plane in 2D (*i.e.* out-of-plane motion). Again, sufficient temporal resolution is required to minimize the amount of motion and consequently the amount of de-correlation.

Ultrasound strain imaging has been used to measure induced deformation and estimate local strains and elasticity in musculoskeletal applications [19]. It has also been applied to study the deformation of actively contracting muscle. Deformation of electronically stimulated muscles *ex vivo* has been investigated [20] and the effects of

muscle fatigue on muscle strain have been studied in animal models [21]. Reports of *in vivo* applications of ultrasound strain imaging in muscles remain limited [22-25], and most studies have focused on the evaluation of tendons in 2D [26, 27].

1.4 Aim and outline of this thesis

In this thesis ultrasound-based methodologies are developed to assess the functional behavior of soft tissues within the musculoskeletal system and new applications are explored. The results of this research are important to enhance our fundamental understanding of muscle functioning, provide valuable data for the characterization and diagnosis of muscular disorders and provide information to obtain reliable biomechanical models that can guide and predict surgical outcomes. To this end, several methods are proposed to quantify local deformation of soft tissue and its relation to its biomechanical status (e.g. morphology and pathology). The developed techniques are validated in phantoms or *ex vivo* tissues and applied in healthy volunteers and in patients with neuromuscular diseases.

In **Chapter 2** we explore the usage of ultrasound imaging to assess the strain in collateral ligaments, which may be used to quantify abnormalities in knee instability. Therefore, two-dimensional ultrasound strain measurement of *ex vivo* human lateral collateral ligaments in an axial loading condition is validated. Additionally, the potential benefits of high frequency ultrasound (>20 MHz) for strain measurement are explored, since the collateral ligaments are relatively small and superficial structures. Ultrasound measurements are compared to surface strain measurements from optical digital image correlation (DIC) techniques in a specially designed experimental set-up to facilitate accurate and reliable data acquisition.

Chapter 3 explores the application of ultrasound speckle tracking to study the functional behavior of muscles in patients with a neuromuscular disease. Muscle deformation of the tibialis anterior in patients with fascioscapulohumeral muscular dystrophy is quantified and compared to healthy muscle deformation. The deformation patterns are compared to force-output and clinical outcome measures for a better understanding of the underlying phenomena related to muscle weakness in muscle disorders.

To gain more insights in the relation between muscle deformation and structural organization of the tissue, **Chapter 4** describes a new frame-work to measure strain and fascicle orientation concurrently. Speckle tracking and an algorithm for the automatic detection of fascicle orientation are combined and applied to ultrasound image sequences of contracting muscles in the lower leg. This approach allows for a complimentary and more comprehensive assessment of muscle functioning during dynamic tasks.

Since muscles are geometrically complex 3D structures and cannot be fully characterized by 2D imaging, **Chapter 5** aims to develop a 3D ultrasound strain imaging technique to assess local strain in three orthogonal directions in 3D space of skeletal muscles during

voluntary contractions. A phantom study that mimics muscle deformation is used as experimental validation of the 3D technique and to compare its performance with respect to a 2D based technique.

Furthermore, ultrasound imaging is applied to visualize spontaneous muscle movements that are important biomarkers in neuromuscular disorders. In **Chapter 6**, an algorithm for automatic detection of muscle motion in combination with the extraction of more detailed information on the properties of the motion is developed and applied to ultrasound data that had been captured during routine clinical care. The outcomes of this algorithm are compared to annotations by experienced clinicians. This approach may lead to improved sensitivity and intra/inter-observer agreement and is a first step towards fully automatic detection and classification of fasciculations in ultrasound videos.

In **Chapter 7** the results of this thesis are summarized and future perspectives discussed.

References

1. Osborne, A., et al., *Prevalence of musculoskeletal disorders among farmers: A systematic review*. Am J Ind Med, 2012. **55**(2): p. 143-58.
2. Woolf, A.D. and B. Pfleger, *Burden of major musculoskeletal conditions*. Bull World Health Organ, 2003. **81**(9): p. 646-56.
3. Duffield, S.J., et al., *The contribution of musculoskeletal disorders in multimorbidity: Implications for practice and policy*. Best Pract Res Clin Rheumatol, 2017. **31**(2): p. 129-144.
4. Fischer, D., U. Bonati, and M.P. Wattjes, *Recent developments in muscle imaging of neuromuscular disorders*. Curr Opin Neurol, 2016. **29**(5): p. 614-20.
5. Zaidman, C.M. and N. van Alfen, *Ultrasound in the Assessment of Myopathic Disorders*. J Clin Neurophysiol, 2016. **33**(2): p. 103-11.
6. Eranki, A., et al., *A novel application of musculoskeletal ultrasound imaging*. J Vis Exp, 2013(79): p. e50595.
7. Moore, C.J., M.D.M. Hossain, and C.M. Gallippi. *2D ARFI and Viscoelastic Response (VisR) anisotropy imaging in skeletal muscle*. in 2017 IEEE International Ultrasonics Symposium (IUS). 2017.
8. Tilp, M., et al., *Changes in fascicle lengths and pennation angles do not contribute to residual force enhancement/depression in voluntary contractions*. J Appl Biomech, 2011. **27**(1): p. 64-73.
9. D'Hooge, J., et al., *Echocardiographic strain and strain-rate imaging: a new tool to study regional myocardial function*. IEEE Trans Med Imaging, 2002. **21**(9): p. 1022-30.
10. Pillen, S. and N. van Alfen, *Skeletal muscle ultrasound*. Neurol Res, 2011. **33**(10): p. 1016-24.
11. Hicks, J.L., et al., *Is My Model Good Enough? Best Practices for Verification and Validation of Musculoskeletal Models and Simulations of Movement*. Journal of Biomechanical Engineering, 2015. **137**(2): p. 020905-020905-24.
12. Marra, M.A., et al., *Anterior referencing of tibial slope in total knee arthroplasty considerably influences knee kinematics: a musculoskeletal simulation study*. Knee Surg Sports Traumatol Arthrosc, 2018. **26**(5): p. 1540-1548.
13. Marra, M.A., et al., *A subject-specific musculoskeletal modeling framework to predict in vivo mechanics of total knee arthroplasty*. J Biomech Eng, 2015. **137**(2): p. 020904.
14. Sikdar, S., Q. Wei, and N. Cortes, *Dynamic ultrasound imaging applications to quantify musculoskeletal function*. Exerc Sport Sci Rev, 2014. **42**(3): p. 126-35.
15. Loizou, C., C. Pattichis, and J. D' Hooge, *Handbook of Speckle Filtering and Tracking in Cardiovascular Ultrasound Imaging and Video*. 2018.
16. Ophir, J., et al., *Elastography: a quantitative method for imaging the elasticity of biological tissues*. Ultrasonic Imaging, 1991. **13**(2): p. 111-134.
17. Lopata, R.G.P., et al., *Performance Evaluation of Methods for Two-Dimensional Displacement and Strain Estimation Using Ultrasound Radio Frequency Data*. Ultrasound in Medicine and Biology, 2009. **35**(5): p. 796-812.
18. Walker, W.F. and G.E. Trahey, *A fundamental limit on delay estimation using partially correlated speckle signals*. IEEE Transactions on Ultrasonics, Ferroelectrics, and Frequency Control, 1995. **UFFC-42**: p. 301-308.
19. Drakonaki, E.E., G.M. Allen, and D.J. Wilson, *Ultrasound elastography for musculoskeletal applications*. Br J Radiol, 2012. **85**(1019): p. 1435-45.
20. Deffieux, T., et al., *Assessment of the mechanical properties of the musculoskeletal system using 2-D and 3-D very high frame rate ultrasound*. IEEE Trans Ultrason Ferroelectr Freq Control, 2009. **55**(10): p. 2177-2190.
21. Witte, R.S., et al. *High Resolution Ultrasound Imaging of Skeletal Muscle Dynamics and Effects of Fatigue*. 2004. Proc. IEEE Ultrasonics Int. Conf., Montreal, Canada.
22. Farron, J., T. Varghese, and D.G. Thelen, *Measurement of tendon strain during muscle twitch contractions using ultrasound elastography*. IEEE Trans Ultrason Ferroelectr Freq Control, 2009. **56**(1): p. 27-35.
23. Peolsson, M., et al., *Modelling human musculoskeletal functional movements using ultrasound imaging*. BMC Med Imaging, 2010. **10**: p. 9.
24. Busato, A., et al., *Ultrasound and analysis of the deformation patterns of the masseter muscle: comparing surgical anatomy, ultrasound and functional anatomy*. Oral Implantol (Rome), 2016. **9**(Suppl 1/2016 to N 4/2016): p. 28-37.
25. Lopata, R.G., et al., *Dynamic imaging of skeletal muscle contraction in three orthogonal directions*. J Appl Physiol (1985), 2010. **109**(3): p. 906-15.

26. Bogaerts, S., et al., *Strain mapping in the Achilles tendon – A systematic review*. Journal of Biomechanics, 2016. **49**(9): p. 1411-1419.
27. Slane, L.C., et al., *Non-uniform deformation of the patellar tendon during passive knee flexion*. J Appl Biomech, 2017: p. 1-25.

2

Strain imaging of the lateral collateral ligament using high frequency and conventional ultrasound imaging: *An ex vivo* comparison

Authors

Kaj Gijsbertse, André M.J. Sprengers, Hamid Naghibi Beidokhti, Maartje M. Nillesen, Chris L. de Korte and Nico Verdonchot

Published in

Journal of Biomechanics; 2017 Nov; 43(11):2537-2545

Abstract

Recent first attempts of *in situ* ultrasound strain imaging in collateral ligaments encountered a number of challenges and illustrated a clear need for additional studies and more thorough validation of the available strain imaging methods. Therefore, in this study we experimentally validated ultrasound strain measurements of *ex vivo* human lateral collateral ligaments in an axial loading condition. Moreover, the use of high frequency ultrasound (>20 MHz) for strain measurement was explored and its performance compared to conventional ultrasound. The ligaments were stretched up to 5% strain and ultrasound measurements were compared to surface strain measurements from optical digital image correlation (DIC) techniques. The results show good correlations between ultrasound based and DIC based strain measures with R^2 values of 0.71 and 0.93 for high frequency and conventional ultrasound, subsequently. The performance of conventional ultrasound was significantly higher compared to high frequency ultrasound strain imaging, as the high frequency based method seemed more prone to errors. This study demonstrates that ultrasound strain imaging is feasible in *ex vivo* lateral collateral ligaments, which are relatively small structures. Additional studies should be designed for a more informed assessment of optimal *in vivo* strain measurements in collateral knee ligaments.

2.1 Introduction

Ultrasound is a widely used imaging modality to assess tendon and ligament abnormalities. Traditional ultrasound techniques are directed towards assessing tissue structure or geometry. However, the biomechanical properties of ligaments may change as a consequence of injury or disease. Quantitative ultrasound imaging techniques can be used to evaluate soft tissue biomechanics. Ultrasound strain imaging is such a technique that can quantify tissue deformation [1] and in the musculoskeletal field it has been mostly applied in tendons such as the Achilles and patellar tendons [2-6].

Within the musculoskeletal field, there are many potential clinical applications of this technique that have not been fully explored. For example, knee instability may be a result of ligamentous insufficiency (e.g. tear, attenuation) and is a major cause of early total knee arthroplasty failures. Also for patients suffering from varus or valgus knee deformities, the strains in the collateral ligaments may not be physiological. In order to quantify these abnormalities ultrasound strain imaging can be a potential technique to assist surgeons and researchers.

First attempts of *in situ* ultrasound strain imaging in the collateral ligaments by Slane and coworkers encountered a number of challenges in both data acquisition and processing [7]. Their study illustrated a clear need for additional work, particularly relating to the collection of ground-truth data and reliable image methodologies for *in vivo* measurements. The small size of the ligaments also complicates data processing and requires more thorough validation studies of the available strain estimation methods. Slane et al. suggested to explore the usage of a higher resolution ultrasound transducer, as the higher spatial resolution of these systems could visualize more structural detail in these small tissues and consequently improve the characterization of ligament displacement and strain. In this paper we analyzed the effects of the latter suggestion and performed high frequency (>20 MHz) ultrasound strain measurements and compared it to strain estimations using conventional (~7 MHz) ultrasound. The performance of both techniques was analyzed in an *ex vivo* experiment with strain values obtained with an optical Digital Image Correlation (DIC) technique serving as a reference.

2.2 Methods

Six fresh-frozen cadavers (78±11 years), without signs of hard and soft tissues injuries were received from the Anatomy Department of Radboudumc with a permission statement for experimental use. The cadaver legs were dissected by an orthopedic surgeon and the lateral collateral ligaments were obtained with bone attachments intact at the insertion sites of the ligament. To facilitate surface strain estimation as obtained with DIC measurements, the ligaments were stained with a methylene blue solution to create a

dark background and sprayed with an white oil-based paint to create highly contrasted speckles [8, 9]. To provide a better grip during testing, each bone part was embedded in bone cement *i.e.* polymethylmethacrylate (PMMA), see also **Figure 2.1**.

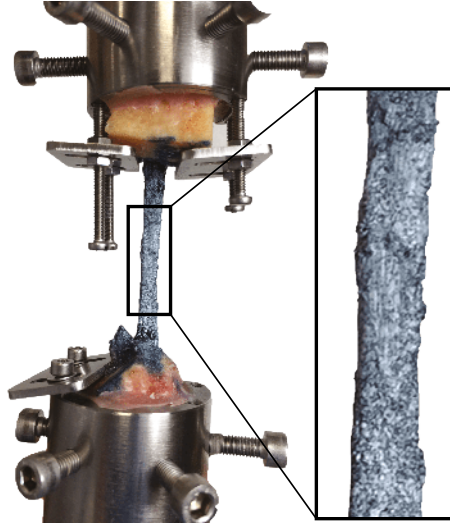


Figure 2.1 Ligament preparation. The ligaments were stained with methylene blue and a white speckle pattern was applied to facilitate digital image correlation techniques. To provide good grip, the bone parts were embedded in PMMA and fixed in custom build grips.

The specimens were submerged in water, with the ends fixed in custom build grips (proximal end in upper grip) of a tensile testing machine (MTS system corporation, Minnesota, USA). The grips allowed free motion of the ligament, except for the axial direction (*i.e.* rotation and translation perpendicular to the axial loading direction). Specimens were preloaded to 10N to reduce slackness and their initial length was measured (using the image data from the DIC method), followed by a preconditioning step of 10 cycles of axial stretching to 5% at a frequency of 1 Hz [10]. Axial stretching was accomplished by displacement driven elongation of the initial measured length of the ligament. After preconditioning, the ligaments were subjected to two trials that both consisted of 5 sinusoidal cycles of axial stretching to 5% at a frequency of 1 Hz. For each trial a different ultrasound system was used to obtain raw ultrasound radio-frequency (RF) data. For one of the trials ultrasound data were acquired using a conventional ultrasound transducer (center frequency $\sim 7\text{MHz}$), and for the other trial a preclinical system with a high resolution transducer (center frequency $\sim 20\text{MHz}$) was used.

Conventional ultrasound data were acquired with an iE33 ultrasound system (Philip Medical Systems, Bothell, USA), equipped with a L11-3 linear array transducer (footprint 39 mm, 576 lines), with a fixed echo depth of 30 mm (1250 samples) and a frame rate of 21 Hz. The high resolution ultrasound acquisition system was a Visualsonics 2100 (FUJIFILM VisualSonics Inc., Toronto, Canada) equipped with an MS250s linear array transducer (footprint 23 mm, 512 lines), with a fixed echo depth of 30 mm (6112 samples) and a frame rate of 21 Hz. As a reference, optical image sequences of the medial surface of the ligament were captured using a SPOT™ Insight 2.0 Color digital camera (SPOT™ Imaging Solutions, Michigan, USA) at a frame rate of 10 Hz (see **Figure 2.2**).

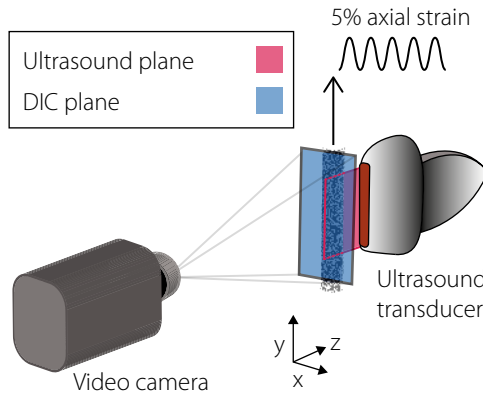


Figure 2.2 Experimental set-up. The ligament is cyclically stretched to 5% strain in axial direction (displacement driven). Ultrasound and optical images were simultaneously acquired from orthogonal planes.

Both ultrasound and optical image data were processed using a custom developed and validated 2D speckle tracking method [11, 12]. Displacements were calculated on an equidistant grid with 0.5 mm spacing within a ROI of 20 x 5 mm within each specimen. The centers of the ROI of the different modalities were manually aligned with each other (transducer positions were visible on the optical images). Inter-frame displacements were calculated by normalized cross-correlation of template kernels (1.2 x 0.6 mm) within larger search kernels (2.2 x 1.1 mm) in the consecutive frame. Sub-pixel displacement estimation was detected by spline fitting of the cross correlation peak. To remove outliers, the displacements were 2D median filtered (1.5 x 2.5 mm kernel). Accumulated displacement estimates over the entire loading cycle were computed from the inter-frame displacements using bilinear interpolation [12]. To synchronize the data and minimize drift as a result of tracking errors, we tracked every stretching phase of the ligaments individually. Starting

frames of the cycle were derived from the entire accumulated lateral displacement, and defined as local peaks in the median displacement curve (**Figure 2.3**). Strain was derived from the accumulated displacements using a 2D least square strain estimator [13, 14] with kernel size of 10 x 1.25 mm.

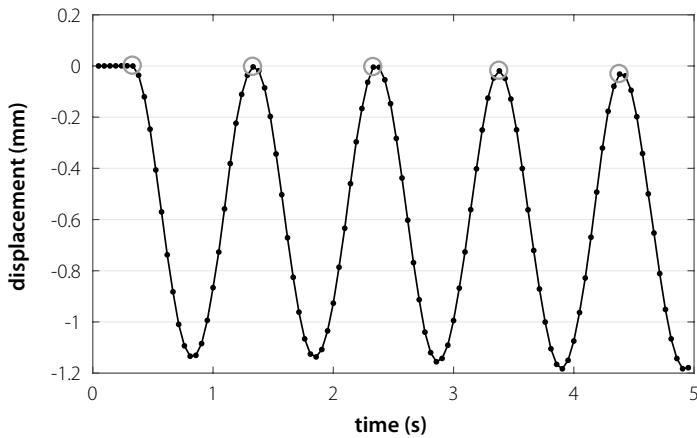


Figure 2.3 Local peak detection of the accumulated lateral displacement was used to detect the starting frames for tracking every stretching phase of the loading cycle.

Median strain curves were calculated from all grid points inside the ROI over the loading cycle and resampled at 20 Hz. Correlation between the strain values derived from DIC and ultrasound techniques were computed and expressed with their coefficient of determination (R^2). Agreement between the techniques were expressed in Bland-Altman plots and the difference values were compared to assess statistical differences (Student T-test). Additionally, ultrasound data and corresponding strain maps were qualitatively evaluated and judged on their resemblance with the results of the DIC technique.

2.3 Results

Displacement and strain maps as obtained with the two ultrasound techniques were similar and showed close resemblance with the reference DIC technique (**Figure 2.4**). The displacement and strain maps show limited variation across the depth of the ligament, indicating that ligaments deform rather homogeneously in this direction. However, the strain is more inhomogeneous along the longitudinal direction (y-axis) and the DIC measurements reveal that the largest strain is present near the insertion sites. The use of

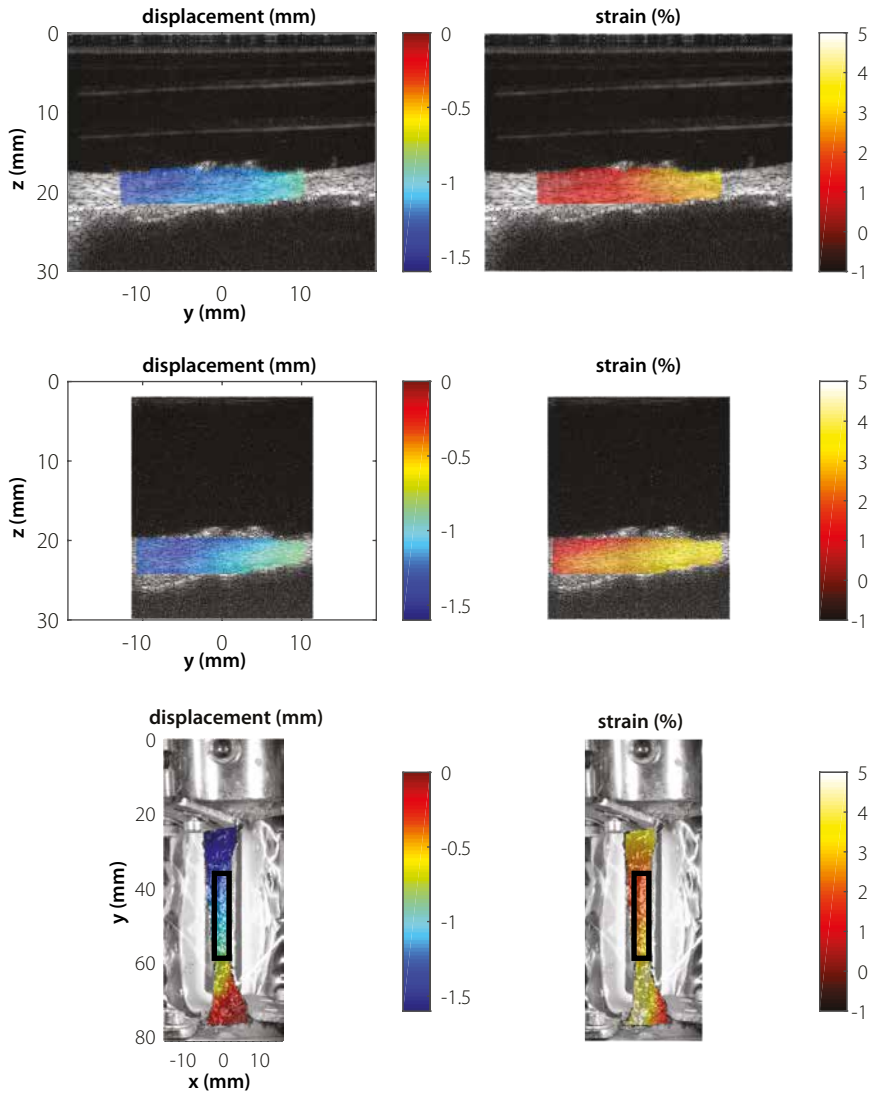


Figure 2.4 Displacement (left) and strain (right) maps at the end of a stretching phase derived from the different imaging modalities. The upper row depicts the conventional ultrasound based results. High frequency based results are shown in the middle row and results from the DIC technique are shown in the lower row. The DIC measurements reveal that the largest strain is not at the mid-substance of the ligament, but present near the insertion sites (outside the ROI).

a high frequency ultrasound system resulted in B-mode images with much finer speckle appearance compared to the conventional system. Yet, the image view is smaller and therefore a smaller part of the ligament is visualized.

Strain values from conventional ultrasound techniques showed very strong correlation with DIC measurements, with a linear coefficient value of $R^2 = 0.93$. The correlation between high frequency ultrasound based and DIC based strain values showed reasonably strong correlation, with a linear coefficient value $R^2 = 0.71$. The correlation between ultrasound based and DIC based strain values for all specimens is depicted in **Figure 2.5A**. Bland-Altman plots depict the agreement of the ultrasound based methods to DIC and are shown in **Figure 2.5B**. Conventional ultrasound underestimates the strain with differences ranging from -1.1% to 0.13% strain with an average of -0.49%. The mean difference by the high frequency method was significantly ($p = 0.035$) larger with an average difference of

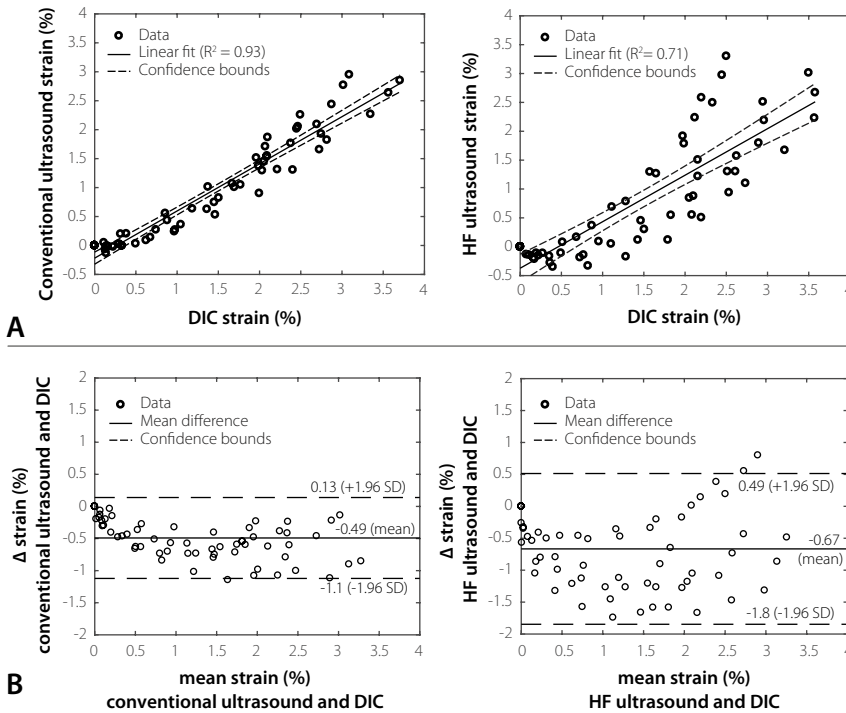


Figure 2.5 Comparison of the different strain estimation techniques, with the left column conventional and right column high frequency versus DIC based strain estimation. **A)** Depicts the linear correlation between the methods. **B)** The difference between ultrasound-based and DIC strain values are plotted against the mean of the two measurements in a Bland-Altman plot.

-0.67 % strain. The estimated local strain from both ultrasound and DIC techniques was lower than was applied globally (grip to grip).

2.4 Discussion

In this study we evaluated the use of high frequency ultrasound strain estimation of axially loaded collateral ligaments *ex vivo* and compared its performance to a conventional ultrasound method. The results demonstrate that conventional ultrasound based strain estimations show very strong correlation with strain values derived from DIC. The correlation obtained in this study is in accordance with earlier findings in strain imaging of tendons [15, 16]. Whereas, high frequency ultrasound strain estimation shows lower performance and only reasonable correlation with DIC measures.

When studying superficial structures, one obvious strategy to increase spatial resolution is to use a high frequency system. An increase in frequency decreases wavelength and consequently decreases both beam width (lateral resolution) and pulse duration (axial resolution), at a cost of penetration depth [17]. As a result of increased spatial resolution, a better performance of high frequency ultrasound systems seems evident in strain imaging, but in this study this approach was unexpectedly found to be inferior to conventional ultrasound based measurements. A possible explanation for this phenomenon might be the smaller elevational beam width, which makes the technique more sensitive to out-of-plane motion, resulting in tracking errors. DIC measures revealed out-of-plane motion (transverse to loading direction) ranging between 0.87 mm and 1.36 mm throughout the loading cycles. Out-of-plane motion is a fundamental challenge and is the inherent limitation of 2D imaging to evaluate 3D tissue motion. Another limitation in ultrasound strain imaging is the lower resolution and lack of phase information in the lateral direction. These challenges might be resolved using additional methods, such as 3D ultrasound imaging techniques [11, 18], displacement compounding [19, 20] or transverse oscillation [21].

The estimated strain of the ligaments was lower than was applied globally. The ligament length could be prone to measurement errors leading to false global reference values. Furthermore, strain may differ spatially [15, 22] and DIC measures indeed shows that strain varied locally with the highest strain values present near the insertion sites (**Figure 2.4**). Therefore, local (mid-substance) ligament strain was directly compared with matching ROI sizes between ultrasound and DIC methods. It is important to note the different imaging planes between the ultrasound and DIC data, which could have contributed to the variability in strain estimation between the methods. In case of the lateral collateral ligament the variability between the surface and internal strain is expected to be low, but this assumption may be invalid when studying structures with more complex anatomical/structural shape and deformation (*e.g.* cruciate ligaments). Moreover, this study addresses

a simple *ex vivo* loading scenario and many difficulties remain prior to clinical translation, including additional challenges in data acquisition as a result of complex anatomy and loading condition that occur in an *in vivo* situation [7]. In a well-controlled tensile test the material would remain more in plane than practically happens and additional studies should be designed for a more informed assessment of optimal *in vivo* strain measurements in the lateral collateral ligaments.

In conclusion, ultrasound strain imaging is feasible in *ex vivo* lateral collateral ligaments. The use of high frequency ultrasound does not seem beneficial compared to conventional ultrasound strain imaging. Despite the fact that high frequency ultrasound results in more detailed images that could help in diagnosis (*e.g.* detect small tears), the technique is more prone to errors that might be caused by out-of-plane motion which is also expected to occur (considerably) during *in vivo* strain measurements [7].

Acknowledgements

This research has received funding from the European Research Council (323091, FP/2007-2013) awarded to N. Verdonchot. Furthermore, the help of Richard van Swam and Sebastiaan van de Groes in the experimental conduct is kindly acknowledged.

References

1. Ophir, J., et al., *Elastography: a quantitative method for imaging the elasticity of biological tissues*. Ultrasonic Imaging, 1991. **13**(2): p. 111-134.
2. Slane, L.C., et al., *Non-uniform deformation of the patellar tendon during passive knee flexion*. J Appl Biomech, 2017: p. 1-25.
3. Slane, L.C., et al., *Evidence of patellar tendon buckling during passive knee extension*. Knee, 2016. **23**(5): p. 801-6.
4. Chimenti, R.L., et al., *Ultrasound Strain Mapping of Achilles Tendon Compressive Strain Patterns During Dorsiflexion*. Journal of biomechanics, 2016. **49**(1): p. 39-44.
5. Slane, L.C. and D.G. Thelen, *Non-Uniform Displacements within the Achilles Tendon observed during Passive and Eccentric Loading*. Journal of biomechanics, 2014. **47**(12): p. 2831-2835.
6. Bogaerts, S., et al., *Strain mapping in the Achilles tendon – A systematic review*. Journal of Biomechanics, 2016. **49**(9): p. 1411-1419.
7. Slane, L.C., et al., *The challenges of measuring in vivo knee collateral ligament strains using ultrasound*. J Biomech, 2017. **61**: p. 258-262.
8. Lionello, G., C. Sirieix, and M. Baleani, *An effective procedure to create a speckle pattern on biological soft tissue for digital image correlation measurements*. J Mech Behav Biomed Mater, 2014. **39**: p. 1-8.
9. Luyckx, T., et al., *Digital image correlation as a tool for three-dimensional strain analysis in human tendon tissue*. J Exp Orthop, 2014. **1**(1): p. 7.
10. Ristaniemi, A., L. Stenroth, and R.K. Korhonen, *PRECONDITIONING PROTOCOL FOR KNEE LIGAMENT TENSILE TESTING*. Congress of the European Society of Biomechanics, 2017.
11. Gijssels, K., et al., *Three-dimensional ultrasound strain imaging of skeletal muscles*. Phys Med Biol, 2017. **62**(2): p. 596-611.
12. Lopata, R.G., et al., *Performance evaluation of methods for two-dimensional displacement and strain estimation using ultrasound radio frequency data*. Ultrasound Med Biol, 2009. **35**(5): p. 796-812.
13. Kallel, F. and J. Ophir, *A least-squares strain estimator for elastography*. Ultrason.Imaging, 1997. **19**(3): p. 195-208.
14. Lopata, R.G.P., et al., *Comparison of One-Dimensional and Two-Dimensional Least-Squares Strain Estimators for Phased Array Displacement Data*. Ultrasonic Imaging, 2009. **31**(1): p. 1-16.
15. Chernak Slane, L. and D.G. Thelen, *The use of 2D ultrasound elastography for measuring tendon motion and strain*. Journal of Biomechanics, 2014. **47**(3): p. 750-754.
16. Okotie, G., et al., *Tendon strain measurements with dynamic ultrasound images: evaluation of digital image correlation*. J Biomech Eng, 2012. **134**(2): p. 024504.
17. Shung, K.K., *Ultrasonic Transducers and Arrays*, in *Diagnostic ultrasound : imaging and blood flow measurements*. 2006, CRC Press. p. 39-78.
18. Carvalho, C., et al., *3D Tendon Strain Estimation Using High-frequency Volumetric Ultrasound Images: A Feasibility Study*. Ultrason Imaging, 2017: p. 161734617724658.
19. Fekkes, S., et al., *2-D Versus 3-D Cross-Correlation-Based Radial and Circumferential Strain Estimation Using Multiplane 2-D Ultrafast Ultrasound in a 3-D Atherosclerotic Carotid Artery Model*. IEEE Trans Ultrason Ferroelectr Freq Control, 2016. **63**(10): p. 1543-1553.
20. Hansen, H.H., et al., *Full 2D displacement vector and strain tensor estimation for superficial tissue using beam-steered ultrasound imaging*. Phys Med Biol, 2010. **55**(11): p. 3201-18.
21. Jensen, J.A. and P. Munk, *A new method for estimation of velocity vectors*. IEEE Transactions on Ultrasonics, Ferroelectrics, and Frequency Control, 1998. **45**(3): p. 837-51.
22. Haraldsson, B.T., et al., *Region-specific mechanical properties of the human patella tendon*. J Appl Physiol (1985), 2005. **98**(3): p. 1006-12.

3

Ultrasound imaging of muscle contraction of the tibialis anterior in patients with facioscapulohumeral dystrophy

Authors

Kaj Gijsbertse, Rianne J.M. Goselink, Saskia Lassche, Maartje M. Nillesen, André M.J. Sprengers, Nico Verdonschot, Nens van Alfen and Chris L. de Korte

Published in

Ultrasound in Medicine and Biology; 2018 May; 17(73):233-237

Abstract

A need exists for biomarkers to diagnose, quantify and longitudinally follow facioscapulo-humeral muscular dystrophy (FSHD) and many other neuromuscular disorders. Furthermore, the pathophysiological mechanisms leading to muscle weakness in most neuromuscular disorders are not completely understood. Dynamic ultrasound imaging (B-mode image sequences) in combination with speckle tracking is an easy, applicable and patient-friendly imaging tool to visualize and quantify muscle deformation. This dynamic information provides insight in the pathophysiological mechanisms and may help to distinguish the various stages of diseased muscle in FSHD. In this proof-of-principle study, we applied a speckle tracking technique to 2-D ultrasound image sequences to quantify the deformation of the tibialis anterior muscle in patients with FSHD and in healthy controls. The resulting deformation patterns were compared with muscle ultrasound echo intensity analysis (a measure of fat infiltration and dystrophy) and clinical outcome measures. Of the four FSHD patients, two patients had severe peroneal weakness and two patients had mild peroneal weakness on clinical examination. We found a markedly varied muscle deformation pattern between these groups: patients with severe peroneal weakness showed a different motion pattern of the tibialis anterior, with overall less displacement of the central tendon region, while healthy patients showed a non-uniform displacement pattern, with the central aponeurosis showing the largest displacement. Hence, dynamic muscle ultrasound of the tibialis anterior muscle in patients with FSHD revealed a distinctively different tissue deformation pattern among persons with and without tibialis anterior weakness. These findings could clarify the understanding of the pathophysiology of muscle weakness in FSHD patients. In addition, the change in muscle deformation shows good correlation with clinical measures and quantitative muscle ultrasound measurements. In conclusion, dynamic ultrasound in combination with speckle tracking allows the study of the effects of muscle pathology in relation to strength, force transmission and movement generation. Although further research is required, this technique can develop into a biomarker to quantify muscle disease severity.

3.1 Introduction

In many neuromuscular diseases a need exists for biomarkers to characterise the severity and pattern of muscle involvement. With advances in the quality and availability of radiologic technologies, the role of muscle imaging is growing in the evaluation of patients with suspected neuromuscular disorders [1] and provide a complementary tool to existing electrophysiological techniques [2, 3]. Skeletal muscle imaging is used as a diagnostic tool to screen and identify the presence and pattern of pathology, and can be used to guide muscle biopsies. Ultrasound has well-recognized advantages of being a cheap, non-ionizing, point-of-care imaging modality with proven clinical validity in detecting neuromuscular disorders [1, 4-7](Simon et al., 2016, Arts et al., 2012). Previous studies have shown that static ultrasound images can be of value in the diagnosis of neuromuscular disorders by enabling the assessment of muscle thickness and the quantification of muscle atrophy (or hypertrophy) and muscle morphology changes [7-11]. Neuromuscular disorders can lead to an increase in muscle echo intensity, *i.e.* a muscle becomes whiter in appearance. An increase in fat and fibrous tissues is responsible for the high echo intensity appearance of muscles, as they increase the number of reflections within the muscle and therefore the mean grey value (echogenicity) of the muscle in the ultrasound image [12, 13].

Facioscapulohumeral muscular dystrophy (FSHD) is one of the most common forms of hereditary myopathy in adults [14, 15]. It derives its name from the muscle groups that are mainly affected at the initial stage of the disease: facial and shoulder girdle muscles. The disease is characterized by asymmetric loss of force and atrophy of muscular tissue starting in the face and shoulder region, with early involvement of the tibialis anterior in many patients [16, 17].

Although we can monitor the progress of neuromuscular diseases using imaging techniques and electrophysiological techniques, the pathophysiological mechanisms that lead to muscle weakness in different muscle disorders, such as FSHD, are not completely understood. With disease progression, healthy muscle tissue will increasingly be replaced by fat and fibrosis. This process can be quite asymmetric and variable along the length of the muscle in FSHD [18]. Because fat and fibrosis do not have electrically-activated contractile properties, these tissues will not contribute to force production during muscle contractions. However, this may not be the only reason that force production changes during disease progression. On the one hand, the progression of muscle tissue replacement not just decreases the amount of muscle tissue available for contraction, but also very likely decreases force transduction over the dystrophic segments to the tendons. On the other hand, even individual FSHD muscle fibres have decreased contractile properties [19].

Quantification of tissue deformation during contraction will be of interest in fundamental and clinical questions with respect to changes in functional behaviour of

muscles at different stages of the dystrophic process in FSHD. Measuring local skeletal muscle deformation *in vivo* might provide new insights how pathological muscle tissue contracts and transmits force, which leads to a better understanding of weakness in muscle disease, and might provide a functional outcome measure to study disease evolution.

Therefore, in this explorative study, we examined muscle tissue deformation during *in vivo* contractions of the tibialis anterior muscle in patients with different clinical stages of FSHD and healthy controls, by using dynamic 2D ultrasound imaging combined with speckle tracking.

3.2 Materials and Methods

A. Participants

This observational study was conducted at the Radboud university medical center, Nijmegen, The Netherlands. Four patients with a DNA-confirmed diagnosis of FSHD who regularly visited the outpatient clinic and four healthy controls were included. Data were obtained between August 2016 and December 2016. All participants gave their informed consent according to the approval from our institutional review board. The study was in accordance with the World Medical Association Declaration of Helsinki on Ethical Principles for Medical Research Involving Human Subjects.

B. Clinical assessment

The following clinical measures were collected: age, gender, height, weight and manual muscle testing scores of the tibialis anterior muscle using the Medical Research Council (MRC) grading system [20]. The age-adjusted clinical severity scale [21, 22] and the FSHD evaluation score [23] were assessed. Both scales have demonstrated a good inter- and intra-reliability in adults. In addition, the ‘walking on heels’ test of the Motor Function Measure [24] was used as a specific functional measure for tibialis anterior muscle strength. The tibialis anterior muscle was chosen for its good accessibility to ultrasound imaging, and because studies have shown that this muscle is one of the most early and severely involved muscles in the lower extremities in FSHD [16, 18, 25].

C. Ultrasound data acquisition

All ultrasound examinations were performed on an Esaote MyLab Twice ultrasound system (Esaote, Genoa - Italy), using a 3-13 MHz broadband linear transducer (LA533) with an axial and lateral image resolution of 0.3 mm and 0.9 mm, respectively. Patients were examined in a supine, relaxed position. Ultrasound data were acquired at the muscle belly of the tibialis anterior with a standardized transducer location at one-third of the distance on the line from interior aspect of the patella to the lateral malleolus [26]. The tibialis

anterior muscle was identified on the ultrasound image and a region of interest (ROI) was drawn manually in the ultrasound images by two different experienced clinicians (N.v.A. and S.L.). Ultrasound image sequences were acquired from both legs with the ultrasound transducer placed longitudinally, creating a sagittal plane representation of the muscle (**Figure 3.1**, right panel). In this plane the (dominant) translational motion of the muscle was visualized. Subjects were instructed to contract their foot dorsiflexors maximally for 3 seconds while their foot was constrained by a dynamometer (CITEC, CIT Technics, Haren – The Netherlands) that recorded the maximum exerted force during contraction. During the contraction of the muscle, ultrasound data were acquired in Digital Imaging and Communications in Medicine (DICOM) format at a frame-rate of 25 Hz.

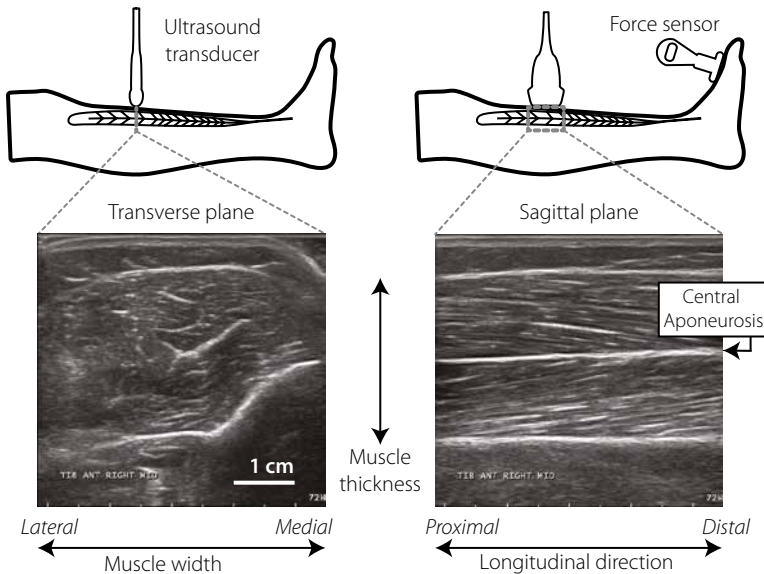


Figure 3.1 Transducer positions for measuring the tibialis anterior and example ultrasound images. Ultrasound imaging sequences were acquired during an isometric contraction in the sagittal plane (right panel). Muscle atrophy was determined using gray scale analysis (echogenicity) of static ultrasound data in the transverse plane (left panel).

D. Speckle tracking of dynamic muscle ultrasound

Tissue displacement was computed retrospectively using a customized Matlab (MathWorks Inc., Natick, MA, USA) based 2D displacement estimation and tracking algorithm, which was developed and validated on simulated, phantom and *in vivo* data [2, 27, 28]. This algorithm estimates the displacement between two consecutive frames by cross-correlating 2D segments of ultrasound data. A grid of nodes (spaced apart 0.5 mm in axial and 1 mm in lateral direction) was positioned within the ROI, at every node displacement estimations were calculated. A kernel of ultrasound data (5.2 x 2.9 mm) centred on the nodes was cross-correlated with a larger search kernel (14.6 x 5.7 mm) within the consecutive frame. For sub-pixel displacement estimation the cross correlation peak was detected using spline fitting of the cross correlation function. Inter-frame axial and lateral displacement estimations were filtered with a median filter of 5 x 5 mm to remove outliers.

Accumulated displacement estimates over the entire contraction were computed from the inter-frame displacements using bilinear interpolation [28]. The longitudinal displacement maps of the muscles at their maximum contraction were visualised on top of the B-mode images, and muscle motion was expressed as the average longitudinal displacement within the ROI. Additionally, the longitudinal displacement maps of all subjects were compared at time points where the averaged longitudinal displacement matched. This allows to compare the deformation pattern at the same level of muscle motion.

Displacement profiles were computed by averaging the longitudinal displacements across the thickness of the muscle and normalized to their maximum measured displacement to allow comparison among subjects. The displacement profiles were expressed as quiver plots.

E. Quantitative analysis of static ultrasound images

For quantitative muscle gray-scale analysis, or 'echogenicity' measurement, 3 images were obtained of tibialis anterior muscles of the left and right leg in the transverse plane (**Figure 3.1**, left panel), using a standardized scanning protocol with a fixed pre-set and image parameters, as previously described [26]. Echogenicity was determined offline by averaging the mean gray value (on a scale from 0-255) of the 3 measurements from the ROI. Muscle echogenicity was then compared to tibialis anterior specific echogenicity reference values [29], which are corrected for gender, age, height and weight, and results were expressed as a z-score (*i.e.* the number of standard deviations from the mean) [30]. A zscore of > 2 (*i.e.* a gray value larger than the value for 95% of the population) was considered abnormal.

3.3 Results

Table 3.1 summarizes the clinical data of the patients and healthy controls. Four patients with genetically confirmed FSHD were included with clinical FSHD scores ranging between 2 and 12. Two patients (Pat3 and Pat4) had peroneal weakness ($MRC \leq 3$) and two patients only had mildly peroneal weakness on clinical examination.

Table 3.1 Clinical data of patients and healthy controls

Subject no.	Age (y)	Gender	MRC score [left, right]	FSHD score
HC1	24	man	-	-
HC2	32	man	-	-
HC3	47	woman	-	-
HC4	27	woman	-	-
Pat1	31	woman	[5,5]	2
Pat2	24	man	[4,4]	3
Pat3	50	man	[3,3]	8
Pat4	37	man	[2,3]	12

The longitudinal tissue displacement of the tibialis anterior of all healthy subjects at maximum contraction is shown in **Figure 3.2**. For all healthy subjects a non-uniform deformation pattern was observed across the thickness of the muscle, with the middle region at the central aponeurosis consistently exhibiting larger displacements than the superficial and deep outer layers of the muscle. The normalized displacement profiles show a parabolic shape with steep flanks. The average longitudinal tissue displacement within the ROI of all healthy subjects was -9.7 ± 1.8 mm.

Patients with only mild tibialis anterior weakness (Pat1 and Pat2) showed similar deformation patterns as healthy subjects (**Figure 3.3**), but the average tissue displacement was slightly lower than healthy controls (-6.5 ± 2.5 mm).

Two patients (Pat3 and Pat4) showed severe tibialis anterior weakness at clinical examination. Dynamic ultrasound data revealed that the muscle tissue displacement of these patients was lower (-2.1 ± 1.0 mm) and deformed in a completely different manner. In **Figure 3.4**, the displacement of muscle tissue of patient 3 is depicted. The deformation pattern is almost homogenous across the thickness of the muscle, with the superficial and deeper regions of the muscle exhibiting similar displacement as the middle region. Patient 4 was the most severely affected patient of this study. We observed a uniform deformation

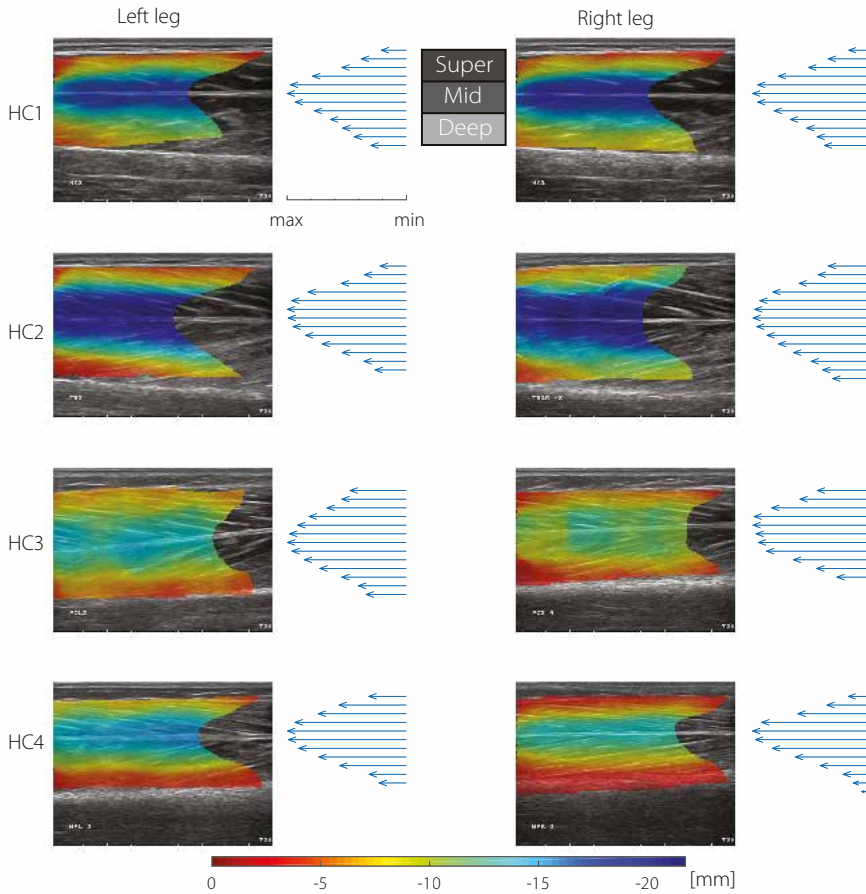


Figure 3.2 Muscle tissue displacement of four healthy controls at their maximum voluntary contraction. The displacement maps depict the longitudinal displacement [mm] of the muscle in the sagittal ultrasound plane. The arrows represent the averaged normalized muscle displacement (displacement profile) across the thickness of the muscle; the mid region at the central aponeurosis shows the largest displacement.

pattern in the superficial and mid region of the muscle at maximum contraction, while the deeper region showed almost no tissue displacement, with a tendency in the opposite direction of the contraction (**Figure 3.5**).

All muscle deformation patterns were analyzed at the point of maximum muscle motion. Additionally, the difference in the muscle deformation patterns among patients without and patients with peroneal weakness was independent of the contraction phase.

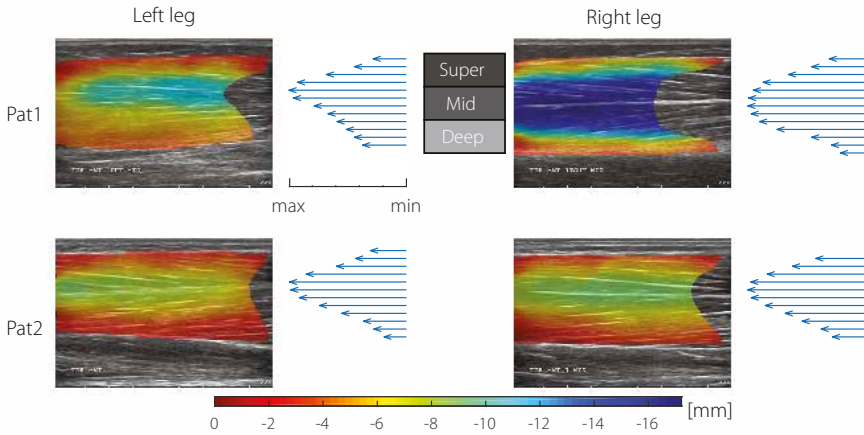


Figure 3.3 Muscle tissue displacement of patient 1 and patient 2 with mild peroneal weakness. Although the average displacement is slightly lower than healthy controls, the displacement patterns are similar; the mid region at the central aponeurosis shows the largest motion.

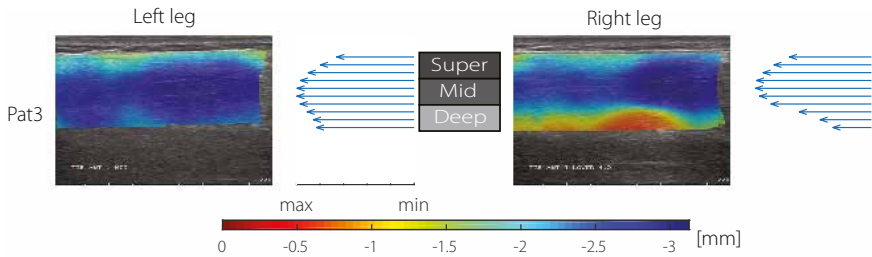


Figure 3.4 Muscle tissue displacement of patient 3 with severe peroneal weakness. The displacement maps are more homogenous across the thickness of the muscle. The superficial and deeper regions are exhibiting almost equal displacement as the mid region.

For equal muscle tissue displacement (for patients at their plateau, and for healthy subjects early in the contraction phase) the variation in deformation pattern was already visible (**Figure 3.6**).

The resulting deformation patterns were compared to muscle echogenicity values, clinical outcome measures and maximum exerted force and showed good agreement (**Table 3.2**). Similar to the averaged measured displacement in the muscles, the peak force

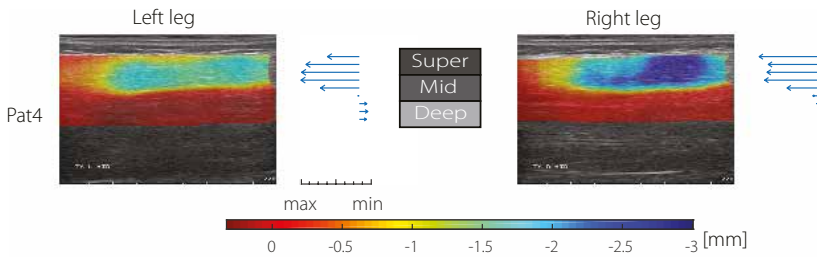


Figure 3.5 Muscle tissue displacement of patient 4 with severe peroneal weakness. The superficial and mid region of the muscle show a homogenous displacement pattern along the depth, but the deeper region shows almost no motion with a tendency in the opposite direction than the contraction direction.

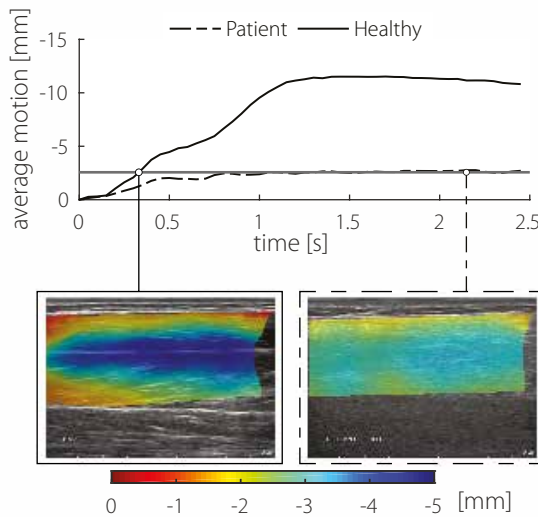


Figure 3.6 Muscle displacement maps of a healthy volunteer (HC 1) and a severely affected patient (patient 3) with peroneal weakness. The selected frames are matched according to their average measured muscle tissue displacement. The displacement patterns within the muscles are quite different which indicates that for similar muscle 'activity' there is a difference in functional behaviour.

Table 3.2 Ultrasound findings; Gray-scale analysis (z-score) and muscle deformation findings

Subject no.	Leg	Peroneal weakness	Force (N)	z-score	Muscle motion (mm)	Muscle tissue displacement findings
HC1	Left	No	175	-2.19	-10.5	Non-uniform deformation pattern, with the muscle region at central aponeurosis showing the largest displacement. The muscle displacement profile shows a parabolic shape.
	Right		200	-2.41	-11.1	
HC2	Left	No	165	0.83	-11.4	
	Right		164	0.05	-11.9	
HC3	Left	No	140	-0.07	-9.1	
	Right		145	0.38	-7.7	
HC4	Left	No	170	-0.36	-9.2	
	Right		140	-0.17	-6.8	
Pat1	Left	Mild	102	-0.46	-6.0	Similar to healthy subjects; largest displacement at central aponeurosis.
	Right		130	-0.36	-10.2	
Pat2	Left	Mild	79	1.44	-4.7	
	Right		70	0.21	-5.13	
Pat3	Left	Severe	33	3.60	-3.1	
	Right		14	2.70	-2.6	
Pat4	Left	Severe	10	3.80	-0.9	
	Right		13	4.47	-1.6	

measurements acquired by the dynamometer showed that FSHD patients produced less muscle force than the healthy controls (56 ± 45 N versus 162 ± 20 N). **Figure 3.7** shows the good correlation between measured force and muscle motion, with a linear coefficient of determination (R^2 value) of 0.91. In addition to the detected weakness, ultrasound echogenicity z-scores were highest for patients with clear tibialis anterior weakness with z-scores between 2.7 and 4.78 corroborating that these muscles were (severely) affected. The echogenicity of patients with only mild tibialis anterior weakness were considered normal, since the z-scores did not exceed levels higher than 2.

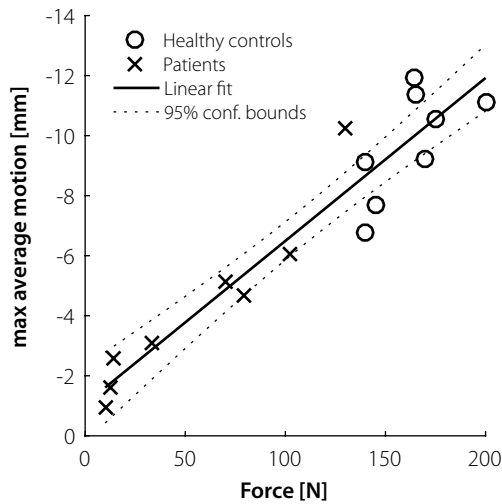


Figure 3.7 Linear regression of peak force [N] and muscle motion [mm]. R^2 value = 0.91.

3.4 Discussion

The results of this explorative study suggest that the deformation pattern of the tibialis anterior muscle with abnormal echogenicity is different from that of a healthy or only mildly affected muscle without clear US abnormalities. Severely affected muscles most notably show decreased motion of the central tendon aponeurosis of the tibialis anterior, which strongly suggests a decrease in force transferred to this central tendon and, hence, a decrease in force output when attempting to flex the ankle. In the most severely affected patient a part of the muscle even showed a very small paradoxical movement, suggesting that this part of the muscle did no longer actively take part in the contractile process, but was rather moved in a passive fashion as result of other still contractile muscle parts.

The observed difference in displacement patterns for equal muscle motion (**Figure 3.6**) indicate that the change in deformation is not a result of lower muscle ‘activity’ as seen in severely affected patients, but suggests a change in functional behaviour and force transmission of affected muscles. Matching the muscle activity between subjects is difficult, since we did not have continuous force measurements. Electronically triggered contraction (*i.e.* twitch contraction) would allow to study displacement and strain rate in a more controlled fashion [2]. This would also eliminate the possibility of co-contraction effects. Stimulation, however, is not very comfortable and may introduce additional practical problems.

Despite that voluntary muscle contractions may not be very accurate to determine the maximum force, the force measurements indicate that muscles of patients with normal echogenicity and deformation patterns were weaker. This suggest the existence of a qualitative mechanism of muscle weakness based on a loss of intrinsic contractile strength. Lassche et al. demonstrated a reduction in sarcomeric force in type II FSHD muscle fibres [19] which could play a role in the development of muscle weakness. Unpublished work by our group corroborate that atrophy and fat infiltration by itself cannot explain the reduced muscle force, as they calculated lower specific muscle tension from musculoskeletal models which compensated for the loss of functional muscle tissue. Furthermore, the distal to proximal progression of fat and fibrotic tissue infiltration not just decreases the amount of muscle tissue available for contraction, but also very likely decreases force transduction and deformation pattern over the dystrophic segments to the distal tendon [31]. Subsequent studies that quantify muscle contraction along the entire length of the muscle are required to reveal local differences in contraction patterns. A multi-dimensional imaging modality is needed for a comprehensive mapping of muscle contraction. Besides the limited field-of-view, 2D displacement estimation techniques are also prone to errors as a result of out-of-plane motion that can arise from muscle twist. Although we were unable to capture the out-of-plane motion, we are confident in the robustness of this method to track motion within the image plane as the peak normalised cross-correlation values were high and qualitative inspection did not reveal significant outof-plane motion. The work presented here utilizes DICOM data and the accuracy of the displacement estimation may benefit from the use of raw ultrasound data (RF-data). This increases the axial (along the ultrasound beam) resolution. Additionally, the estimation of the lateral displacement can be improved using compounding techniques, as described by Hansen and co-workers [32]. However, these techniques require dedicated equipment/sequences and access to RF data, which are not typically available on ultrasound machines used in clinical practice. Three-dimensional ultrasound techniques have been applied to study the contraction of skeletal muscles [10, 27, 33]. However, a trade-off exists among spatial resolution, field-of-view and temporal resolution in these 3D techniques. Alternatively, magnetic resonance imaging (MRI) allows the study of muscle contraction throughout the full length of the muscle [34-39]. While MRI measures can provide detailed information

about muscle structures, its ability to quantify muscle deformation during natural activities (e.g. gait) is limited. Ultrasound imaging systems are developing towards portable systems that allow us to study muscle contraction during highly dynamic tasks [40].

Our findings as presented in this study are based on a small group of healthy controls and patients diagnosed with FSHD. More extensive studies are needed to confirm these data. Longitudinal studies that provide insight in the change of muscle functioning as a function of disease progression may help to understand why muscles in neuromuscular diseases become weaker. Local assessment of muscle deformation can be of interest in many other neuromuscular diseases, such as inclusion body myositis. Furthermore, speckle tracking also provides a tool to extract detailed information of the presence of fasciculations or fibrillations as seen in motor neuron diseases [41].

In conclusion, this work provides a tool to quantify muscle motion and evidence of changing functional behaviour of affected muscles in FSHD patients. The quantitative characterization of muscle contraction provides new insights in the way pathological muscle tissue deforms and transmits force, which leads to a better understanding of the underlying phenomena related to weakness in muscle disease.

Acknowledgements

The research leading to these results has received funding from the European Research Council under the European Union's Seventh Framework Programme (FP/2007-2013) / ERC Grant Agreement n. 323091 awarded to N. Verdonschot.

References

1. Simon, N.G., Y.I. Noto, and C.M. Zaidman, *Skeletal muscle imaging in neuromuscular disease*. J Clin Neurosci, 2016. **33**: p. 1-10.
2. Lopata, R.G., et al., *Dynamic imaging of skeletal muscle contraction in three orthogonal directions*. J Appl Physiol (1985), 2010. **109**(3): p. 906-15.
3. Zwarts, M.J., G. Drost, and D.F. Stegeman, *Recent progress in the diagnostic use of surface EMG for neurological diseases*. J Electromyogr Kinesiol, 2000. **10**(5): p. 287-91.
4. Arts, I.M., et al., *Muscle ultrasonography: a diagnostic tool for amyotrophic lateral sclerosis*. Clin Neurophysiol, 2012. **123**(8): p. 1662-7.
5. Heckmatt, J.Z., V. Dubowitz, and S. Leeman, *Detection of pathological change in dystrophic muscle with B-scan ultrasound imaging*. Lancet, 1980. **1**(8183): p. 1389-90.
6. Pillen, S., I.M. Arts, and M.J. Zwarts, *Muscle ultrasound in neuromuscular disorders*. Muscle Nerve, 2008. **37**(6): p. 679-93.
7. Zaidman, C.M. and N. van Alfen, *Ultrasound in the Assessment of Myopathic Disorders*. J Clin Neurophysiol, 2016. **33**(2): p. 103-11.
8. Janssen, B.H., et al., *Quantitative muscle ultrasound versus quantitative magnetic resonance imaging in facioscapulohumeral dystrophy*. Muscle Nerve, 2014. **50**(6): p. 968-75.
9. Pillen, S., et al., *Quantitative skeletal muscle ultrasound: diagnostic value in childhood neuromuscular disease*. Neuromuscul Disord, 2007. **17**(7): p. 509-16.
10. Raiteri, B.J., A.G. Cresswell, and G.A. Lichtwark, *Three-dimensional geometrical changes of the human tibialis anterior muscle and its central aponeurosis measured with three-dimensional ultrasound during isometric contractions*. PeerJ, 2016. **4**: p. e2260.
11. Reimers, K., et al., *Skeletal muscle sonography: a correlative study of echogenicity and morphology*. J Ultrasound Med, 1993. **12**(2): p. 73-7.
12. Pillen, S., et al., *Skeletal muscle ultrasound: correlation between fibrous tissue and echo intensity*. Ultrasound Med Biol, 2009. **35**(3): p. 443-6.
13. Pillen, S. and N. van Alfen, *Skeletal muscle ultrasound*. Neurol Res, 2011. **33**(10): p. 1016-24.
14. Deenen, J.C., et al., *The Epidemiology of Neuromuscular Disorders: A Comprehensive Overview of the Literature*. J Neuromuscul Dis, 2015. **2**(1): p. 73-85.
15. Lunt, P.W., et al., *Correlation between fragment size at D4F104S1 and age at onset or at wheelchair use, with a possible generational effect, accounts for much phenotypic variation in 4q35-facioscapulohumeral muscular dystrophy (FSHD)*. Hum Mol Genet, 1995. **4**(5): p. 951-8.
16. Mul, K., et al., *Integrating clinical and genetic observations in facioscapulohumeral muscular dystrophy*. Curr Opin Neurol, 2016. **29**(5): p. 606-13.
17. Tawil, R., *Facioscapulohumeral muscular dystrophy*. Neurotherapeutics, 2008. **5**(4): p. 601-6.
18. Janssen, B.H., et al., *Distinct disease phases in muscles of facioscapulohumeral dystrophy patients identified by MR detected fat infiltration*. PLoS One, 2014. **9**(1): p. e85416.
19. Lassche, S., et al., *Sarcomeric dysfunction contributes to muscle weakness in facioscapulohumeral muscular dystrophy*. Neurology, 2013. **80**(8): p. 733-7.
20. Vanhoutte, E.K., et al., *Modifying the Medical Research Council grading system through Rasch analyses*. Brain, 2012. **135**(Pt 5): p. 1639-49.
21. Ricci, E., et al., *Progress in the molecular diagnosis of facioscapulohumeral muscular dystrophy and correlation between the number of KpnI repeats at the 4q35 locus and clinical phenotype*. Ann Neurol, 1999. **45**(6): p. 751-7.
22. van Overveld, P.G., et al., *Variable hypomethylation of D4Z4 in facioscapulohumeral muscular dystrophy*. Ann Neurol, 2005. **58**(4): p. 569-76.
23. Lamperti, C., et al., *A standardized clinical evaluation of patients affected by facioscapulohumeral muscular dystrophy: The FSHD clinical score*. Muscle Nerve, 2010. **42**(2): p. 213-7.
24. Berard, C., et al., *A motor function measure scale for neuromuscular diseases. Construction and validation study*. Neuromuscular Disorders, 2005. **15**(7): p. 463-470.
25. Tasca, G., et al., *Different molecular signatures in magnetic resonance imaging-staged facioscapulohumeral muscular dystrophy muscles*. PLoS One, 2012. **7**(6): p. e38779.

26. Scholten, R.R., et al., *Quantitative ultrasonography of skeletal muscles in children: normal values*. Muscle Nerve, 2003. **27**(6): p. 693-8.
27. Gijssbertse, K., et al., *Three-dimensional ultrasound strain imaging of skeletal muscles*. Phys Med Biol, 2017. **62**(2): p. 596-611.
28. Lopata, R.G., et al., *Performance evaluation of methods for two-dimensional displacement and strain estimation using ultrasound radio frequency data*. Ultrasound Med Biol, 2009. **35**(5): p. 796-812.
29. Nijboer-Oosterveld, J., N. Van Alfen, and S. Pillen, *New normal values for quantitative muscle ultrasound: obesity increases muscle echo intensity*. Muscle Nerve, 2011. **43**(1): p. 142-3.
30. Pillen, S., et al., *Quantitative skeletal muscle ultrasonography in children with suspected neuromuscular disease*. Muscle Nerve, 2003. **27**(6): p. 699-705.
31. Lacourpaille, L., et al., *New insights on contraction efficiency in patients with Duchenne muscular dystrophy*. J Appl Physiol (1985), 2014. **117**(6): p. 658-62.
32. Hansen, H.H., et al., *Full 2D displacement vector and strain tensor estimation for superficial tissue using beam-steered ultrasound imaging*. Phys Med Biol, 2010. **55**(11): p. 3201-18.
33. Deffieux, T., et al., *Assessment of the mechanical properties of the musculoskeletal system using 2-D and 3-D very high frame rate ultrasound*. IEEE Trans Ultrason Ferroelectr Freq Control, 2009. **55**(10): p. 2177-2190.
34. Dresner, M.A., et al., *Magnetic resonance elastography of skeletal muscle*. Journal of Magnetic Resonance Imaging, 2001. **13**(2): p. 269-276.
35. Moerman, K.M., et al., *Validation of continuously tagged MRI for the measurement of dynamic 3D skeletal muscle tissue deformation*. Med Phys, 2012. **39**(4): p. 1793-810.
36. Zhong, X., et al., *Imaging two-dimensional displacements and strains in skeletal muscle during joint motion by cine DENSE MR*. J.Biomech., 2008. **41**(3): p. 532-540.
37. Englund, E.K., et al., *Combined diffusion and strain tensor MRI reveals a heterogeneous, planar pattern of strain development during isometric muscle contraction*. Am J Physiol Regul Integr Comp Physiol, 2011. **300**(5): p. R1079-90.
38. Pappas, G.P., et al., *Nonuniform shortening in the biceps brachii during elbow flexion*. J Appl Physiol (1985), 2002. **92**(6): p. 2381-9.
39. Mazzoli, V., et al., *Assessment of passive muscle elongation using Diffusion Tensor MRI: Correlation between fiber length and diffusion coefficients*. NMR Biomed, 2016. **29**(12): p. 1813-1824.
40. Eranki, A., et al., *A novel application of musculoskeletal ultrasound imaging*. J Vis Exp, 2013(79): p. e50595.
41. Harding, P.J., et al., *Ultrasound-Based Detection of Fasciculations in Healthy and Diseased Muscles*. IEEE Trans Biomed Eng, 2016. **63**(3): p. 512-8.

4

Continuous analysis of skeletal muscle strain with respect to fascicle orientation using ultrasound

Authors

Kaj Gijsbertse, André M.J. Sprengers, Max A. Bakker, Maartje M. Nillesen, Linda Heskamp, Chris L. de Korte and Nico Verdonchot

Submitted to

Journal of Medical Engineering and Physics; 2018 March

Abstract

The relation between muscle fiber orientation and muscle deformation is complex and includes a non-collinear alignment of the direction of shortening with the muscle fiber direction. To study the dynamic behavior of this relation, we present a 2D ultrasound based method to quantify local muscle deformation concurrently with fiber orientation *in vivo*. Our method combines a cross-correlation based speckle tracking technique to measure the muscle deformation with a local Radon-transformation based technique to detect the fiber orientation. This method was tested in eight healthy volunteers during an isometric contraction of the tibialis anterior muscle. The results reveal a heterogeneous pattern of strain development with largest deformation at the muscle belly region. The change of fiber direction was small and limited to seven degrees in the most extreme cases. The principal shortening direction deviated from the fiber direction. This deviation varied spatially and over time, where the deviation was large at the beginning of the contraction and converges to $\sim 30^\circ$ for higher strain levels at the plateau of the contraction phase. In conclusion, the results corroborates the complex relation between muscle fiber direction and contraction direction, and adds to the quantitative characterization of this dynamic relation during contraction. This tool allows for a more comprehensive assessment of muscle functioning during dynamic tasks, which can be used to obtain more accurate biomechanical models and to study differences in functional behavior in healthy and pathologic muscle tissue.

4.1 Introduction

The evaluation of muscle morphology and the way muscle contract and transmit force is important for understanding the working mechanism of healthy muscles as well as muscles in neuromuscular disorders. Morphological parameters such as fascicle length and fascicle orientation have been extensively studied using imaging modalities such as Magnetic Resonance Imaging (MRI) and Ultrasound. These morphological parameters are used in biomechanical modeling to estimate the force-generating capacity of muscles [1-3] and to quantify muscle functioning for addressing research questions and for clinical diagnosis [4-6]. Besides morphological parameters, quantification of deformation (strain) of muscles during activities provide additional insights in the way healthy or pathological muscle contract and transmit force [7]. Combining methods to evaluate strain development in relation to changes in muscle morphology leads to a more complete understanding of muscle functioning.

MRI data have provided evidence that the relation between fascicle orientation and muscle deformation pattern is complex. This includes spatially heterogeneous strain distributions [8, 9] and non-collinear alignment of the direction of shortening with the muscle fiber direction [10]. However, these MR techniques are highly time consuming and require subjects to repeat a contraction several times, which induces muscle fatigue leading to lower reproducibility and might hamper applications in patients. Consequently, morphological parameters are frequently assessed quasi-dynamically and thus unable to reveal the true dynamic behavior. Moreover, the ability of MRI to study muscle contraction during natural activities (*e.g.* gait) is limited. To overcome these limitations, ultrasound has the well-recognized advantage of being an imaging modality with high spatial and temporal resolution that allows to study muscle contraction during highly dynamic tasks.

Muscle fascicles are bundles of skeletal muscle fibers surrounded by connective tissue that appear as hyperechoic line structures in ultrasound images and previous studies have shown that ultrasound can be used to measure muscle fascicle lengths during activities, such as standing, walking, and running [11-14]. For the tracking of fascicle orientation, most of the methods are based on the detection of linear features of the fascicles and apply Hough [15] or Radon [16-18] transformations and Gabor filtering [19] of ultrasound images. A technique to quantify the deformation of tissue is called ultrasound strain imaging and has been applied to skeletal muscles *in vivo* [20-23]. With this technique, the displacement of tissue can be assessed by dividing the ultrasound data in segments and then track these segments over time using cross-correlation techniques. Subsequently the spatial derivative of the displacement field is computed to determine strain, as was first introduced by Ophir et al. [24].

Combining these ultrasound techniques allows to study muscle deformation and interpret it with respect to fiber orientation in a true dynamic fashion. This might provide a valuable complementary method to study the functional behavior of muscles. In this

paper we propose a 2D ultrasound based framework to quantify local muscle deformation concurrently with fascicle orientation during *in vivo* contraction of the tibialis anterior muscle.

4.2 Methods

For a comprehensive mapping of muscle functioning we applied a cross-correlation based strain estimation technique to quantify the deformation of muscle besides local fiber orientation detection using a Radon transformation-based algorithm.

A. Experimental protocol

We included eight healthy male volunteers in the age range of 18-35 years. All subjects gave written informed consent according to the World Medical Association Declaration of Helsinki for Medical Research Involving Human Subjects and our institutional review board (NL6013509116). The subjects were in a supine position on a bed, with their right leg positioned in a custom designed ergometer (**Figure 4.1**). Isometric voluntary contractions provide a standardized and reproducible procedure to study muscle functioning [10, 21]. Therefore, the foot was fixed to the pedal of the ergometer which was connected to a force sensor (Sauter FL500, Kern & Sohn GmbH, Balingen - Germany) that recorded the exerted force. Maximum voluntary contraction (MVC) was determined by instructing each subject to deliver their maximum effort of (isometric) dorsiflexion twice for a period of ~3s. The MVC was calculated as the average of the two maximal force recordings. Subsequently, the subjects were instructed to dorsiflex their ankle (*i.e.* contraction of the tibialis anterior) up to 50% of their MVC within a period of 3.5s. The level of 50% was chosen because it was demonstrated that most architectural parameters, such as fascicle orientation, fascicle length and muscle thickness change markedly for contractions up to this level, but change little at higher levels of contraction [25, 26]. Additionally, studying contractions at 50% MVC prevents fatigue, and allows to compare our results with previous studies in a similar situation. To guide the subject, the force exerted by the subject was displayed together with the required force level. During this exercise, two-dimensional ultrasound data were acquired of the tibialis anterior muscle. This exercise was conducted twice for two separate longitudinal ultrasound acquisitions; one with the ultrasound transducer positioned at the proximal part of the muscle, and another with the transducer placed at the distal end, to cover the entire muscle (see also **Figure 4.1**). The junction of the two acquisitions was at the muscle belly of the tibialis anterior muscle with a standardized location at one-third of the distance on the line from the interior aspect of the patella to the lateral malleolus [27]. Ultrasound image sequences were acquired using a Acuson S2000 system (Siemens Medical Solutions, Mountain View, CA, USA) equipped with a 14L5BV transducer (footprint of 15.4 cm), and exported in radio-frequency (RF)

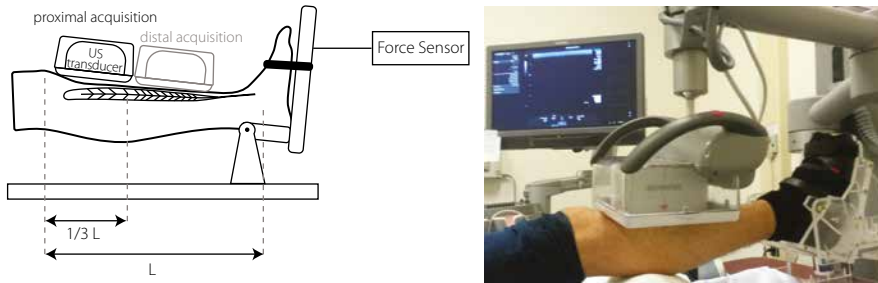


Figure 4.1 Experimental set-up. The leg of the subject was positioned in the ergometer and their foot constrained to a pedal which measured the exerted force during the isometric dorsiflexion. Ultrasound data was acquired at two different locations (proximal and distal), with the junction of the two acquisitions at the muscle belly of the tibialis anterior muscle with a standardized location at one-third of the distance on the line from the interior aspect of the patella to the lateral malleolus (left image). The photo on the right depicts the proximal placement of the ultrasound transducer on the leg.

format at a frame rate of 24 Hz and an axial-lateral spatial resolution of 0.02×0.3 mm. The tibialis anterior muscle was identified on the ultrasound image and a region of interest (ROI) was drawn manually (K.G.) (**Figure 4.2**). To facilitate local data assessment, the ROI was divided in an upper and lower region (*i.e.* above and below the central aponeurosis). These region were then divided into three sub-regions, which were $1/3$ of the muscle length within the image (L_p = proximal muscle length, and L_d = distal muscle length) resulting in six sub-regions per acquisition (see also **Figure 4.2**).

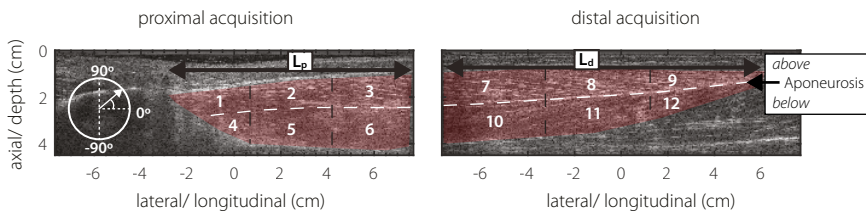


Figure 4.2 Muscle region definition and coordinate system for strain and fiber direction within the ultrasound data for the two image acquisition locations (proximal and distal). The tibialis anterior muscle is annotated by the red region and was divided in 12 sub-regions for local data assessment.

B. Fiber orientation detection

Local fiber orientation was detected, for each ultrasound time-frame in the acquired image sequence, based on a Radon transform method as described by Zhao et al [16]. Briefly, ultrasound data were re-sampled to a uniform grid with a resolution of 0.3 mm. Kernels (6.3 x 6.3 mm) of ultrasound data were retrieved at points on an equidistant grid with 0.6 mm spacing within the ROI. Kernels with low average intensity values (< 140 [signal amplitude unit]) were considered as kernels without visible fascicles and were ignored from the analysis. Each kernel was normalized to have intensities with zero mean and a standard deviation of one. Subsequently, a Radon transformation was applied to find the local fiber direction within that kernel. From previous studies it is known that the fiber direction is within a certain range during contraction [28, 29]. Therefore, to reduce calculation time, the Radon transform was applied within an angle range of -45° to 45° with step size 0.5° . After the Radon transformation, linear features were represented as peaks at their corresponding angle in Radon space (*i.e.* sinogram). The most prominent linear feature (*i.e.* fiber direction) was detected by finding the maximum of the sums of absolute values in Radon space for every angle. This summation allows for detection of the most prominent fiber direction in the kernel, and not just the most singular fiber which is represented by the highest peak in the sinogram. To remove outliers, the detected fiber directions in the ultrasound image were 2D median filtered (5.0 x 10.0 mm kernel).

C. Ultrasound strain imaging

Muscle deformation was computed using an customized MATLAB-based (Math-Works Inc, Natick, MA, USA) 2D strain estimation algorithm, which was developed and validated on simulated, phantom and *in vivo* data [20, 21, 30]. Displacements were calculated on the same grid as was used for the local fiber orientation. Inter-frame displacements were calculated for every grid point by normalized cross-correlation of template kernels (2.1 x 3.3 mm) within larger search kernels (2.5 x 6.3 mm) in the consecutive frame, of ultrasound data. For sub-pixel displacement estimation the cross correlation peak was detected using spline fitting of the cross correlation function. To remove outliers, the displacements were 2D median filtered (5.0 x 10.0 mm kernel). Accumulated displacement estimates over the contraction phase were computed from the inter-frame displacements using bilinear interpolation [30]. To compute the axial and lateral components of the 2D strain tensor (E), a least-squares strain estimator with a kernel size of 10 x 15 mm was applied to the measured displacements [31, 32]. Subsequently, the strain tensor was diagonalized and principal strains were computed as the eigenvalues of E , and the directions of the principal strains are represented by the eigenvectors of E [10]. Principal strains consisted of one positive, ϵ_p (expansion) and one negative, ϵ_n (contracting) component, orthogonal to each other (see results). The contraction direction can be considered in first approximation to be related to the fiber orientation. Therefore, the direction of the negative strain component (ϵ_n) was compared to the local fiber orientation. For low strain values ($< 5\%$)

early in the contraction phase, the strain direction was discarded as it might not be fully defined/reliable for these low values. The negative strain values were expressed in a color map and superimposed over of the B-mode image. Strain and fiber directions were also visualized in the B-mode image and expressed as local small lines with their angles corresponding to the strain/fiber orientation. The average strain and its direction together with the fiber orientation for each of the twelve regions for each subject were plotted over time to visualize the local development during the contraction phase. The contraction phase was defined as a period of three seconds after the point where the strain magnitude exceeded the level of 1%. Additionally, the absolute difference between the strain direction and fiber orientation was also plotted for each region and subject.

4.3 Results

The negative (contraction) principal strain component (ϵ_N) and fiber direction during contraction of the proximal muscle region of one subject is shown in **Figure 4.3**. The strain varies locally in both magnitude and direction and show low values around the central aponeurosis. The direction of local strain deviates from the fiber direction and is also spatially dependent; at the most proximal side, *i.e.* muscle origin, of the muscle the deviation appears smaller compared to the more distal region, *i.e.* muscle belly. The images are shown for six time points during the contraction and reveal how the strain and fiber orientation changes over time.

Time evolution of strain and fiber direction for all six regions in the proximal muscle per individual subject (dashed grey lines) and the mean curves of the eight subjects (solid black lines) are depicted in **Figure 4.4**. Strain increases during the contraction and is largest in region 3, the upper half (above the aponeurosis) of the muscle belly region, with average strain values of $\epsilon_p = 37.4 \pm 11.0$ % and $\epsilon_N = -16.8 \pm 3.0$ % at the end of the contraction phase (**Figure 4.4A**). The direction of the negative strain component deviates from the fiber direction, but this angle difference converges for higher strain values (end of contraction phase) to $\sim 30^\circ$ (**Figure 4.4B-D**). The smallest deviation between negative strain and fiber angle can be found near the insertion side of the muscle (region 1 and 4) where mean angle differences range from $36.6 \pm 9.8^\circ$ at the start of contraction to $14.8 \pm 6.2^\circ$ at the end of the contraction phase. Similar results are observed for the distal muscle region (**Figure 5**), with increasing strain during the contraction and maximum strain values near the muscle belly region (region 7). The distal muscle region shows the largest fiber angles, with largest values in the most distal region (region 12) of $7.4 \pm 3.3^\circ$ at the end of the contraction. Noteworthy, the orientation of fibers does not change dramatically during contraction and is limited to a change of $\sim 7^\circ$ in the most extreme cases.

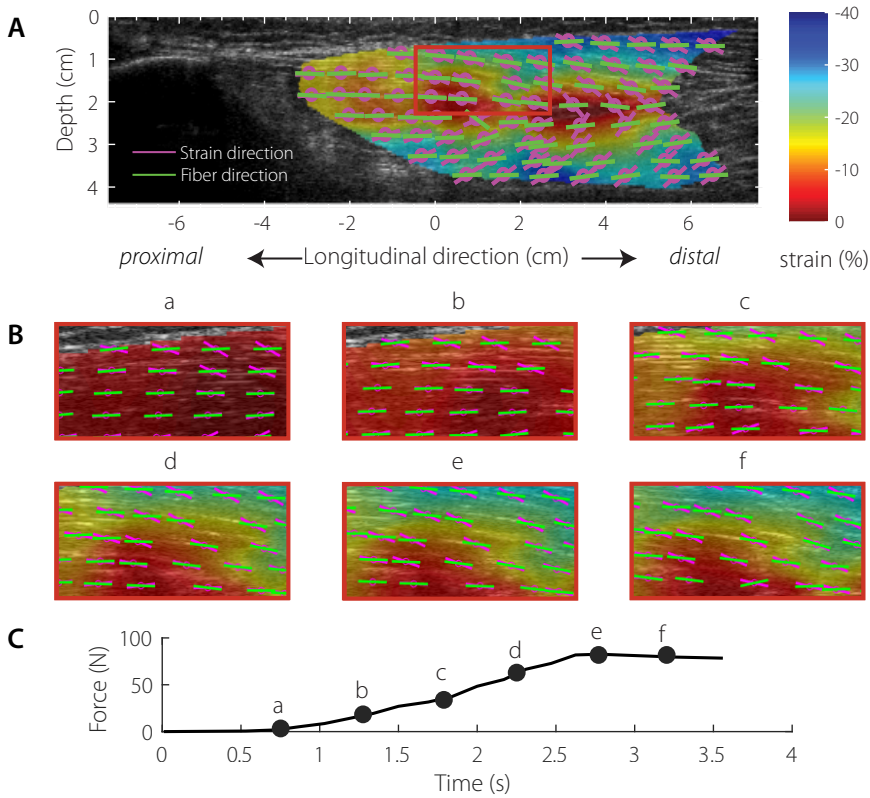


Figure 4.3 **A**) The negative (contraction) principal strain amplitude (color bar) and direction (pink lines) and locally detected fiber orientation (green lines) during muscle contraction of the proximal muscle region. **B**) The local strain and fiber orientation for six different time points (a-f) of the contraction for the red box in **A**. **C**) Experimentally measured force during the contraction period depicting the six-time points.

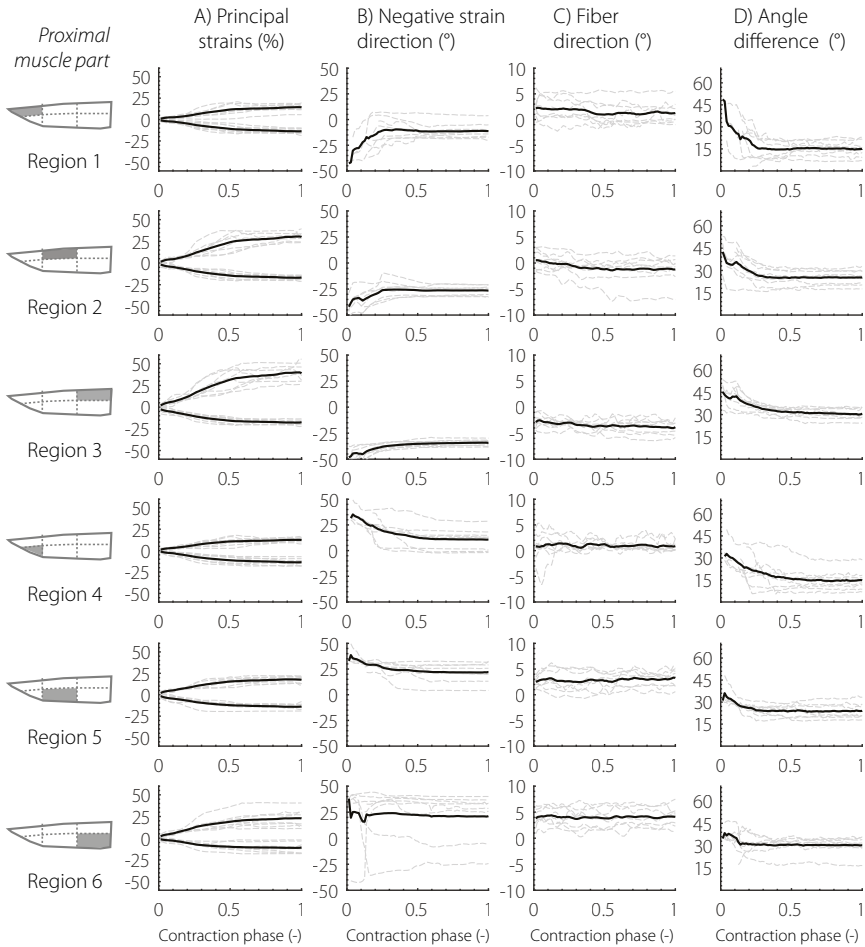


Figure 4.4 Strain and fiber orientation over time for the 6 different regions of the **proximal** muscle for the individual subjects (dashed grey lines) and average over all eight subjects (solid black lines). **A)** Principal strain. **B)** Negative strain direction. **C)** Fiber direction **D)** Angle difference between the negative strain direction and fiber direction.

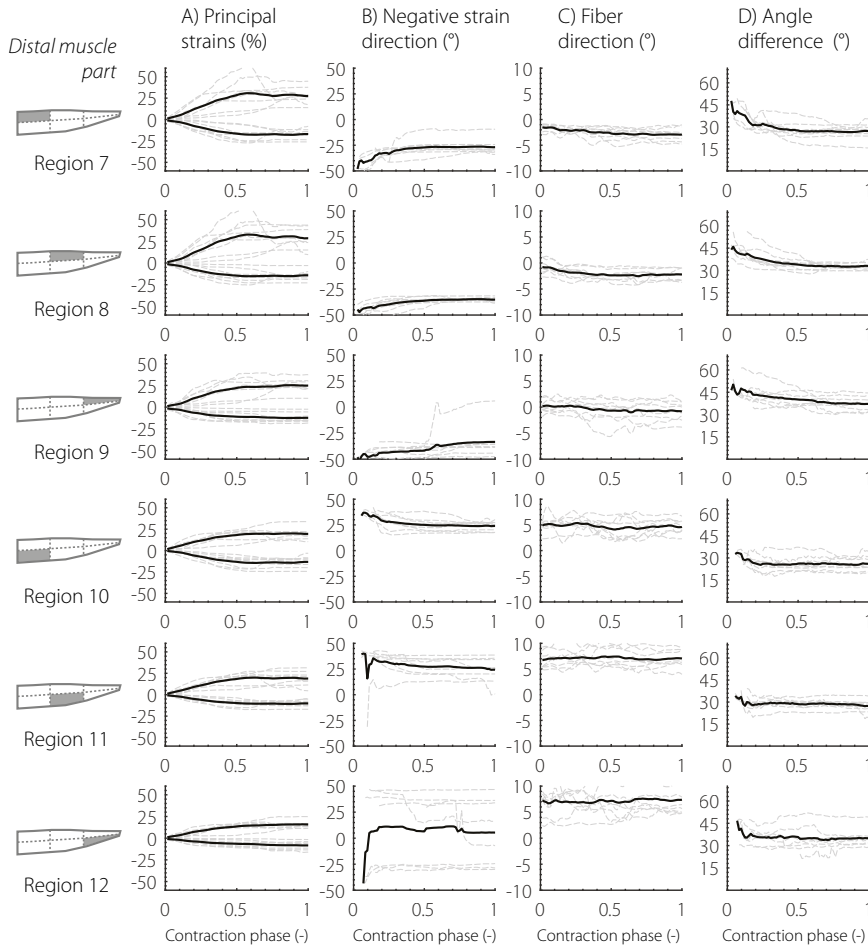


Figure 4.5 Strain and fiber orientation over time for the 6 different regions of the **distal** muscle for the individual subjects (dashed grey lines) and average over all eight subjects (solid black line). **A)** Principal strain. **B)** Negative strain direction. **C)** Fiber direction **D)** Angle difference between the negative strain direction and fiber direction.

4.4 Discussion

This paper presented an ultrasound based framework to measure strain in skeletal muscle concurrently with fascicle direction during contraction. The high temporal resolution of ultrasound enabled true dynamic assessment of muscle functioning. Using the described method, 2D principal strain components were measured locally during contraction,

revealing the deformation magnitude and its direction along the length of the muscle. Strain magnitude increased during contraction and the direction of strain changed. The contraction direction, *i.e.* negative strain, deviated from the fascicle direction. Moreover, this deviation between fiber and deformation direction changes during contraction, adding to and corroborating the complexity of the relation between these two parameters throughout the entire contraction cycle.

The results reveal a spatially heterogeneous strain distribution with the largest strain magnitudes at the muscle belly, which is in accordance with earlier findings [9]. Also the magnitude of strain is similar to those previously described for isometric muscle contraction [20, 21]. Positive components of the principal strain were larger than the negative component, which suggest the existence of another negative strain component in order to retain a constant volume (*i.e.* incompressibility) [33]. This finding of incompressibility of skeletal muscle is also supported by findings based on 4D MRI [10, 34], however their formation and diagonalization of the 3D strain tensor revealed a consistent, planar pattern of strain development. This indicates that the general assumption in many models of muscles expanding radially [35] is not necessary true but their deformation is complex and might vary, which could be depending on type of contraction (*e.g.* isometric, isotonic, or isokinetic) and surrounding or connecting tissue. For example, the shortening of a muscle during an isometric contraction is expected to be smaller than muscles contracting concentrically. Additionally, when studying voluntary contractions, co-contracting muscles are likely to influence each other's deformation resulting in complex strain patterns. Studying voluntary contractions may be less reproducible compared to electric stimulated contractions [21], but are more comfortable and carry fewer practical issues. The reproducibility of the voluntary contraction and the proposed ultrasound techniques is indicated by the similarity of the strain and fiber curves as obtained from eight the different participants.

The most markedly change in muscle morphological parameters is within 30% MVC and fiber orientation changes little for higher contraction levels [25, 26]. Muscle fiber direction showed limited ($< 7^\circ$) change during the 50% MVC, which is comparable to the findings of Raiteri et al. who reported an average change of 4° within the tibialis anterior muscle during an isometric contraction based on 3D ultrasound measurements [29]. Most studies calculate one pennation angle of a muscle, which is the angle between the fascicle insertion into the central aponeurosis, but this may introduce difficulties since both fascicles and central aponeurosis are curved [36]. Our method allows for a view-independent comparison of stain and fiber direction, locally, without the requirement of a consistently orientated reference frame definition.

The direction of the negative (contraction) principal strain component (ϵ_N) deviated from the fiber, this deviation varied during the contraction both spatially and over time. The angle difference was approximately 30° , depending on the location within the muscle at the end-phase of the 50% MVC and corresponds with values as reported in MR studies [10, 37]. This non-collinearity is believed to be caused by architectural heterogeneity in

terms of fiber lengths and fiber orientation [10]. Also, the variation in fascicle lengths and fascicle curvature causes non-uniform fascicle strains [38]. Our method provides complementary information with respect to the dynamic behavior of this relation during contraction. At the beginning of the contraction this deviation is large but converges for larger strain values, which is comparable to results of studies focusing on tendon mechanics that showed that the fibers become more aligned under passive load [39]. Furthermore, this observation is in line with the previously described phenomenon of large change in muscle architecture for contraction levels up to 30% MVC. It is likely that there are active and passive parts within the muscle during a submaximal muscle contraction, as only a subset of the motor units are recruited. For increasing contraction levels, more motor units and their corresponding muscle fibers are involved, which influence each other's motion. This could partly explain the complex temporal and spatial dependency of the deviation between muscle fiber orientation and muscle deformation.

It is important to note that the muscle was imaged in two separate 2D acquisitions. Variation in contraction speed or fashion together with malalignment between the two ultrasound acquisitions could have contributed to some of the variability in strain values or fiber orientation within muscle regions that are adjacent to each other. Although we have applied one of the largest clinically available linear array transducers the field-of-view is limited compared to other modalities such as MRI. Besides the limited field-of-view of 2D ultrasound, displacement estimation techniques are also prone to errors as a result of out-of-plane motion that can arise from muscle twist. This is the inherent limitation of using a 2D imaging approach to evaluate 3D tissue motion is a fundamental challenge of this approach. To measure the full 3D strain tensor in 3D space, the proposed ultrasound techniques methods can be extended to 3D ultrasound data [20, 29, 40]. However, 3D ultrasound comes at the cost of reduced spatial and temporal resolution that reduces the performance of strain estimation. Obviously, also the performance of fiber detection is related to the spatial resolution. Sufficient frame rate is required to study fast motion, such as muscle contraction and to prevent decorrelation of ultrasound data between frames. This can be accomplished with multiple triggered contractions, but leads to increased experimental and computational time and higher muscle fatigue that may reduce the reproducibility of the contraction. Alternatively, magnetic resonance imaging allows the study of muscle contraction throughout the full length of the muscle [9, 10, 41-44] but requires faster image acquisition to compete with the high temporal resolution of ultrasound. Recent developments in accelerated self-gated MRI, might help to resolve this challenge [34].

In conclusion, we combined different ultrasound-based methods to evaluate muscle deformation concurrently with muscle fiber orientation during contraction. The results of this study corroborates the complex relation between muscle fiber direction and contraction direction, and adds to the quantitative characterization of this dynamic relation. This tool allows for a more comprehensive assessment of muscle functioning

during dynamic tasks, which can be used to obtain more accurate biomechanical models and to study differences in functional behavior in healthy and pathologic muscle tissue.

Acknowledgements

The research leading to these results has received funding from the European Research Council under the European Union's Seventh Framework Programme (FP/2007-2013) / ERC Grant Agreement n. 323091 awarded to N. Verdonschot. Furthermore, the help of Anniek Driessen in the preparation of the experiments and the analysis of the preliminary results is kindly acknowledged.

Ethical approval

All participants in this study gave written informed consent according to the World Medical Association Declaration of Helsinki for Medical Research Involving Human Subjects and our institutional review board (NL6013509116).

References

1. Hicks, J.L., et al., *Is My Model Good Enough? Best Practices for Verification and Validation of Musculoskeletal Models and Simulations of Movement*. Journal of Biomechanical Engineering, 2015. **137**(2): p. 020905-020905-24.
2. Lieber, R.L., et al., *Skeletal muscle mechanics, energetics and plasticity*. J Neuroeng Rehabil, 2017. **14**(1): p. 108.
3. Marra, M.A., et al., *A subject-specific musculoskeletal modeling framework to predict in vivo mechanics of total knee arthroplasty*. J Biomech Eng, 2015. **137**(2): p. 020904.
4. Lieber, R.L. and J. Friden, *Clinical significance of skeletal muscle architecture*. Clin Orthop Relat Res, 2001(383): p. 140-51.
5. Mohagheghi, A.A., et al., *In vivo gastrocnemius muscle fascicle length in children with and without diplegic cerebral palsy*. Dev Med Child Neurol, 2008. **50**(1): p. 44-50.
6. Li, L., K.Y. Tong, and X. Hu, *The effect of poststroke impairments on brachialis muscle architecture as measured by ultrasound*. Arch Phys Med Rehabil, 2007. **88**(2): p. 243-50.
7. Gijssbertse, K., et al., *Ultrasound Imaging of Muscle Contraction of the Tibialis Anterior in Patients with Facioscapulo-humeral Dystrophy*. Ultrasound Med Biol, 2017. **43**(11): p. 2537-2545.
8. Jensen, E.R., et al., *Characterization of three dimensional volumetric strain distribution during passive tension of the human tibialis anterior using Cine Phase Contrast MRI*. J Biomech, 2016. **49**(14): p. 3430-3436.
9. Pappas, G.P., et al., *Nonuniform shortening in the biceps brachii during elbow flexion*. J Appl Physiol (1985), 2002. **92**(6): p. 2381-9.
10. Englund, E.K., et al., *Combined diffusion and strain tensor MRI reveals a heterogeneous, planar pattern of strain development during isometric muscle contraction*. Am J Physiol Regul Integr Comp Physiol, 2011. **300**(5): p. R1079-90.
11. Aggelousis, N., et al., *Reproducibility of fascicle length and pennation angle of gastrocnemius medialis in human gait in vivo*. Gait Posture, 2010. **31**(1): p. 73-7.
12. Lichtwark, G.A. and A.M. Wilson, *Optimal muscle fascicle length and tendon stiffness for maximising gastrocnemius efficiency during human walking and running*. J Theor Biol, 2008. **252**(4): p. 662-73.
13. Loram, I.D., C.N. Maganaris, and M. Lakie, *Use of ultrasound to make noninvasive in vivo measurement of continuous changes in human muscle contractile length*. J Appl Physiol (1985), 2006. **100**(4): p. 1311-23.
14. Chleboun, G.S., et al., *Fascicle Length Change of the Human Tibialis Anterior and Vastus Lateralis During Walking*. Journal of Orthopaedic & Sports Physical Therapy, 2007. **37**(7): p. 372-379.
15. Zhou, Y. and Y.P. Zheng, *Estimation of muscle fiber orientation in ultrasound images using revolving hough transform (RVHT)*. Ultrasound Med Biol, 2008. **34**(9): p. 1474-81.
16. Zhao, H. and L.Q. Zhang, *Automatic tracking of muscle fascicles in ultrasound images using localized Radon transform*. IEEE Trans Biomed Eng, 2011. **58**(7): p. 2094-101.
17. Chen, X., et al., *Continuous fascicle orientation measurement of medial gastrocnemius muscle in ultrasonography using frequency domain Radon transform*. Biomedical Signal Processing and Control, 2015. **20**(Supplement C): p. 117-124.
18. Rana, M., G. Hamarneh, and J.M. Wakeling, *Automated tracking of muscle fascicle orientation in B-mode ultrasound images*. J Biomech, 2009. **42**(13): p. 2068-73.
19. Han, P., et al., *Automatic thickness estimation for skeletal muscle in ultrasonography: evaluation of two enhancement methods*. Biomed Eng Online, 2013. **12**: p. 6.
20. Gijssbertse, K., et al., *Three-dimensional ultrasound strain imaging of skeletal muscles*. Phys Med Biol, 2017. **62**(2): p. 596-611.
21. Lopata, R.G., et al., *Dynamic imaging of skeletal muscle contraction in three orthogonal directions*. J Appl Physiol (1985), 2010. **109**(3): p. 906-15.
22. Witte, R.S., et al., *High Resolution Ultrasound Imaging of Skeletal Muscle Dynamics and Effects of Fatigue*. 2004. Proc. IEEE Ultrasonics Int. Conf., Montreal, Canada.
23. Affagard, J.S., P. Feissel, and S.F. Bensamoun, *Use of digital image correlation and ultrasound: analysis of thigh muscle displacement fields*. Conf Proc IEEE Eng Med Biol Soc, 2015. **2015**: p. 3827-30.
24. Ophir, J., et al., *Elastography: a quantitative method for imaging the elasticity of biological tissues*. Ultrasonic Imaging, 1991. **13**(2): p. 111-134.

25. Hodges, P.W., et al., *Measurement of muscle contraction with ultrasound imaging*. Muscle Nerve, 2003. **27**(6): p. 682-92.
26. Li, J., et al., *The sensitive and efficient detection of quadriceps muscle thickness changes in cross-sectional plane using ultrasonography: a feasibility investigation*. IEEE J Biomed Health Inform, 2014. **18**(2): p. 628-35.
27. Scholten, R.R., et al., *Quantitative ultrasonography of skeletal muscles in children: Normal values*. Muscle & Nerve, 2003. **27**(6): p. 693-698.
28. Maganaris, C.N. and V. Baltzopoulos, *Predictability of in vivo changes in pennation angle of human tibialis anterior muscle from rest to maximum isometric dorsiflexion*. Eur J Appl Physiol Occup Physiol, 1999. **79**(3): p. 294-7.
29. Raiteri, B.J., A.G. Cresswell, and G.A. Lichtwark, *Three-dimensional geometrical changes of the human tibialis anterior muscle and its central aponeurosis measured with three-dimensional ultrasound during isometric contractions*. PeerJ, 2016. **4**: p. e2260.
30. Lopata, R.G., et al., *Performance evaluation of methods for two-dimensional displacement and strain estimation using ultrasound radio frequency data*. Ultrasound Med Biol, 2009. **35**(5): p. 796-812.
31. Kallel, F. and J. Ophir, *A least-squares strain estimator for elastography*. Ultrason.Imaging, 1997. **19**(3): p. 195-208.
32. Lopata, R.G.P., et al., *Comparison of One-Dimensional and Two-Dimensional Least-Squares Strain Estimators for Phased Array Displacement Data*. Ultrasonic Imaging, 2009. **31**(1): p. 1-16.
33. Baskin, R.J. and P.J. Paolini, *Volume change and pressure development in muscle during contraction*. Am J Physiol, 1967. **213**(4): p. 1025-30.
34. Mazzoli, V., et al., *Accelerated 4D self-gated MRI of tibiofemoral kinematics*. NMR Biomed, 2017. **30**(11).
35. Wakeling, J.M. and A. Randhawa, *Transverse Strains in Muscle Fascicles during Voluntary Contraction: A 2D Frequency Decomposition of B-Mode Ultrasound Images*. Int J Biomed Imaging, 2014. **2014**: p. 352910.
36. Randhawa, A. and J.M. Wakeling, *Multidimensional models for predicting muscle structure and fascicle pennation*. Journal of Theoretical Biology, 2015. **382**: p. 57-63.
37. Mazzoli, V., et al., *Combined accelerated 4D phase contrast and 3D diffusion tensor imaging reveals a complex relation between strain and muscle architecture in contracting leg muscles*. in proceeding ISMRM conference 2017. 2017.
38. Blemker, S.S., P.M. Pinsky, and S.L. Delp, *A 3D model of muscle reveals the causes of nonuniform strains in the biceps brachii*. J Biomech, 2005. **38**(4): p. 657-65.
39. Lake, S.P., et al., *Effect of fiber distribution and realignment on the nonlinear and inhomogeneous mechanical properties of human supraspinatus tendon under longitudinal tensile loading*. J Orthop Res, 2009. **27**(12): p. 1596-602.
40. Weide, G., et al., *3D Ultrasound Imaging: Fast and Cost-effective Morphometry of Musculoskeletal Tissue*. J Vis Exp, 2017(129).
41. Dresner, M.A., et al., *Magnetic resonance elastography of skeletal muscle*. Journal of Magnetic Resonance Imaging, 2001. **13**(2): p. 269-276.
42. Mazzoli, V., et al., *Assessment of passive muscle elongation using Diffusion Tensor MRI: Correlation between fiber length and diffusion coefficients*. NMR Biomed, 2016. **29**(12): p. 1813-1824.
43. Moerman, K.M., et al., *Validation of continuously tagged MRI for the measurement of dynamic 3D skeletal muscle tissue deformation*. Med Phys, 2012. **39**(4): p. 1793-810.
44. Zhong, X., et al., *Imaging two-dimensional displacements and strains in skeletal muscle during joint motion by cine DENSE MR*. J.Biomech., 2008. **41**(3): p. 532-540.

5

Three-dimensional ultrasound strain imaging of skeletal muscles

Authors

Kaj Gijsbertse, André M.J. Sprengers, Maartje M. Nillesen, Hendrik H Hansen, Richard G. Lopata, Nico Verdonchot and Chris L. de Korte

Published in

Physics in Medicine and Biology; 2017 Jan; 62(2):596-611

Abstract

In this study, a multi-dimensional strain estimation method is presented to assess local relative deformation in three orthogonal directions in 3D space of skeletal muscles during voluntary contractions. A rigid translation and compressive deformation of a block phantom mimics muscle contraction and is used as experimental validation of the 3D technique to compare its performance with respect to a 2D based technique. Axial, lateral and elevational (in case of 3D) displacements are estimated using a coarse-to-fine normalized cross-correlation method. After transformation of the displacements to a Cartesian coordinate system, strain is derived using a least-squares strain estimator. The performance of both methods is compared by calculating the root-mean-squared error of the estimated displacements with the calculated theoretical displacements of the phantom experiments.

We observe that the 3D technique delivers more accurate displacement estimations compared to the 2D technique, especially in the translation experiment where out-of-plane motion hampers the 2D technique. *In vivo* application of the 3D technique in the *musculus vastus intermedius* shows good correlation between measured strain and the force pattern. Similarity of the strain curves of repetitive measurements indicates the reproducibility of voluntary contractions. These results indicate that 3D ultrasound is a valuable imaging tool to quantify complex tissue motion, especially when there is motion in three directions, which results in out-of-plane errors for 2D techniques.

5.1 Introduction

The aetiology of many musculoskeletal diseases is related to the biomechanical condition of the affected muscle. Techniques that provide systematic and quantitative data of abnormal tissue deformation could be of great diagnostic value for treatment of musculoskeletal diseases or injuries. To study the deformation of muscles, different imaging modalities have been used, including MRI and ultrasonography [1-3]. The high temporal resolution of ultrasound allows for assessment of dynamic muscle behavior during contraction. Hence, ultrasound imaging of muscles may provide insight in the process of force production, the subsequent deformations and its dependency on muscle structure and hierarchy. Giles et al. have suggested to use 2D ultrasound to assess quadriceps muscle size and relate it to muscle functioning in patients with patellofemoral pain [2]. Furthermore, quantitative measures of muscles derived from ultrasound techniques, such as hierarchical or mechanical properties provide valuable information for calibration and validation of musculoskeletal models [4].

There are different ultrasound techniques which provide quantitative measures of mechanical properties and muscle dynamics. One of the first *in vivo* efforts was performed with a Doppler-based technique to assess muscle contraction [5]. More recently, vector tissue Doppler imaging was performed to measure contraction velocity, strain and strain rate during dynamic activity [6]. Ultrasound strain imaging is a widely used technique for measuring induced deformation (tumor detection, plaque characterization) and active deformation (heart) of tissue and has also been applied to skeletal muscles *in vivo* [3, 7-9]. With this technique, the displacement of tissue is assessed by correlating segments of ultrasound data acquired sequentially. Subsequently the spatial derivative of the displacement field is computed to determine strain.

Muscle contraction is anisotropic and of a 3D nature due to the anisotropic material properties and contractile element orientations of muscle tissue, and is characterized by translations and deformations. Therefore a multi-dimensional imaging modality is required to reveal functional muscle behavior. However, most of the reported studies are limited to 1D or 2D and are, therefore, unable to reveal the 3D anisotropic behavior of the muscle. Furthermore, errors in the strain estimation might be introduced as a result of out-of-plane motion. Consequently, a full 3D imaging technique is required to reduce these errors and yield the full 3D strain tensor. Three-dimensional strain imaging has been applied to study the heart [10], but the technique has not been validated. In cardiovascular data the displacement and strain of interest obey a coordinate system that is more or less aligned with the transducer coordinate system. Therefore, it is interesting to study the performance of 3D strain imaging in cases where the main direction of the displacements and strains are not aligned with the utilized coordinate system, such as the deformation of skeletal muscles.

In the present study we investigated the use of 3D ultrasound for strain estimation in skeletal muscles, and its potential advantages over 2D-based strain estimation. 2D and 3D ultrasound acquisitions were performed in a deformable phantom for experimental validation. The 3D technique was subsequently evaluated *in vivo* to measure muscle deformation of the *musculus vastus intermedius* in a healthy volunteer.

5.2 Material and Methods

A. Three-dimensional Ultrasound Acquisition

Real-time 3D radio-frequency (RF) ultrasound data were acquired with an iE33 ultrasound system (Philip Medical Systems, Bothell, USA), equipped with an X7-2 matrix array transducer (2-7 MHz) and an RF-interface which sampled the RF data with a frequency of 16 MHz. Subsequently, the RF-data were up-sampled by spline interpolation in both lateral and elevational direction by a factor of 3, to increase the spatial density. Up-sampling the RF-data is commonly used to improve the lateral and elevational displacement estimation [11-14].

B. Displacement and Strain estimation

To estimate the displacement field, a multi-step normalized cross-correlation based technique was used [10, 12]. This technique estimates the displacements between two consecutive frames by cross-correlating either 2D or 3D segments of ultrasound data in two steps. In the first step the global motion of the tissue was estimated using relatively large segments of envelope data (*i.e.* demodulated RF data using the Hilbert transform). In the second step, the axial displacement estimates were refined by using smaller segments of RF-data. For all cross-correlation computations the data were processed along the scan-lines in a rectangular format. For accurate sub-sample displacement estimation the cross correlation peak was detected using spline fitting of the cross correlation function. Displacement and strain values were obtained every 0.5 mm (10 sample points) in the axial direction and for each original RF-line (*i.e.* non-interpolated lateral and elevational direction). It must be noted that lateral and elevational window sizes cannot be expressed in units such as millimeters, since they are depth dependent due to diverging image lines. Inter-frame displacement estimates were filtered with a median filter to remove outliers. Accumulated displacement estimates were computed from the inter-frame displacements using bilinear interpolation. After transformation of the displacements to a Cartesian coordinate system, strain was derived using a least-squares strain estimator (LSQSE) [15]. To investigate the effect of out-of-plane motion on the displacement estimation we compared the performance of the 3D technique with the performance of a 2D technique. In case of the 2D technique, 2D segments from the 3D data were selected (*i.e.* no data in elevational direction). Settings for the displacement estimation are summarized in **Table 5.1**.

Table 5.1 Displacement estimation settings.

	Iteration 1	Iteration 2
Used data	Envelope	RF
Axial segment size	5 mm	2.5 mm
Axial search range	10 mm	0.2 mm
Lateral segment size	25 lines	13 lines
Lateral search range	12 lines	0 lines
Elevational segment size ^a	25 lines	13 lines
Elevational search range ^a	5 lines	0 lines
Median filter	3.0 mm x 7 x 7 ^a lines	
LSQSE filter	5.5 mm x 11 x 11 ^a lines	
^a Only applicable for the 3D method		

C. Experimental Validation (Phantom study set-up)

For validation of the displacement and strain estimation technique, a phantom study was conducted. A block phantom (10x10x10 cm³) was constructed from a homogeneous 10% gelatin (Dr. Oetker, Ede – The Netherlands) solution. Scattering properties of soft tissue were mimicked by adding 1% Silica particles (15-30 µm SiC, E. Merck, Darmstadt – Germany) to the solution [16]. The material was assumed to be linearly elastic and incompressible (Poisson's ratio 0.5).

Two experimental situations were used to mimic the behavior of muscle contraction. The first experiment consisted of a rigid translation. A linear translation stage was used to move the transducer 1 mm over the phantom in the y-direction (**Figure 5.1**). The second experiment applied a compressive deformation of 2.5 mm in the z-direction, resulting in a theoretical deformation of -2.5% and 1.25% strain in the z- and x/y-direction, respectively. This deformation was realized using a compressor setup, which moved a plate to uniformly apply displacement to the top plane of the phantom. The ultrasound transducer was fixed in the center of the compressor plate and the bottom plate was constrained from moving. Both plates were lubricated aiming to achieve free-slip boundary conditions. For both experimental situations 3D ultrasound data were acquired before and after the applied translation or deformation (**Figure 5.2**).

As a reference (*i.e.* ground truth), the theoretical displacements and strains within the phantom were derived using classic continuum mechanics; using Hooke's law the displacement and strain at every point within the field of view of the ultrasound acquisition were calculated given the applied deformation.

To assess the performance of the displacement and strain estimation the root-mean-squared error (RMSE) was calculated using the estimated displacements/strains and the theoretically derived values according to:

$$RMSE = \sqrt{\frac{\sum_{i=1}^M \sum_{j=1}^N \sum_{k=1}^P (\delta_{i,j,k}^{est} - \delta_{i,j,k}^{ref})^2}{M \cdot N \cdot P}}, \quad (\text{eq. 5.1})$$

where $\delta_{i,j,k}^{est}$ is the estimated displacement (or strain) value on coordinate (i,j,k) and $\delta_{i,j,k}^{ref}$ the corresponding theoretically derived value for all points $M \cdot N \cdot P$ inside the region of interest (ROI), see also **Figure 5.2**. RMSE values were assessed for displacement and strain in the transducer's coordinate system (i.e. axial, lateral and elevational), and Cartesian coordinate system.

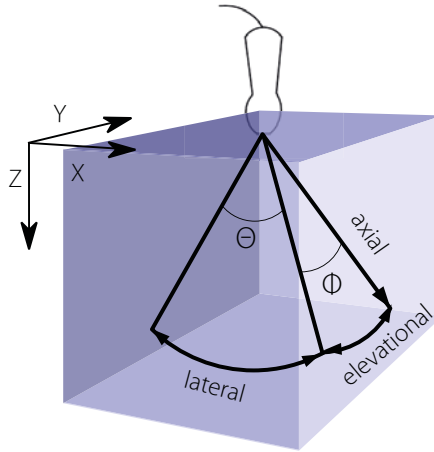


Figure 5.1 Phantom block and representation of both the transducer and Cartesian coordinate system.

D. In Vivo Application

To demonstrate the *in vivo* feasibility of 3D strain imaging of skeletal muscles, the *musculus vastus intermedius* (VI) of a human volunteer (female, 27 years) was examined during voluntary isometric contractions. The *in vivo* data was acquired in accordance with the World Medical Association Declaration of Helsinki on Ethical Principles for Medical Research Involving Human Subjects. Informed consent of the healthy volunteer was obtained. The volunteer was positioned in a chair with both the right hip and knee at 90

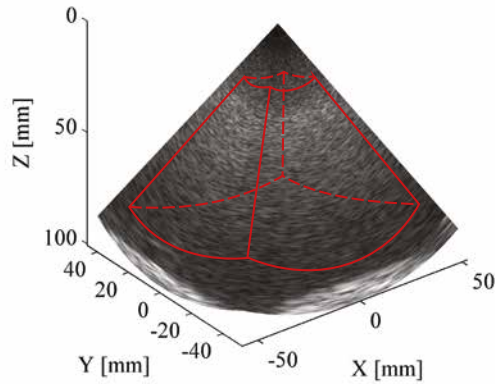


Figure 5.2 3D B-mode image of the block phantom with the region of interest for analysis indicated in red.

degrees of flexion (see **Figure 5.3**). The lower leg was cuffed to a force sensor, which constrained the movement of the leg and recorded the exerted force. Maximum voluntary contraction (MVC) was determined by asking the subject to deliver her maximum effort of isometric knee extension twice for a period of 3 seconds with one minute rest in-between. The MVC was calculated as the average of the two force recordings. Subsequently, the subject was instructed to follow a block shaped curve of 2.5 seconds at 30% of the maximum voluntary contraction twice, with 5 minutes rest in-between. To facilitate the sub-maximal MVC, the force exerted by the subject was displayed together with the predefined pattern for visual feedback (see **Figure 5.4**). The level of 30% was chosen, because it was demonstrated that most architectural parameters, such as pennation angle, fascicle length and muscle thickness change markedly with contractions up to 30% MVC, but change little at higher levels of contraction [17, 18]. Additionally, studying contractions at 30% MVC prevents fatigue, limits the contraction rate and limits the contribution of opposing forces caused by the stiffness of the surrounding tissue.

The ultrasound transducer was positioned at the middle of the thigh on its superior aspect, with the axial-elevation plane (*i.e.* z-y plane) aligned with the anatomical sagittal plane (**Figure 5.3**). A bag filled with acoustic-gel was placed between the transducer and skin to secure the acoustic coupling between the probe and skin during muscle contractions. Additionally, this offset increased the imaged volume of the muscle in the field of view. At an image depth of 8 cm, 3D ultrasound data were acquired with a frame rate of 35 Hz. The *V* muscle was annotated manually by a trained observer (**Figure 5.5**).

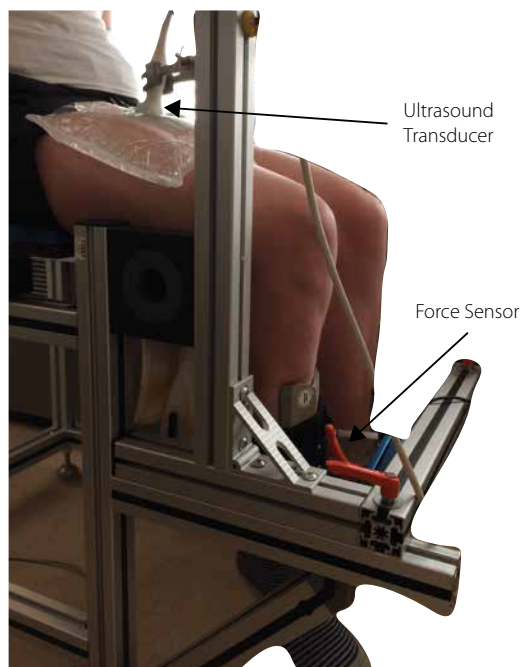


Figure 5.3 Experimental set-up for collecting in vivo ultrasound data from the subject's right leg during isometric contraction of the quadriceps muscles. The exerted force was recorded using a force sensor at the lower leg. 3D ultrasound data were acquired at the center of the quadriceps muscle.

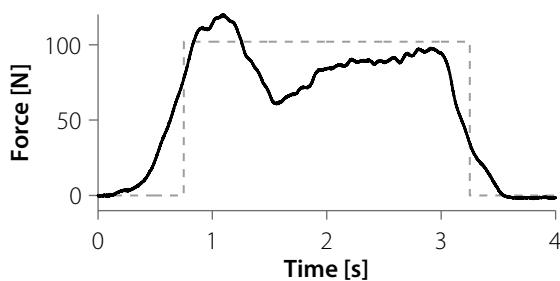


Figure 5.4 Predefined force pattern (dashed line) and exerted force (solid line) as displayed for visual feedback to the subject.

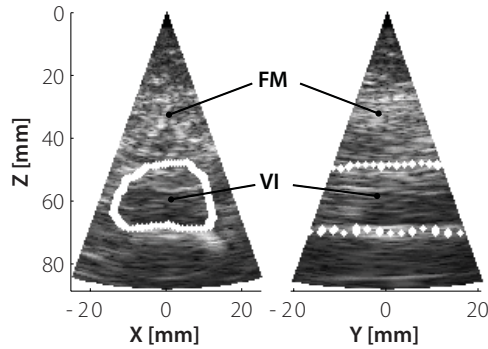


Figure 5.5 B-mode images of two orthogonal planes from the 3D ultrasound acquisition. Left: a cross-sectional plane (orthogonal to muscle). Right: the longitudinal view (aligned with the anatomical sagittal plane). The *m. vastus intermedius* (VI) is located posterior to the *m. rectus femoris* (FM) and was annotated by a trained observer and is indicated by the dashed lines.

5.3 Results

A. Experimental Validation

The rigid translation experiment clearly illustrates the effect of out-of-plane (elevational) motion on the displacement estimation. **Figure 5.6** shows the theoretical axial, lateral and elevational displacement images for the rigid translation experiment and the measured displacement images obtained with the 2D and 3D technique. The displacement images obtained with the 3D technique show good agreement with the theoretical values, whereas the displacement images obtained with the 2D technique show large deviations due to the out-of-plane motion. **Table 5.2** summarizes the RMSE for the two techniques in transducer units (*i.e.* samples) and in millimeters. Axial displacement estimations are converted into millimeters by multiplying with the sampling distance, and lateral/elevational displacement estimations by multiplying with the beam spacing. RMSE values of the 3D technique indicate good performance, as the values are in the sub-sample domain. The 3D technique clearly outperforms the 2D technique with RMSE values of 0.03 mm versus 0.81 mm in axial direction and 0.04 mm versus 0.43 mm in lateral direction. The elevational displacement (restricted for the 2D technique) was resolved by the 3D technique with a RMSE value of 0.09 mm. The axial, lateral and elevational displacement estimations are combined to obtain the displacement in x, y and z-direction (*i.e.* Cartesian space). The Cartesian RMSE values for the 3D technique are summarized in **Table 5.3**, for the 2D technique the displacement in Cartesian space could not be derived (fairly) due to the absence of the elevational component. The rigid translation of 1 mm in the y-direction

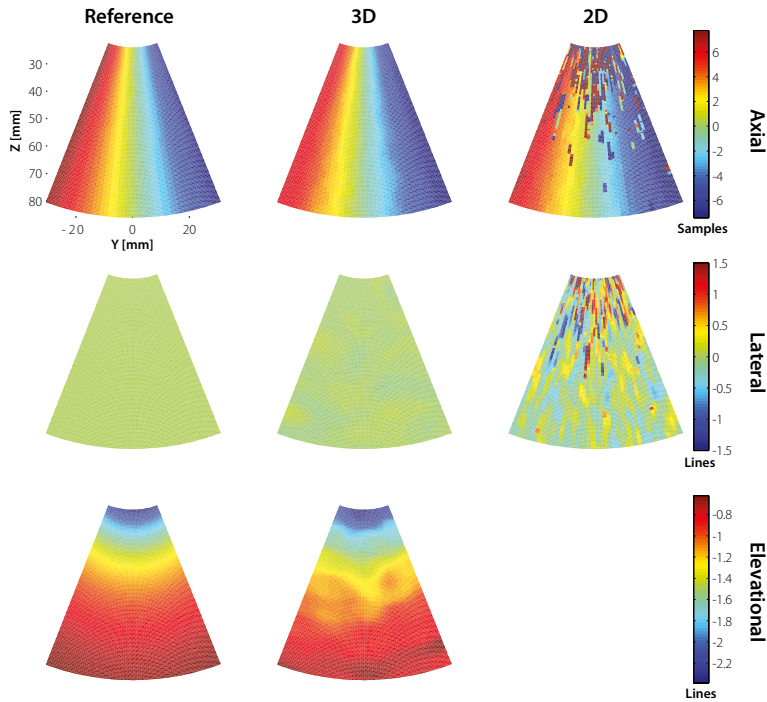


Figure 5.6 Displacement images in transducers units on the central Y-Z image plane from the translation experiment. Left column: reference values, which were theoretically derived. Middle and right column show the displacement images derived from the 3D and 2D technique, respectively.

Table 5.2 Displacement RMSE values in transducer space of the rigid translation of 1 mm along y-axis.		
	2D	3D
<i>Axial displacement error</i>	16.86 [samples] 0.81 [mm]	0.72 [samples] 0.03 [mm]
<i>Lateral displacement error</i>	0.64 [samples] 0.43 [mm]	0.04 [samples] 0.04 [mm]
<i>Elevational displacement error</i>	-	0.09 [samples] 0.10 [mm]

Table 5.3 Displacement and strain RMSE values in Cartesian space for both translation and compression experiments derived with the 3D technique.

	Translation Experiment	Compression Experiment
X displacement error [mm]	0.04	0.11
Y displacement error [mm]	0.09	0.09
Z displacement error [mm]	0.04	0.06
X strain error [%]	-	0.7
Y strain error [%]	-	0.9
Z strain error [%]	-	0.5

was measured using the 3D technique with a RMSE of 0.09 mm. **Figure 5.7** depicts the displacement in y-direction derived from the 3D technique.

Figure 5.8 shows the theoretically axial, lateral and elevational displacement images and the measured displacement images obtained with the 2D and 3D technique for the compressive deformation experiment. To illustrate the effect of out-of-plane motion, the figure depicts the displacement in a plane off-center ($\Phi = 13.83^\circ$), since there is no elevational-motion in the center image plane. Although the amount of out-of-plane motion present in the compressive deformation experiment is smaller than for the rigid translation,

5

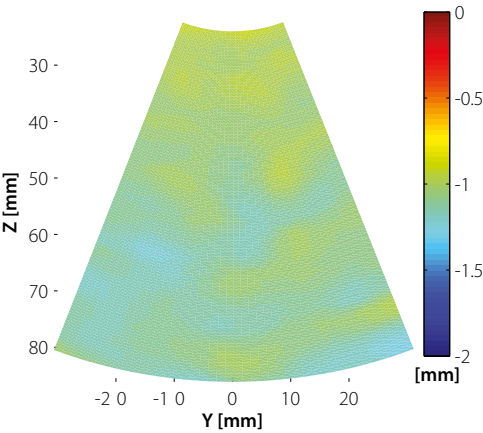


Figure 5.7 Displacement image in y-direction [mm] derived from the 3D technique on the central Y-Z image plane. The rigid translation of 1 mm in the y-direction was measured with a RMSE of 0.09 mm.

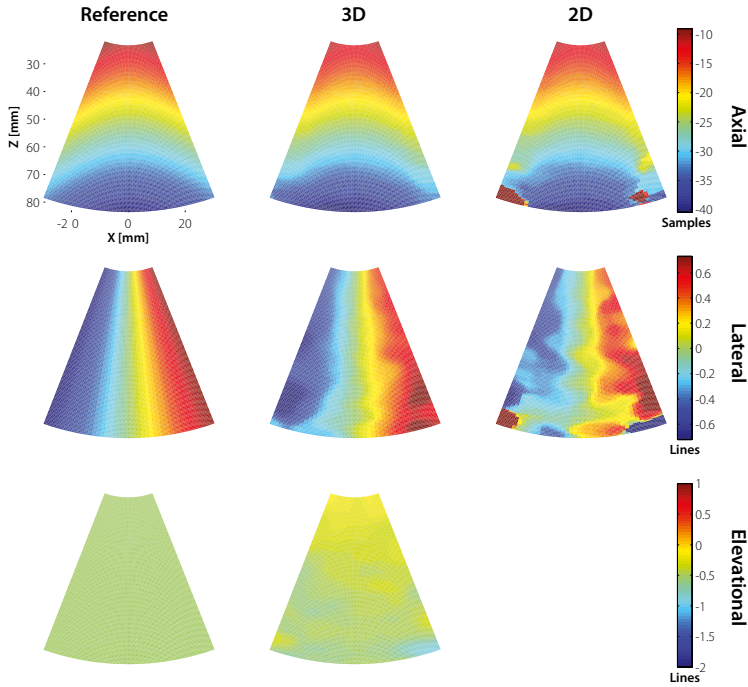


Figure 5.8 Displacement images in transducers units on the Y-X image plane at $\Phi = 13.83^\circ$ from the compression experiment. Left column: reference values. Middle and right column show the displacement images derived from the 3D and 2D technique, respectively.

the performance findings are similar. When using the 3D technique a higher accuracy is achieved with RMSE values of 0.05 mm and 0.11 in axial and lateral direction respectively, compared to RMSE values of 0.35 mm and 0.36 mm using the 2D technique (see also **Table 5.4**). After transformation of the axial, lateral and elevational displacement values to Cartesian space, strain was derived using the LSQSE method. We observed RMSE of the strain values of 0.7%, 0.9% and 0.5% in the x, y and z-direction respectively (**Table 5.3**). The measured displacement and strain images in Cartesian space are shown in **Figure 5.9**.

Table 5.4 Displacement RMSE values in transducer space of the compressive deformation of 2.5mm along the z-axis.

	2D	3D
Axial displacement error	7.33 [samples] 0.35 [mm]	1.04 [samples] 0.05 [mm]
Lateral displacement error	0.28 [samples] 0.36 [mm]	0.11 [samples] 0.11 [mm]
Elevational displacement error	-	0.12 [samples] 0.11 [mm]

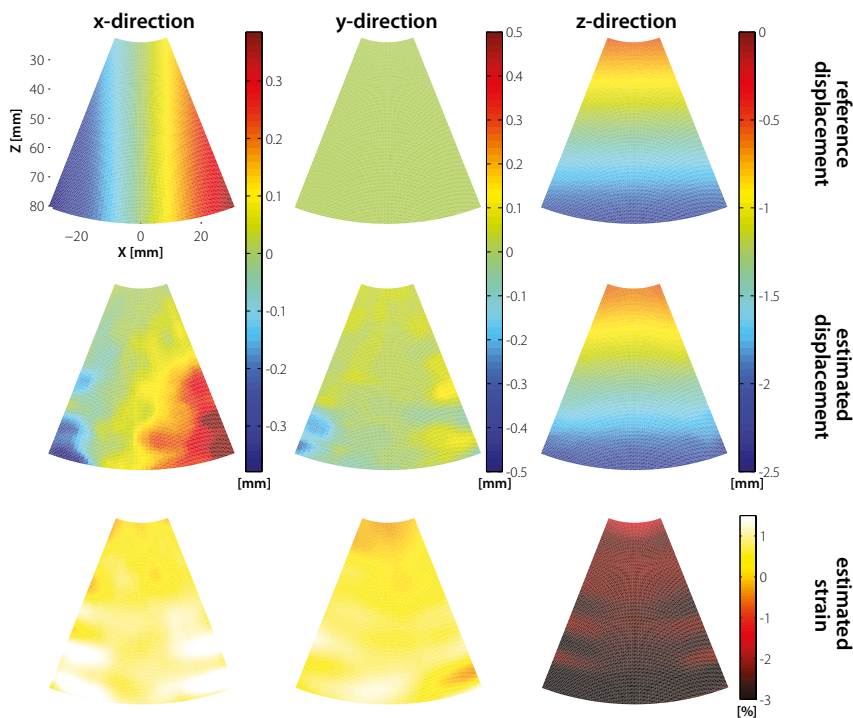


Figure 5.9 Displacement and strain images in Cartesian space. The upper row shows the reference displacement images in x, y and z-direction on the central X-Z image plane. The middle row shows the estimated displacement images and the lower row depicts the derived strain after applying the LSQSE kernel on the displacement images obtained with the 3D technique.

B. In Vivo Application

Figure 5.10 plots the mean strain of the VI muscle in three orthogonal directions during the voluntary contraction at 30% MVC for both measurements. The strain in x-direction (ϵ_{xx}) is the horizontal strain in the cross-sectional view. The strain in the y-direction (ϵ_{yy}) is the horizontal strain in the longitudinal view (along the contraction direction). The strain in the z-direction (ϵ_{zz}) is the vertical strain (see also **Figure 5.11**). Since we studied an isometric contraction, the shortening of the muscle is limited. Therefore, the strain in y-direction is low with a maximum mean strain of -7%. The strain curves in the x- and z-direction show a good resemblance to the predefined force shape. Contracting the muscle results in increased thickness (bulging) of the muscle, which is represented by the strain in z-direction. The thickness of the muscle increased approximately 20% during the contraction. In the x-direction we observe a negative mean strain value, with a maximum value of -12%. The deformation of the muscle is different in all three directions, which illustrate the complexity of the deformation. The reproducibility of the voluntary contraction is indicated by the similarity of the strain curves for the two measurements. **Figure 5.11** depicts strain in z-direction in the cross-sectional and longitudinal view and visualize the local strain distribution within the muscle. We can observe a fairly homogeneous distribution of the strain at the plateau of 30% MVC.

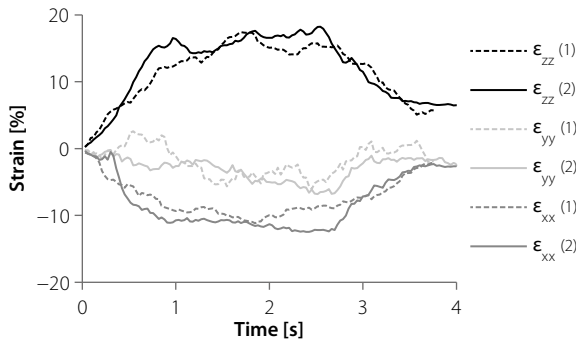


Figure 5.10 Strain curves (experiment in duplo) of the VI muscle in three orthogonal directions during an isometric contraction at 30% of MVC. The strain in the horizontal strain in the cross-sectional view, ϵ_{xx} . The strain in the horizontal strain in the longitudinal view (along the contraction direction) ϵ_{yy} . And the strain in the vertical direction (thickness of the muscle) ϵ_{zz} .

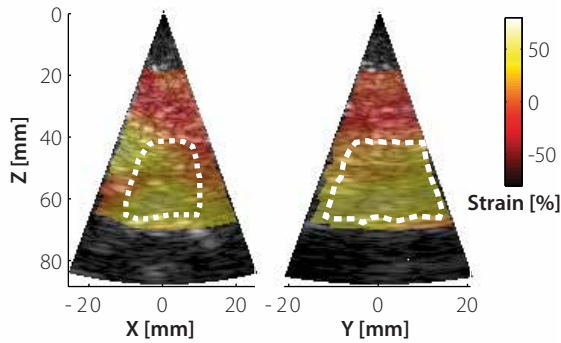


Figure 5.11 Strain images in the center cross-sectional and longitudinal view. Here an example of the strain in z-direction during the plateau phase of the contraction is visualized. The dashed lines indicate the ROI in the m. vastus intermedius.

5.4 Discussion

Three-dimensional ultrasound imaging enables the quantitative measurement of complex tissue motion. Three-dimensional imaging has shown to be a valuable tool to quantify tissue motion, especially when there is motion in three directions, which results in out-of-plane motion for 2D techniques. In this study the performance of a 3D based strain imaging technique was experimentally evaluated and compared to a 2D based technique. An important observation of this study is the good agreement of displacement and strain estimation in z-direction with the theoretically predicted values, but a relatively high RMSE for the x- and y-direction. This is probably caused by the relatively low line density and non-equidistant line spacing of the used transducer. Luo et al. [14] showed that a smaller pitch and a wider beam width reduces the error of the lateral displacement estimation. He also showed that spline interpolation of the RF data (as implemented in this study) improves the lateral displacement estimation. Additionally, the conversion from displacements in the transducer coordinate system to Cartesian coordinates reduces performance of the displacement estimation even further [19]. These factors could also explain the noisy strain curves in the y-direction of the *in vivo* demonstration. Since we studied an isometric contraction, the strain in y-direction (along the contraction direction) was expected to be low, but errors in the inter-frame displacement estimations are accumulated during tracking of the tissue. Theoretically the strain curves should return to zero after contraction, but tracking errors also may explain the drift we observe in the strain curves. Additional regularization may help overcome this problem. Further improvement of the strain results could be accomplished by means of re-correlation techniques [20].

Overall, the results indicate that the use of 3D ultrasound data to estimate tissue deformation outperforms the use of 2D data. Please note that for the results, obtained by the 2D displacement method, 2D data (single planes) were selected from the 3D datasets acquired with the matrix array transducer. This transducer has lower spatial resolution (*i.e.* lower sampling frequency and line density) than dedicated transducers for 2D acquisition. Furthermore, it is debated whether multi-dimensional kernels are applicable, valid and beneficial when diverging line data are used [21, 22]. It is therefore interesting for future studies to quantitatively compare the performance of displacement estimation using a matrix array transducer and a linear array transducer.

The use of phantoms to validate displacement algorithms can be discussed, as the behavior of phantoms cannot be controlled perfectly. Hence, errors in the displacement estimation could be a result of small heterogeneities in the phantom or incorrect experimental conduct. Furthermore, the physical properties of a phantom are of great importance; the speed of sound and the stiffness of the phantom must be controlled to ensure correct boundary conditions for the theoretical calculations. To this extent, in this study much care was taken to construct the tissue mimicking phantom. In general, the resulting ultrasound images and displacement estimations suggest that the phantom experiments were conducted properly without any notable artifacts and the resulting displacement estimates thus provide good insight in the performance of both methods.

The results of the *in vivo* study of the *m. vastus intermedius* show that the 3D algorithm can measure deformations of human muscles in the leg. To our knowledge this is the first study that reported full 3D ultrasound strain imaging of skeletal muscles. Muscle thickness increased during the voluntary contraction, which was also reported by Akima et al [23]. Interestingly, the inverse pattern of muscle thickness change in the *m. vastus intermedius* was reported by Li et al [18]; they observed a reduction in muscle thickness during contraction. Due to different techniques and acquisition locations on the muscle, comparing the studies is difficult. The limitation of the present study is the measurement of one subject and should be realized on other participants.

Studying voluntary contractions may be less reproducible compared to electric stimulated contractions, but are more comfortable and carry fewer practical issues. Furthermore, voluntary contractions can be performed in virtually any skeletal muscle and represent more natural functional behavior. The *m. vastus intermedius* was chosen because of its good accessibility for ultrasound imaging. Superficial to the *m. vastus intermedius* lays the *m. rectus femoris* which was also visible in the ultrasound data, but due to the small image sector at that depth it moves out of the image plane rapidly.

Ultrasound strain imaging provides information of global and local deformation and could be of use in musculoskeletal studies on force transmission. It may be a complementary diagnostic technique as a measurement of function in several myopathic disorders, such as: muscular dystrophies, mitochondrial and metabolic myopathies or immune and inflammatory myopathies. Further research is needed to understand the link between

muscle excitation, force and strain in more detail. For further verification and validation of the measured strains and its relation to muscle functioning, EMG (electromyography) and magnetic resonance techniques will be included in future studies.

Concluding, the present study investigated the feasibility of a 3D strain estimation method in skeletal muscles during an isometric voluntary contraction. The method was experimentally evaluated and showed good performance. Additionally, displacement and strain estimation results using 3D ultrasound segments are more accurate than estimation using 2D segments. Application of the 3D technique *in vivo* is feasible and results in high quality strain images. The method was able to track 3D motion of the tissue in 3D space and enabled the measurement of local deformation.

Acknowledgements

The research leading to these results has received funding from the European Research Council under the European Union's Seventh Framework Programme (FP/2007-2013) / ERC Grant Agreement n. 323091 awarded to N. Verdonschot.

References

1. Dresner, M.A., et al., *Magnetic resonance elastography of skeletal muscle*. Journal of Magnetic Resonance Imaging, 2001. **13**(2): p. 269-276.
2. Giles, L.S., et al., *Can ultrasound measurements of muscle thickness be used to measure the size of individual quadriceps muscles in people with patellofemoral pain?* Phys Ther Sport, 2015. **16**(1): p. 45-52.
3. Affagard, J.S., P. Feissel, and S.F. Bensamoun, *Measurement of the quadriceps muscle displacement and strain fields with ultrasound and Digital Image Correlation (DIC) techniques*. IRBM, 2015. **36**(3): p. 170-177.
4. Hicks, J.L., et al., *Is my model good enough? Best practices for verification and validation of musculoskeletal models and simulations of movement*. J Biomech Eng, 2015. **137**(2): p. 020905.
5. Grubb, N.R., et al., *Skeletal muscle contraction in healthy volunteers: assessment with Doppler tissue imaging*. Radiology, 1995. **194**(3): p. 837-842.
6. Eranki, A., et al., *A novel application of musculoskeletal ultrasound imaging*. J Vis Exp, 2013(79): p. e50595.
7. Witte, R.S., et al. *High Resolution Ultrasound Imaging of Skeletal Muscle Dynamics and Effects of Fatigue*. 2004. Proc. IEEE Ultrasonics Int. Conf., Montreal, Canada.
8. Lopata, R.G., et al., *Dynamic imaging of skeletal muscle contraction in three orthogonal directions*. J Appl Physiol (1985), 2010. **109**(3): p. 906-15.
9. Deffieux, T., et al., *Assessment of the mechanical properties of the musculoskeletal system using 2-D and 3-D very high frame rate ultrasound*. IEEE Trans Ultrason Ferroelectr Freq Control, 2009. **55**(10): p. 2177-2190.
10. Lopata, R.G., et al., *Three-Dimensional Cardiac Strain Imaging in Healthy Children Using RF-Data*. Ultrasound in Medicine and Biology, 2011. **37**(9): p. 1399-1408.
11. Farron, J., T. Varghese, and D.G. Thelen, *Measurement of Tendon Strain During Muscle Twitch Contractions Using Ultrasound Elastography*. Ieee Transactions on Ultrasonics Ferroelectrics and Frequency Control, 2009. **56**(1): p. 27-35.
12. Lopata, R.G., et al., *Performance evaluation of methods for two-dimensional displacement and strain estimation using ultrasound radio frequency data*. Ultrasound Med Biol, 2009. **35**(5): p. 796-812.
13. Luo, J., W.N. Lee, and E.E. Konofagou, *Fundamental performance assessment of 2-D myocardial elastography in a phased-array configuration*. IEEE Trans Ultrason Ferroelectr Freq Control, 2009. **56**(10): p. 2320-7.
14. Luo, J. and E.E. Konofagou, *Effects of various parameters on lateral displacement estimation in ultrasound elastography*. Ultrasound Med Biol, 2009. **35**(8): p. 1352-66.
15. Lopata, R.G.P., et al., *Comparison of One-Dimensional and Two-Dimensional Least-Squares Strain Estimators for Phased Array Displacement Data*. Ultrasonic Imaging, 2009. **31**(1): p. 1-16.
16. Madsen, E.L., et al., *Tissue mimicking materials for ultrasound phantoms*. Medical physics, 1978. **15**(5): p. 391-394.
17. Hodges, P.W., et al., *Measurement of muscle contraction with ultrasound imaging*. Muscle Nerve, 2003. **27**(6): p. 682-92.
18. Li, J., et al., *The sensitive and efficient detection of quadriceps muscle thickness changes in cross-sectional plane using ultrasonography: a feasibility investigation*. IEEE J Biomed Health Inform, 2014. **18**(2): p. 628-35.
19. Zahiri Azar, R., O. Goksel, and S.E. Salcudean, *Sub-sample displacement estimation from digitized ultrasound RF signals using multi-dimensional polynomial fitting of the cross-correlation function*. IEEE Trans Ultrason Ferroelectr Freq Control, 2010. **57**(11): p. 2403-20.
20. Lopata, R.G., et al., *Performance of two dimensional displacement and strain estimation techniques using a phased array transducer*. Ultrasound Med Biol, 2009. **35**(12): p. 2031-41.
21. Langeland, S., et al. *A parametric study on processing parameters for two-dimensional cardiac strain estimation: an in vivo study*. Proc. IEEE Ultrasonics Int. Conf., Rotterdam, The Netherlands.
22. Kaluzynski, K., et al., *Strain rate imaging using two-dimensional speckle tracking*. IEEE Trans.Ultrason.Ferroelectr. Freq.Control, 2001. **48**(4): p. 1111-1123.
23. Akima, H. and A. Saito, *Inverse activation between the deeper vastus intermedius and superficial muscles in the quadriceps during dynamic knee extensions*. Muscle Nerve, 2013. **47**(5): p. 682-90.

6

Computer aided detection of fasciculations and other movements in muscle with ultrasound: development and clinical application

Authors

Kaj Gijsbertse, Max A. Bakker, André M.J. Sprengers, Juerd Wijntjes, Saskia Lassche, Nico Verdonchot, Chris L. de Korte and Nens van Alfen

In press

Journal of Clinical Neurophysiology

Abstract

In patients suspected of amyotrophic lateral sclerosis, fasciculations are important indicators for the diagnosis. Up to now, the presence of fasciculations in ultrasound images is routinely performed online by observing the live ultrasound video image, whereas offline analysis of ultrasound videos is sometimes used for research purposes. However, observation of video images by a human operator limits the objective information gained from the data. It is expected that automated detection of motion in combination with more detailed information on the properties of the motions leads to improved sensitivity and will also improve intra- and inter-operator agreement on the presence of fasciculations.

In this study we present the development of an automatic algorithm for the detection of muscle tissue movement present in ultrasound data. We use a stepwise process of identifying any movement, feeding back this information to human observers, and then further refining the differentiation of the movements based on their specific parameters in an iterative learning process. A data-set (10 ultrasound recordings) including a variety of neuromuscular conditions and targeted muscles was analyzed with the proposed method and compared to manually identified motions by experienced clinicians.

The results showed that the algorithm is capable of reliable motion detection in ultrasound image sequences. Guided by the algorithm, observers found more fasciculations compared to visual analysis alone. This might improve the reliable and early detection of movements indicating a diagnosis of neuromuscular disease. Additionally, other types of movement were also detected. We calculated physiologic features of these movements, to serve as input for subsequent machine learning techniques that can fully automate both the detection and classification of intramuscular movement with ultrasound.

6.1 Introduction

Muscle ultrasound imaging is an increasingly important addition to the diagnostic arsenal for diagnosing neuromuscular disease, providing an anatomical assessment of muscle structure to complement standard neurological examination and electrophysiologic function testing [2]. In addition to its well-known advantages of being patient-friendly, non-invasive and a bedside applicable imaging technique, also the dynamic nature of ultrasound images as a result of the high temporal resolution enables visualization of spontaneous or voluntary muscle movements, including fasciculations.

Fasciculations are spontaneous contractions of a group of muscle fibers innervated by a single motor axon (*i.e.* one motor unit). They can be physiologic in certain muscles under specific circumstances (such as calf fasciculations after sports activities), but in the context of clinical symptoms they are often a sign of motor neuron or peripheral nerve pathology. Since the Awaji modification of the El Escorial criteria for amyotrophic lateral sclerosis (ALS), fasciculations are an important clue to confirm the involvement of the peripheral nervous system in patients with suspected ALS [4]. In ALS, ultrasound has a consistently higher detection rate of fasciculations compared to clinical examination (*e.g.* visual inspection) or electromyography (EMG) [5-7].

However, visual detection of such brief muscle contractions within ultrasound image sequences by a human observer is time consuming and subjective, resulting in under-detection and unwanted intra- and inter-observer variation [8, 9]. To overcome these limitations, computer-aided techniques have been introduced for automated image interpretation. Only one previous study has reported on the application of computer-aided techniques in the detection of fasciculations [12]. The authors proposed an optical flow technique to quantify muscle motion and calculate mutual information, to measure the interdependence of the motion and discriminate between muscle twitches (*e.g.* fasciculations) and muscle tissue at rest. They found good agreement between manual and computational detection of muscle twitches in two different muscles (biceps brachii and medial gastrocnemius). However, not all twitches in muscle tissue observed during ultrasound are fasciculations. Other tissue movements caused by voluntary contractions of small parts of a muscle (including contraction pseudotremor, which is the isolated contraction of enlarged, neurogenic motor units during slight antigravity movement), muscle fibrillation after denervation, vascular pulsations, and imaging artefacts such as probe motion or scatter artefacts close to bony surfaces. For the purpose of helping the clinician to detect and quantify fasciculations, automated ultrasound analysis should not only detect, but also discriminate fasciculations from these other types of muscle ultrasound movements. To do this, physiologic information on the specific characteristics of these different types of motion is required to distinguish between the different observed movements in the ultrasound data.

Using a human observer as the gold standard for detection of a specific type of movement in an ultrasound video is potentially prone to error, especially when many simultaneous movements are present in the real-time image flow, as human observation and interpretation will select some features for its attention, but will ignore others. To overcome this, observers would need to selectively look at every image region (or pixel, ideally) in a frame-by-frame approach, which is expected to be more accurate, but is also very time consuming and unsuitable for routine clinical evaluation of an ultrasound study. However, initially such a frame-by-frame evaluation is necessary in a certain image set, to develop/train an automated detection algorithm.

In this study we introduce a computationally cheap frame-work for the automatic detection of motion within ultrasound images sequences. We take the first steps of an iterative process that starts with human observation, then compare the results to automated detection of any image motion using an ultrasound background subtraction-based method, feed this information back to the human observer who next selectively evaluates every movement detected in a frame-by-frame visual analysis. With this approach, we provide physiologic information of the detected motions that might be used to classify the different detected events. In this paper, we show that this approach can detect fasciculations (*i.e.* has sensitivity), and is potentially able to differentiate fasciculations from other movements (*i.e.* has specificity), paving the way towards automatic classification, or machine learning.

6.2 Methods

A. Clinical and ultrasound data collection

This retrospective study retrieved a set of 42 ultrasound image sequences (*i.e.* videos) from 11 patients seen at the neuromuscular outpatient clinic of the Radboud university medical center (**Figure 6.1**, step A). As the study protocol only involved the post-hoc review of anonymized data that had been captured during routine clinical care, no ethics approval was deemed necessary for this study. Patients had been referred for the workup of different neuromuscular disorders, such as suspected myopathy, unexplained myalgia and fatigue, unexplained extremity or axial weakness, suspected motor neuron disease, and hereditary polyneuropathy. The ultrasound videos were retrieved from different muscles. Patient characteristics and muscles studied can be found in **Table 6.1**. All ultrasound examinations were performed on an Esaote MyLab Twice system (Esaote, Genoa - Italy), equipped with a 3-13 MHz broadband linear transducer (LA533), using a standard pre-set and image parameters described earlier [13]. Image depth was set at 4 cm for all muscles except the rectus femoris, for which the depth was set at 6 cm. For every acquisition, 30 seconds of ultrasound video were recorded from the relaxed muscle, using a framerate of 20 Hz. All ultrasound data were initially scored by experienced clinicians (JW, NvA, SL);

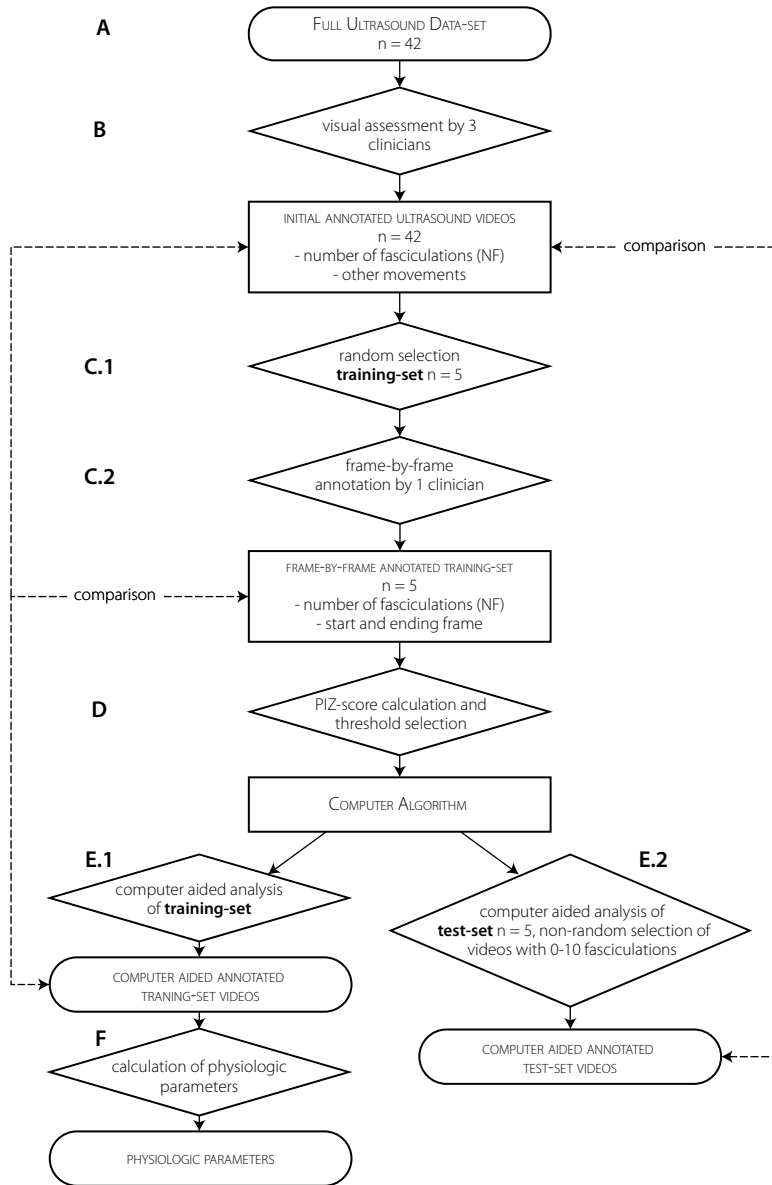


Figure 6.1 Flow-chart of described methods. The process starts with human observation of a large ultrasound database (A-B), next a selection and frame-by-frame annotation of a training set (step C) to develop a computer algorithm for automated detection of movements (step D) and the evaluation of the algorithm with the training and test-set (step E.1 and E.2). Finally, physiologic parameters for the different muscles were extracted from the training set (step F).

Table 6.1 All patient data

Participant	Sex	Age at exam	Diagnosis	Examined muscles
#1	Male	62	amyotrophic lateral sclerosis	<u>biceps brachii L</u> ^{T4} rectus femoris R masseter R flexor carpi radialis R first dorsal interosseous L
#2	Male	74	amyotrophic lateral sclerosis	rectus femoris R,L
#3	Male	64	amyotrophic lateral sclerosis	medial gastrocnemius L <u>tibialis anterior R</u> ^{T1} first dorsal interosseous L
#4	Female	12	focal inflammatory neuropathy	flexor carpi radialis R medial gastrocnemius R,L
#5	Female	53	lumbosacral radiculopathy	masseter R rectus femoris L <u>medial gastrocnemius L</u> ^{TR4}
#6	Male	54	rigid spine myopathy	<u>medial gastrocnemius L</u> ^{TR3}
#7	Female	9	hereditary motor and sensory neuropathy type 4c	medial gastrocnemius L ^{T3} tibialis anterior L
#8	Male	64	progressive spinal muscular atrophy	flexor carpi radialis R <u>first dorsal interosseous L</u> ^{TR2} medial gastrocnemius R,L <u>rectus femoris R</u> ^{T5}
#9	Male	58	cramp fasciculation syndrome with S1 radiculopathy	<u>first dorsal interosseous R,L</u> ^{TR1}
#10	Male	41	myalgia and exercise intolerance, no underlying neuromuscular disorder found	medial gastrocnemius R tibialis anterior L flexor carpi radialis L
#11	Male	47	reinnervated muscle, no underlying neuromuscular disorder found	geniohyoid masseter R <u>flexor carpi radialis R</u> ^{T2} <u>rectus femoris R,L</u> ^{TR5} tibialis anterior L sternocleidomastoid R medial gastrocnemius R,L

TR = training-set, I = test-set

see below **Figure 6.1**, step B). To develop the algorithm (section D), a training set of 5 videos was selected from the available videos by the main researcher (KG; **Figure 6.1**, step C.1; also see **Table 6.2**) to include a variation of image sequences that contained few, some or many movement events. Subsequently, another subset consisting of 5 videos was selected to test the developed algorithm *i.e.* test-set (**Figure 6.1**, step E.2; also see **Table 6.3**). More details of the selection of the data-sets are provided in their corresponding section; see below section C and section E.

Table 6.2 Training-set patient data

Participant	Muscle	Heckmatt-score	Initial number of fasciculations
Training #1	first dorsal interosseous L	1	6
Training #2	first dorsal interosseous L	1	3
Training #3	medial gastrocnemius L	2	13
Training #4	medial gastrocnemius L	1	3
Training #5	Rectus femoris L	1	3

Table 6.3 Test-set patient data

Participant	Muscle	Heckmatt-score	Initial number of fasciculations
Test #1	tibialis anterior R	3	4
Test #2	flexor carpi radialis R	1	0
Test #3	medial gastrocnemius L	3	1
Test #4	biceps brachii L	2	0
Test #5	rectus femoris R	1	1

B. Observer study

For the initial scoring of the videos (see **Figure 6.1**, step B), the ultrasound image sequences were visually assessed by three experienced neuromuscular clinicians: 2 clinical neurophysiologists (NvA, JW) and one neuromuscular fellow (SL). The clinicians were asked to state whether fasciculations were present or not in the image sequences, and to count the total number of fasciculations (NF) during the 30s video. Any other present movement, such as vascular pulsation, probe motion artefacts or voluntary muscle

contraction, were scored by the observers as well. Muscle echogenicity was assessed from the ultrasound videos, and scored semi-quantitatively by using the Heckmatt grading scale [14]. This scale represents a visual grading of muscle echogenicity which corresponds to changes in muscle tissue architecture such as fibrosis and fatty degeneration, with the rating scale as follows: 1-normal, 2-mildly increased muscle echoes with normal bone reflection, 3- moderately increased muscle echoes with reduced bone reflection, 4-severely increased muscle echoes with absent bone reflection.

C. Training set for algorithm development

To develop the algorithm, a subset of 5 ultrasound image sequences (30s epochs of 600 frames each) was randomly selected to obtain a training-set (**Figure 6.1**, step C.1 and **Table 6.2**). The training-set comprised three different muscles (dorsal interossei, gastrocnemius, rectus femoris) that had a Heckmatt-score of either 1 or 2. One clinical observer (NvA) marked the time frames in which fasciculations occurred in this training set by using a frame-by-frame visual analysis (**Figure 6.1**, step C.2). This resulted in labeled example data, which we used to develop and optimize our detection algorithm for the detection of fasciculations (see section D and **Figure 6.1**, step D). These initially found fasciculations were later compared to the number of fasciculations found with the help of the developed algorithm to evaluate its performance.

D. The algorithm for automatic detection of movement

Our motion detection method (implemented in Matlab, MathWorks Inc., Natick, MA, USA) comprised a modified background subtraction (or frame-difference) method, which is a frequently used step in many optical motion capturing systems [15]. By subtracting static background from an image sequence, static areas will cancel out to zero revealing the non-zero areas where motion has occurred. In ultrasound applications this method has for example been applied to remove vascular wall tissue movements from image sequences, which enhances the remaining signal of blood in the ultrasound images for blood flow estimation [16].

To detect movement, we subtracted the background image from the contiguous image sequence. The background image at every time point t was computed by averaging a series of images (double sided window size = 31 frames). Subsequently, the difference image was divided by the standard deviation of the image within the same time series. This results in a measure that yields the extent of pixel intensity variability (PIZ-score, see **equation 6.1**) which is the equivalent of the z-score of pixel intensity and represents tissue motion (see also **Figure 6.2** and **Figure 6.3**).

$$PIZ(m, n, t) = \frac{|f(m, n, t) - \bar{f}(m, n, t)|}{s(m, n, t)}, \quad (\text{eq. 6.1})$$

where f is the image intensity value and s the standard deviation of the intensity value. With m and n the pixels indices in x and y -direction, and t the time frame.

To cluster pixels into event regions, *e.g.* regions of the ultrasound image with suspected motion, the PIZ values were 2D Gaussian smoothed ($\sigma = 10$ pixels) and connected in space and time using 3D flood filling with an empirical derived PIZ score of 1.5. Pixels without noteworthy signal (*i.e.* $\bar{f}(m, n, t) < 30$) or that have a low variation (*i.e.* $s(m, n, t) < 5$) were ignored. The maximum of the PIZ for every time point converts the 2D+t image information into a 1-D signal. The magnitude of that signal represents the likelihood of an ultrasound frame containing motion. Based on the first analysis of the training-set a threshold PIZ of 1.5 was chosen to include all fasciculations identified by the clinical observers (see **Figure 6.1**, step D and **Figure 6.4**) and to establish future detection of clinical evident fasciculations by the algorithm.

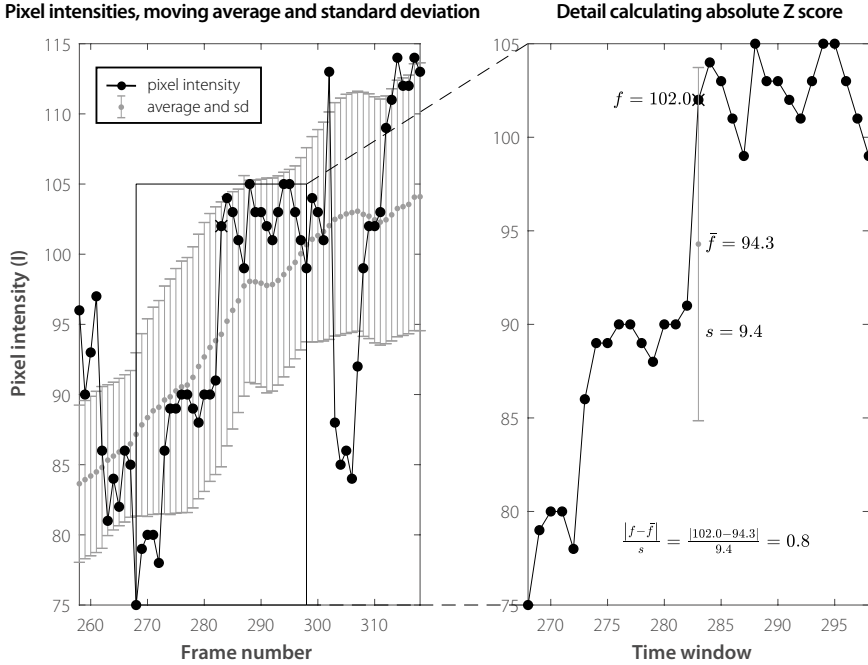


Figure 6.2 Calculation of the standardized pixel intensity variation (PIZ-score). For each pixel over time (m, n, t), the background (moving average within time window,) was subtracted from the intensity (I) value and divided by the standard deviation.

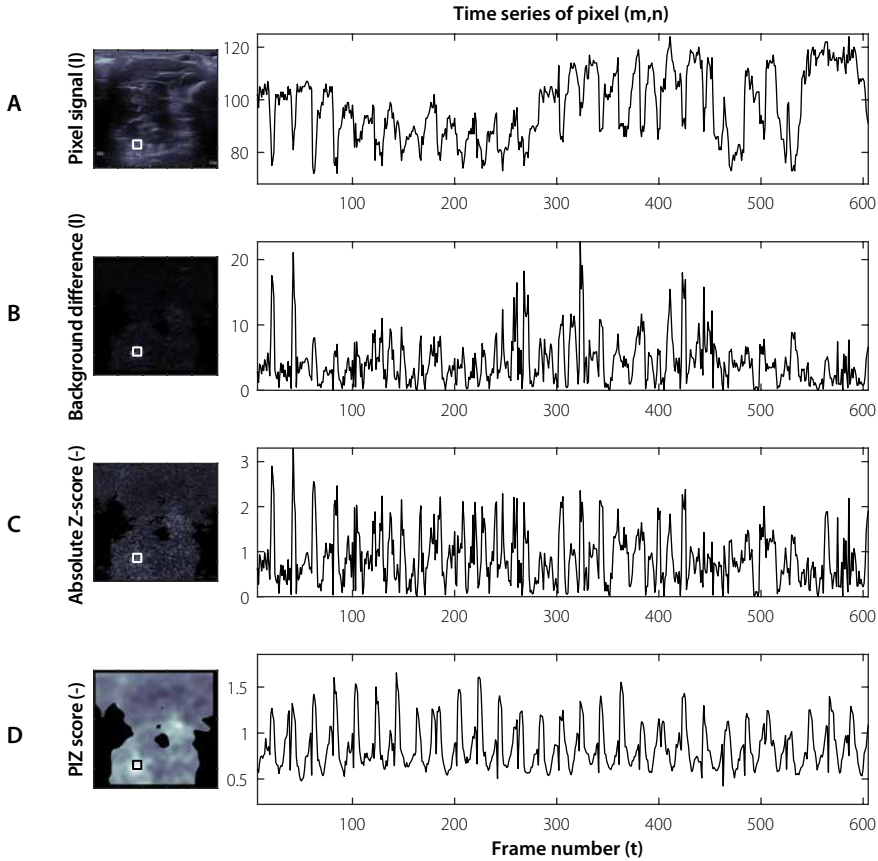


Figure 6.3 Calculation of standardized pixel intensity variation (PIZ-score) to detect motion in ultrasound videos. **A)** Shows the pixel intensity, or gray scale representation of the ultrasound data. **B)** Shows the result after (static) background subtraction and **C)** the result after dividing by the standard deviation. The PIZ-scores are filtered and clustered resulting in **D)**. Please note that the pixel (m, n) was selected inside a region where vascular pulsation was visible resulting in the periodic PIZ-score signal.

E. Computer aided detection of fasciculations

The algorithm developed in step D was next tested on the training-set, to assess whether the clinician had missed any fasciculations in the manual annotation (see **Figure 6.1-E.1**), and on five additional ultrasound sequences (the test-set) to evaluate the performance of the algorithm on unfamiliar data *i.e.* data not used to ‘train’ the algorithm (see also **Figure 6.1-E.2**). The test-set comprised five muscles (biceps brachii, flexor carpi radialis,

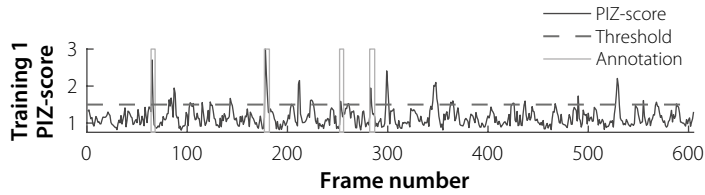


Figure 6.4 Example of manually annotation of fasciculations for an ultrasound sequence from the training-set and the derivation of the pixel intensity variation (PIZ-score). The black line represents the maximum PIZ-score of the entire image over time, a threshold of 1.5 was chosen to include all 4 manually annotated fasciculations (gray vertical lines). When the PIZ-score value exceeds the threshold, the motion was classified as a movement event.

rectus femoris, tibialis anterior, gastrocnemius) with Heckmatt-scores between 1 and 3 (see **Table 6.3**). The test-set contained manually selected ultrasound sequences with low fasciculations severity scores, and also included videos without the presence of fasciculations, which allowed us to test if our algorithm did not miss any ‘critical’ cases *i.e.* the absence of fasciculations that would alter a diagnosis.

The outcome of the algorithm consisted primarily of a number of movement events for each ultrasound video. Every image was next divided into 25 areas, numbered as seen in **Figure 6.5** to further guide the clinical observers. For every movement event, the corresponding time frame and location within the ultrasound image were recorded, and presented to the clinical observer, who then specifically evaluated these frames in the video to classify the events into the following categories: fasciculations, voluntary contractions, contraction pseudotremor (*i.e.* slight antigravity contraction of one or a few enlarged motor units), vascular pulsations, image artefacts, or any other movement type. The results of the algorithm-guided clinical annotation were compared to the initial visual annotation by the clinicians (see **Figure 6.1**, step E) to detect any differences.

F. Physiologic parameters

Besides fasciculation, the ultrasound videos also contained other movement types, as expected. To enable automatic classification of these movements and separate them from the fasciculations detected, we aimed to extract parameters informed by (physio)-logic properties, such as frequency of occurrence, duration and the extent of tissue involved in the motion (see **Table 6.4**). Therefore, for every detected movement event in the training-set we calculated the following five parameters:

1. *Duration (# frames)*: The number of ultrasound frames that correspond to a detected event.
2. *Area (# pixels, mm²)*: The number of pixels that are involved in a detected event and the area they cover.

3. *Occurrence*: The average of instances the pixels within the event are involved in the total number of detected events.
4. *Periodicity (f)*: For every pixel within the event we compute the power spectrum of the *PIZ* signal. The average of the maxima of the power spectra represents the periodicity. We searched for the maximum within the expected normal range of frequencies for the heart rate (50-120 bpm).
5. *Concurrent global deviation (l)*: The average of for all pixels of the entire image frame corresponding to the detected event. This measure represents the amount of surrounding motion.

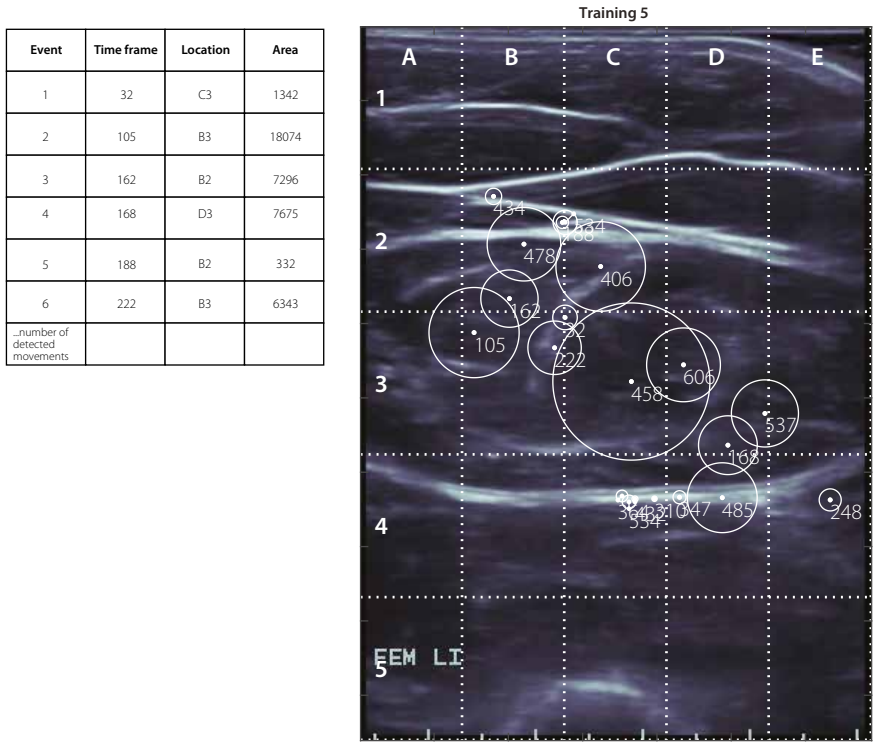


Figure 6.5 Presentation of the outcome of the developed motion detection method for video #5 from the training-set. The movement events were listed with their corresponding time frame, location and area. Additionally, an ultrasound frame was presented with the events annotated with circles and a time frame stamp, where the radius of the circles represented the involved area of the event.

Table 6.4 Motion events and physiologic parameters

Phenomenon	Periodicity	Tissue area involved in motion	Spatial predictability	Duration	Physiology
<i>Fasciculations</i> ^{a,b}	Irregular, < 4 Hz	estimated 1-5 mm diameter	random	~0.25s	Single axon hyperexcitability discharge with contraction of the motor units' muscle fibers. Can occur simultaneously.
<i>Contraction pseudotremor</i> ^c	(pseudo) rhythmic crescendo or decrescendo rate, 5-10 Hz	estimated 1-5 mm diameter	predictable	~0.1s	Denervation
<i>Vascular pulsation</i>	50-120 Bpm, 0.83-2 Hz	2-10 mm diameter	highly predictable, local		Vascular pulsation
<i>Probe motion</i>	unpredictable	affects entire image, 0.5- 2 cm	predictable, affects entire image	n/a	Operator artefact
<i>Fibrillations</i> ^d	regular, > 5 Hz	estimated 0.1-0.3 mm diameter	predictable, local	50-100 μ s	Denervation
<i>Voluntary contraction</i>	irregular	several cm, depending on muscle	whole muscle outline		Voluntary muscle movement

^a : de Carvalho and Swash [1]^b : Conradi, Grimby [3]^c : Riggs, Gutmann [10]^d : Preston and Shapiro [11]

6.3 Results

In this section, we first present the outcomes of the manually and guided annotation of fasciculations in the training-set (**Figure 6.1**, step E.1) and subsequently test-set of ultrasound image sequences (**Figure 6.1**, step E.2). Secondly, we present the physiologic features we calculated for every motion event (**Figure 6.1**, step F).

A. Manual versus computer algorithm-guided fasciculation detection

Table 6.5 summarizes the outcomes of the manually and algorithm-guided detection of fasciculations. The initial manually annotated number of fasciculations (NF) in the training-set ranged between $NF = 1$ and $NF = 6$ within an ultrasound image sequence, with a total of $NF = 19$ for all videos. When the observer subsequently reviewed the ultrasound sequences again with guidance of the movement events listed by our algorithm, more fasciculations were found, with a total NF of 49. The total difference between manually and algorithm-guided annotation within the training-set was 30, and ranged between 0 and 14 per video of the training-set. **Figure 6.6** shows that all manual annotated fasciculations were found, except for one fasciculation event that was annotated as a contraction pseudotremor in the algorithm-guided evaluation.

Of note, the number of manual (frame-by-frame) annotated fasciculations in training video #3 had a very wide range between the observers from the initial visual screening: from 13 to 1. These movements were classified as contraction pseudotremor in the frame-by-frame annotation. With the aid of the computer algorithm the number of detected fasciculations again increased, to 15. This indicates that there is a considerable effect of observer-variability possibly related to the presence of contraction pseudotremor.

From the original 600 frames per video in the training-set, only a fraction of the data (145 movement events from 3000 frames, or ~5%) needed to be reviewed to classify the automatically detected motion events, depending on the number of detected events, which were 29 on average and ranged between 20 and 39 per video for the fasciculations combined with all other movements. Especially contractions, both voluntary but also contraction pseudotremor, were observed in almost every recording, and resulted in additional detected events besides fasciculations.

For the ultrasound image sequences from the test-set, we observed a global decrease in annotated fasciculations with the help of the computer algorithm (see also **Table 6.5**). Initially the observers annotated a total of $NF = 6$ in all videos of this test-set, whereas with the computer guidance fewer fasciculations were annotated $NF = 4$. The difference between manually (initial scoring) and computer guided annotation within this test-set was within the range of: -3 and 1. We observed that the decrease of total number of fasciculations found was the result of a single video (test #1), in which some of the fasciculations occurred in the same region as a contraction pseudotremor and were not

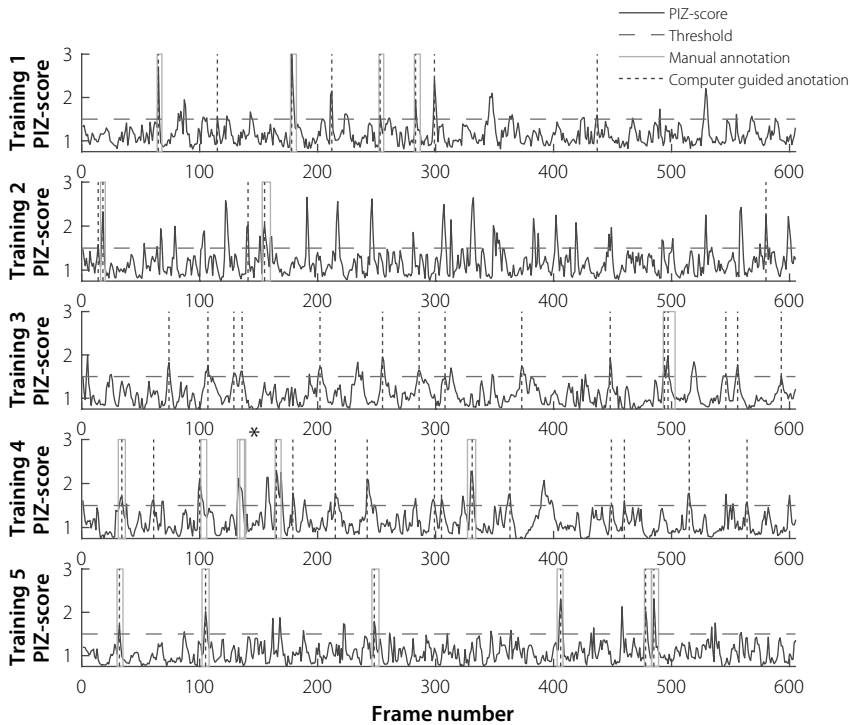


Figure 6.6 PIZ-score (standardized pixel intensity variation) for five ultrasound sequences within the training-set. Motion events were detected when this score exceeded the threshold of 1.5 (horizontal dashed line). The gray solid lines represent the manually annotated fasciculations (start and end frame), and the dashed vertical lines represent the computer guided annotated fasciculations. The manual frame-by-frame annotation identified 19 fasciculations, whereas with the guidance of the computer algorithm 49 fasciculations were found. The asterisk (*) indicate the missed fasciculation by the algorithm.

detected as a result of large pixel variation over time in that area (*i.e.* a high standard deviation in the image sequence results in low PIZ-score). The number of fasciculations in the other videos were correctly found or increased similar to the results of the training-set. The total number of automatically detected movement events was 44 (out of 3000 frames, or 1.5%) and showed that there were less movements in the videos within the test-set compared to the training-set. On average the videos in the test-set contained 9 movements, with the number of movement events ranging between 5 and 11. Consequently, clinicians had to review fewer frames in these videos compared to the videos in the training-set.

Table 6.5 Manual and computer guided annotations of fasciculations					
Data	Initial manual count	Frame by frame count of Fasciculations	Computer guided count of Fasciculations	Total automatically detected events/ movement	Other motion observed
Training #1	6	4	8	29	vascular pulsation, contractions, contractions pseudotremor
Training #2	3	2	5	39	contractions, contractions pseudotremor, probe motion
Training #3	13	1	15	25	probe motion, contractions, pseudotremor
Training #4	3	6	15	32	probe motion, vascular pulsation, contractions pseudotremor
Training #5	3	6	6	20	probe motion, vascular pulsation
Training-set (total)	28	19	49	145	
Test #1	4	-	1	9	contractions pseudotremor, vascular pulsation
Test #2	0	-	0	11	probe motion, vascular pulsation
Test #3	1	-	1	8	contractions
Test #4	0	-	0	5	contractions, probe motion
Test #5	1	-	2	11	vascular pulsations, probe motion
Test-set (total)	6	-	4	44	
Please note that the values presented in the second column are the same as presented in Tables 6.2 and 6.3 .					

B. Physiologic parameters of detected movements

Figure 6.7 illustrates the average values of the parameters of duration, area, occurrence, periodicity and surrounding motion for every classified movement event from the training-set (see also **Figure 6.1**, step F). Duration and area were not found to distinguish between fasciculations and other movement events. Occurrence reflects the repetitive behavior of events and was highest for contractions pseudotremor with an average value of 11.4 ± 3.7 times. In other words, pixels within the region of a pseudotremor contraction were involved in 11.4 additional detected movement events in the video (most likely another pseudotremor contraction). Vascular pulsations were clearly recognizable with the use of the periodicity parameter, which had the highest average value of 5.9 ± 5.2 (power, I^2). Motions that were classified as artefacts, were frequently caused by probe motion, and these events showed the largest pixel intensity variation for the entire image 6.9 ± 6.3 (I).

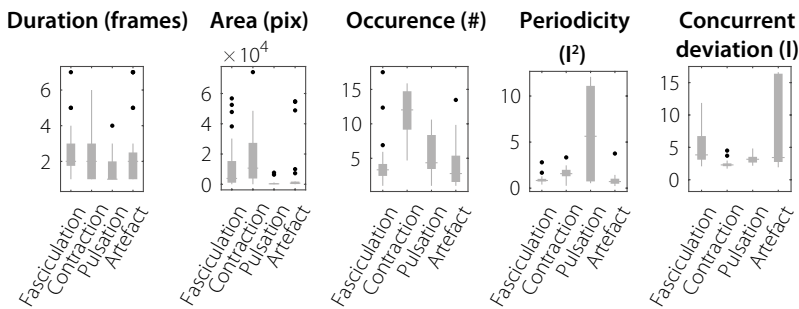


Figure 6.7 Physiologic parameters per categorized motion event; the average duration, area, occurrence, periodicity and concurrent global deviation are depicted for all classified events in the training-set.

6.4 Discussion

In this study we developed the first steps of an algorithm for the automatic detection and specification of motion in muscle ultrasound image sequences acquired during clinical practice. We found that the algorithm found all manual detected fasciculations in the test-set, except for three fasciculations in one challenging video, indicating a high level of accuracy; 4/5 videos in the-test were correctly annotated with the help of the algorithm. This makes an automated approach an attractive method to objectively screen for the presence of fasciculations in muscle ultrasound videos, and confirms the findings of a previous study by Harding et al. [12].

Using the algorithm, clinicians were able to detect more fasciculations than using offline visual analysis alone, and the use of the algorithm to prescreen the videos could save clinicians time that would have been needed to review the full ultrasound video. There were in total 189 movement events found by the algorithm in the training and test-set combined (6000 frames total), depending on the number of frames required to investigate a movement event, this will save considerable time. For instance, when 10 frames are required to investigate a movement event this will lead to a time reduction of approximately 70% ($189 \text{ events} \times 10 \text{ frames} / 6000 \text{ frames}$). This shows that computer-guidance may also be an attractive approach for fasciculation detection that will help improve sensitivity and saves a considerable amount of time for the human observer.

Furthermore, with help of the algorithm combined with revision by the clinician, the ultrasound videos consistently were found to contain additional movements, especially repetitive contractions of single motor units (either voluntary or anti-gravity contraction). These movements can potentially confound the visual analysis of muscle ultrasound videos, especially when it is performed online. The movements were found to have specific characteristics that would tell them apart from each other. Using the computer algorithm, enhanced with a standard detection method for these features, is expected to give good detection accuracy and prevent confounding of the different movements, thus improving specificity of the muscle ultrasound video analysis.

The analysis of the test-set indicate that the algorithm is capable of coping with the large variability of ultrasound data that exist in clinical examinations. It included acquisitions from different muscles of patients with varying diseases and disease stages. Although there was a good agreement between the number of fasciculations found, it is unclear if the automatically detected events included the originally annotated fasciculations, since we only have the number of fasciculations and not the starting frames within the test-set. The algorithm failed to present all fasciculations to the observer in one of the test-set recordings (test#1). A thorough inspection of this data revealed that the missed fasciculations occurred at the location of a pseudotremor, which confounds the automated detection by presenting a high level of background movement in a certain image area. Further research is required to optimize the algorithm for this sort of challenging data. Further, certain confounding movements, such as contraction pseudotremor or anti-gravity contractions can be prevented by making sure the patient is completely relaxed during the examination.

Agreement between observers has been shown to be influenced by the number of fasciculations present in the data being analyzed; fewer fasciculations corresponds to lower agreement [12]. Consequently, a comprehensive evaluation of the algorithm on the test-test is difficult since the initial annotations were scored by different observers. Additional studies on the reliability of the algorithm should include a more comprehensive collection of ground-truth data, such as the collection of EMG data and data on intra/inter-observer variability.

The additional physiologic data extracted from the ultrasound movement events in this study indicate these parameters can be used to discriminate fasciculations from other types of motion. Vascular pulsation events showed highest periodicity values and can be excluded using this information. Additionally, probe motion artefacts might be discarded using the average pixel variation of the entire image. To improve the computer-aided detection, the physiologic data can be displayed as an overlay over the ultrasound images to help the observer in the classification (see **Figure 6.8**). Ideally, these parameters are incorporated in a machine learning algorithm, such as a random-forest classifier or neural network, for fully automatic detection and classification. The feasibility of using machine learning for this application will be studied in future work. This requires further investigation of the variability of the derived parameters/features. For example, the magnitude of the periodicity will be affected negatively by probe motion. Therefore, it might be important to have more strict requirements of ultrasound recordings and acquisition protocols to prevent unnecessary difficulties in the image processing. Furthermore, the method could be optimized for each specific muscle, since it might be the case that other parameters are optimal for different muscles.

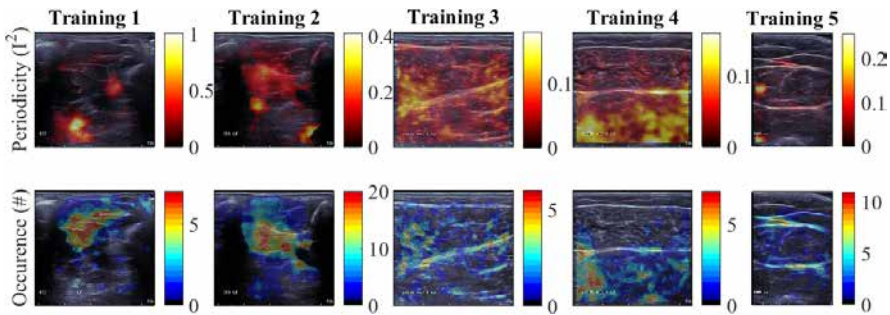


Figure 6.8 Possible presentation of physiologic parameters to further guide observers in the classification of motion events. Upper row depicts the periodicity (power of spectrum) for five ultrasound image sequences and reveal the locations of vascular pulsation. The lower row depicts the occurrence-map of events and indicates occurrence *i.e.* how often a pixel/region is involved in motion events.

The method proposed for automated fasciculation detection is a computationally cheap (*i.e.* fast) alternative for other motion detection techniques such as optical flow [12]. However, the proposed method is not capable of quantifying motion. Additional information, such as the characterization of the motion pattern may help distinguish between fasciculations and other involuntary contractions. For example, myokymia appears as “brief but sustained, tractive movements” of the muscle, which contrasts with

the brief rotary muscle movements that are typical for fasciculations [2]. Our method may be used as a pre-processing step to detect ultrasound frames that contain motion, and subsequently, extract quantitative information of the tissue motion using optical flow or speckle tracking [17, 18]. Further exploration of the use of the proposed algorithm will include its potential for detecting other biomarkers in neuromuscular diseases, such as myokymia or fibrillations.

In conclusion, the findings above confirm the potential clinical usefulness of an automated approach to movement analysis in muscle ultrasound videos. The derived additional physiologic features together with quantitative techniques have the potential to improve diagnosis and may lead to fully automatic classification of motions in neuromuscular diseases.

References

1. de Carvalho, M. and M. Swash, *Fasciculation potentials: a study of amyotrophic lateral sclerosis and other neurogenic disorders*. Muscle Nerve, 1998. **21**(3): p. 336-44.
2. Simon, N.G., *Dynamic muscle ultrasound - Another extension of the clinical examination*. Clin Neurophysiol, 2015. **126**(8): p. 1466-7.
3. Conradi, S., L. Grimby, and G. Lundemo, *Pathophysiology of fasciculations in ALS as studied by electromyography of single motor units*. Muscle Nerve, 1982. **5**(3): p. 202-8.
4. Geevasinga, N., et al., *Awaji criteria improves the diagnostic sensitivity in amyotrophic lateral sclerosis: A systematic review using individual patient data*. Clin Neurophysiol, 2016. **127**(7): p. 2684-91.
5. Grimm, A., et al., *Muscle ultrasonography as an additional diagnostic tool for the diagnosis of amyotrophic lateral sclerosis*. Clin Neurophysiol, 2015. **126**(4): p. 820-7.
6. Misawa, S., et al., *Ultrasonographic detection of fasciculations markedly increases diagnostic sensitivity of ALS*. Neurology, 2011. **77**(16): p. 1532-7.
7. Regensburger, M., et al., *Detection radius of EMG for fasciculations: Empiric study combining ultrasonography and electromyography*. Clin Neurophysiol, 2017.
8. Pillen, S., et al., *Muscles alive: ultrasound detects fibrillations*. Clin Neurophysiol, 2009. **120**(5): p. 932-6.
9. Reimers, C.D., et al., *Fasciculations: clinical, electromyographic, and ultrasonographic assessment*. J Neurol, 1996. **243**(8): p. 579-84.
10. Riggs, J.E., L. Gutmann, and S.S. Schochet, Jr., *Contraction pseudotremor of chronic denervation*. Arch Neurol, 1983. **40**(8): p. 518-9.
11. Preston, D.C. and B.E. Shapiro, *14 - Basic Electromyography: Analysis of Spontaneous Activity*, in *Electromyography and Neuromuscular Disorders (Third Edition)*. 2013, W.B. Saunders: London. p. 220-234.
12. Harding, P.J., et al., *Ultrasound-Based Detection of Fasciculations in Healthy and Diseased Muscles*. IEEE Trans Biomed Eng, 2016. **63**(3): p. 512-8.
13. Scholten, R.R., et al., *Quantitative ultrasonography of skeletal muscles in children: Normal values*. Muscle & Nerve, 2003. **27**(6): p. 693-698.
14. Heckmatt, J.Z., S. Leeman, and V. Dubowitz, *Ultrasound imaging in the diagnosis of muscle disease*. J Pediatr, 1982. **101**(5): p. 656-60.
15. Ramya, P. and R. Rajeswari, *A Modified Frame Difference Method Using Correlation Coefficient for Background Subtraction*. Procedia Computer Science, 2016. **93**: p. 478-485.
16. Jin, D. and Y. Wang, *Doppler ultrasound wall removal based on the spatial correlation of wavelet coefficients*. Medical & Biological Engineering & Computing, 2007. **45**(11): p. 1105-1111.
17. Gijsbertse, K., et al., *Ultrasound Imaging of Muscle Contraction of the Tibialis Anterior in Patients with Facioscapulo-humeral Dystrophy*. Ultrasound Med Biol, 2017. **43**(11): p. 2537-2545.
18. Gijsbertse, K., et al., *Three-dimensional ultrasound strain imaging of skeletal muscles*. Phys Med Biol, 2017. **62**(2): p. 596-611.

7

Summary and general discussion

The work in this thesis describes the development and application of ultrasound-based methodologies to assess the functional behavior of muscles, tendons and ligaments within the musculoskeletal system. Ultrasound is an excellent technique to assess the deformation of tissues. Due to its high spatial and temporal resolution, this deformation can be quantified with high accuracy. In cardiology, ultrasound-based speckle tracking is a well-established technique to assess myocardial deformation. However, for musculoskeletal imaging, these techniques were not fully explored yet. In this thesis, new techniques have been developed to quantify muscle deformation, as well as deformation of ligaments. Additionally, a technique to detect fasciculations and other muscle movements in ultrasound data has been developed and applied to clinical data. This functional information increases our fundamental understanding of muscle function and can be of potential use as a follow up biomarker in neuromuscular diseases. Moreover, it aids in the regeneration, optimization and validation of biomechanical models that can be used to optimize surgery and functional outcome of the patient. This chapter summarizes and discusses the main findings of the research performed in this thesis and outlines future perspectives related to dynamic ultrasound imaging of the musculoskeletal system.

7.1 Summary

Accurate quantitative information on strain in ligaments is needed to detect abnormalities in muscular disorders and improve our understanding of injury mechanisms. Clinicians can use this information to assess the biomechanical status of tissue and to study changes in longitudinal studies. From a biomechanical perspective, this information is useful to generate and validate patient-specific models. **Chapter 2** describes the results of ultrasound strain imaging in lateral collateral ligaments *ex vivo*. The goals were to investigate the performance of ultrasound strain imaging in small structures and to explore the potential benefits of high frequency ultrasound (>20 MHz) compared to conventional ultrasound (~7 MHz). Therefore, an experimental set-up was designed that allowed for axial stretching of the ligaments whilst ultrasound and digital image data could be recorded concurrently. The ligaments were stretched up to 5% strain and ultrasound measurements were compared to surface strain measurements from optical digital image correlation (DIC) techniques. The results showed good correlations between ultrasound based and DIC based strain measures with R^2 values of 0.71 and 0.93 for high frequency and conventional ultrasound, respectively. This study demonstrated that ultrasound strain imaging is feasible in *ex vivo* lateral collateral ligaments, which are relatively small structures. Although the use of high frequency ultrasound was expected to be beneficial when studying superficial structures because of the increased spatial resolution, this study showed that high frequency imaging was found to be inferior to conventional ultrasound-based measurements. A possible explanation for this phenomenon

might be the smaller elevational beam width in high frequency imaging, which makes the technique more sensitive to out-of-plane motion, resulting in tracking errors. Since this study was performed in a well-controlled *ex vivo* experiment, additional studies should be designed for a more informed assessment of optimal *in vivo* strain measurements in collateral knee ligaments.

After strain imaging of passively stretched ligaments we focused on actively contracting muscles. The deformation pattern of muscles is complex and depends on muscle architecture and its (pathological) condition. To study how pathological muscles contract and transmit force, we applied 2D speckle tracking to quantify the deformation of the tibialis anterior muscle in patients with fascioscapulohumeral dystrophy (FSHD) and compared it to healthy muscle deformation in **Chapter 3**. The results showed that the deformation pattern of muscles with abnormal echogenicity is different from that of healthy or only mildly affected muscles without ultrasound abnormalities, possibly related to the decreased amount of muscle tissue available for contraction and force transduction. Severely affected muscles showed decreased motion of the central tendon aponeurosis, which suggests a decrease in force transferred to this tendon and thus a diminished force output. Furthermore, the resulting deformation patterns showed good agreement with clinical outcome measures, muscle echogenicity values, and maximum exerted force. This dynamic information provides insight in the pathophysiological mechanisms and may help to distinguish the different stages of diseased muscle in FSHD and follow disease progression.

Since the deformation of a muscle is depending on its architecture such as fiber direction, we developed an algorithm in **Chapter 4** that allowed to analyze muscle contraction concurrently with muscle fiber orientation in 2D. Our method combined ultrasound strain imaging, to measure muscle deformation, with a local Radon-transformation based technique to automatically detect the fiber orientation. This method was tested in eight healthy volunteers during an isometric contraction of the tibialis anterior muscle. The results revealed a spatially heterogeneous pattern of strain development that increased during contraction. The principal shortening direction deviated from the fiber direction as was also shown by MR studies [1]. With ultrasound we were able to measure this relation spatially and over time and the results showed that this deviation was large ($\sim 45^\circ$) at the beginning of the contraction and converged to $\sim 30^\circ$ for higher strain levels at the plateau of the contraction phase. This study supports the current consensus that the relation between muscle fiber direction and contraction direction is complex and adds to the quantitative characterization of this dynamic relation during contraction.

To fully characterize the complex 3D deformation of muscle, a 3D strain measurement method is required. Therefore, in **Chapter 5**, we developed a 3D ultrasound strain imaging technique. The performance of this 3D technique was experimentally validated in a phantom study and compared to 2D strain estimation. Furthermore, the feasibility of *in vivo* 3D strain estimation of the quadriceps muscles during voluntary contraction was explored. The results of the phantom study showed good performance of the 3D

technique and showed to reduce errors as a result of out-of-plane motion compared to the 2D technique. Although the technique has high accuracy in axial direction, the performance of 3D strain imaging in the lateral and elevational direction was limited as a result of diverging ultrasound beams in the phased-array matrix transducer. Application of the 3D technique *in vivo* is feasible and the method was able to track 3D motion of the tissue in 3D space. This allowed for measurement of local deformation, where the thickening of the muscle showed good resemblance with the measured force.

Finally, in **Chapter 6**, we presented the development and application of an algorithm towards automatic detection and classification of spontaneous movements (e.g. fasciculations) in ultrasound recordings. We used a stepwise process of identifying any movement, feeding back this information to human observers, and then further refining the differentiation of the movements based on their specific parameters in an iterative learning process. The results showed that the algorithm is capable of reliable detection of movement of tissue in ultrasound image sequences. With the guidance of the algorithm, observers found more fasciculations compared to subjective annotation, which might improve reliable and early diagnosis of neuromuscular diseases. Many other movements were also detected, for which we calculated physiologic features that might serve as input for subsequent machine learning techniques to fully automate the detection and classification of intramuscular movement with ultrasound.

7.2 General discussion

The set-ups, ultrasound image processing and analysis techniques as described in this thesis allow for the functional assessment of soft tissues in the musculoskeletal system. Ultrasound strain imaging enables quantification of tissue deformation *in vivo* and thus provides information on muscle contraction and force transmission. With this approach, healthy and pathologic tissue functioning can be differentiated as it may reveal individual or combined contribution of different tissues to altered deformation patterns or pathological loading conditions in muscular disorders. For example, patellofemoral pain or excessive lateral patellar tracking may be due to dysfunction of the *musculus vastus medialis* or its opposing muscle, the *musculus vastus lateralis*. Additionally, the medial patellofemoral ligament (MPFL) plays an important role in patellar stability. With ultrasound strain imaging it would be possible to directly assess differences in muscle functioning or the biomechanical status of the MPFL and their role in patellofemoral pain. Similarly, knee instability may be a result of ligamentous insufficiency (e.g. tear, weakening) and is a major cause of early total knee arthroplasty failures. Also, for patients suffering from varus or valgus knee deformities, the deformation in the collateral ligaments may not be physiological. In order to quantify these abnormalities ultrasound strain imaging can be used to assist surgeons and researchers.

Insights in the activation patterns or the way different muscles are contributing to certain tasks lead to a comprehensive understanding of musculoskeletal functioning. Ultrasound provides a non-invasive and easily accessible technique to assess soft tissue deformation and this thesis shows the feasibility of making this technique available for the clinic to assess the biomechanical status of tissue. However, the feasibility to assess the function of ligaments *in vivo* remains challenging as a result of their small size in combination with complex loading and deformation patterns. In musculoskeletal modeling, information of the deformation of tissue may be incorporated into biomechanical models and provide additional insights of musculoskeletal functioning at a subject-specific level. Furthermore, the measurement of morphological parameters from ultrasound data can be used in biomechanical modeling to reduce the unknown parameters during the optimization process [2].

Strain measurements can be performed concurrently with other biomechanical techniques, such as joint kinematics from motion capture techniques, electromyography for timing of muscle activation and force plates for ground reaction force. Integration of these complementary techniques could lead to a better understanding of dynamic muscle function and the underlying mechanisms in musculoskeletal diseases.

For accurate performance of the presented ultrasound-based techniques there are several technical and clinical considerations, ranging from transducer properties, data-acquisition, post-processing and interpretation. **Chapter 3**, **Chapter 4** and **Chapter 5** describe methods to quantify muscle deformation *in vivo* during isometric contractions. Isometric contractions are easily applicable and reproducible and therefore allow muscle examination in a controllable way. However, in many daily activities *e.g.* gait, muscle contraction is not isometric, but isotonic (concentric/eccentric). This will most certainly lead to different deformation profiles of muscles and require further performance analysis of the proposed techniques in these dynamic tasks. For example, optimal block-matching parameters for reliable displacement estimation are dependent on the amount of tissue displacement but are often not known a-priori. Furthermore, there are various parameters that affect the accuracy and precision of ultrasound displacement (and consequently strain) estimation. Most importantly the performance depends on the characteristics of the transducer used such as center frequency (band width), beam width and pitch (*i.e.* the distance between transducer elements). Additionally, the lateral displacement of the tissue and interpolation method of the cross-correlation function are parameters that influence the sub-sample performance of displacement estimation. The effect of the pitch on the lateral displacement estimation was found to be larger than the beam width effect for linear array transducers [3]. However, when applying a phased array transducer (**Chapter 5**) the beam spacing is not equal to the pitch and increases with depth. Consequently, the performance of displacement estimation varies spatially and is believed to be better closer to the transducer where the beam spacing is smaller. Choosing the best possible equipment for the expected deformation is therefore important. Moreover,

an important limitation in ultrasound lateral displacement/strain estimation is the lower resolution and lack of phase information in this direction. These challenges might be resolved using additional methods, such as line interpolation [3], displacement compounding [4] or transverse oscillation [5]. The line interpolation approach was applied in our 3D strain estimation method (**Chapter 5**), but the benefit of other approaches may be explored in the future to improve lateral (and elevational) displacement/strain estimation.

The manner in which muscle contracts or functions depends on its architecture or morphology. These architectural parameters such as pennation angle and strain/thickening of the muscle change during muscle contraction, which can be measured with ultrasound. However, the relationship between the architectural changes is not linear with force output [6, 7], consequently muscle deformation cannot directly be translated to muscle force. Furthermore, strain is a relative measure and when derived from ultrasound images it depends on the orientation of the ultrasound image. Therefore, for quantitative assessment and comparison to other functional data such as force output, muscle activation derived from EMG or resulting motion, placement of the transducer relative to the anatomy is an important consideration. These aspects need to be evaluated prior to quantify muscle activity based on ultrasound strain measurements. The combination of ultrasound strain imaging and fiber orientation can help elucidating the relation between muscle architecture and function. It is commonly assumed in many musculoskeletal models that muscles shorten along their longitudinal axis and expand radially. However, the results of **Chapter 4** and **Chapter 5** indicate that this general assumption is not necessarily true and muscle deformation is complex and might vary depending on the type of contraction (*e.g.* isometric, isotonic, or isokinetic) and surrounding or connecting tissue. It is fascinating how muscle architecture and co-contractions permit skeletal muscle to function effectively over a wide range of tasks. With the help of ultrasound imaging techniques, the distinct mechanisms of different contractions and muscle architecture can be further illuminated.

The evaluation of muscle morphology and the way muscles contract and transmit force is important for understanding the working mechanism of healthy muscles as well as muscles in neuromuscular disorders. Muscles affected by diseases, such as FSHD, experience architectural changes due to fat infiltration and muscle tissue atrophy, which may be responsible for the decreased lateral force transmission in patients. Morphological parameters such as fascicle length and fascicle orientation are used in biomechanical modeling to estimate the force-generating capacity of muscles [2, 8, 9] and to quantify muscle functioning for addressing research questions and for clinical diagnosis [10-12]. Besides morphological parameters, quantification of deformation (strain) of muscles during activities provides additional insights in the way healthy or pathological muscles contract and transmit force (**Chapter 3**). With the proposed methods it is possible to quantitatively characterize the relationship between muscle deformation and the

underlying architecture *in vivo* (**Chapter 4**). Yet, it is unclear how the proposed methods perform in patients with neuromuscular disease. Most techniques are validated for healthy volunteers and a limited number of patients, and since the force production or the appearance of pathological tissue may differ compared to healthy tissue, these techniques may encounter difficulties or may not work at all for severely affected patients. Alternatively, other ultrasound-based approaches may be suitable for the assessment of the biomechanical properties of soft tissues within the musculoskeletal system. For example, shear wave imaging provides a direct estimate of the elastic modulus of the tissue without the requirement of dynamic loading conditions. Shear wave elastography employs an acoustic radiation force impulse (*i.e.* push pulse), or a mechanical vibration device to evoke a shear wave. The applied push pulse results in a shear wave traveling longitudinally through the muscle. This shear wave induces tissue displacements, which are detected by ultrafast image acquisitions. Subsequently, the shear wave velocity can be derived from the tracked tissue displacement, which can be directly related to the elastic modulus and superimposed in color over the B-mode images. The stiffness value can be measured locally within a region of interest on the shear wave image. Under rigorous laboratory conditions, shear wave elastography of skeletal muscle acquired reliable, real-time, non-invasive, high resolution and quantitative data on the mechanical properties. However, under clinical conditions the reproducibility will most likely be limited. It is known to produce noisy and erroneous results when data is collected close to bones, and a recent study using found shear wave imaging results to be unreliable during *in vivo* collections [13]. Furthermore, shear wave imaging does not allow to study the deformation of tissue under dynamic loading. A combination of shear wave imaging and strain imaging might be a good approach to assess the dynamic as well as the static mechanical properties and thus provide important information for diagnosis but also to feed biomechanical models.

Skeletal muscles are relatively large and require a sufficient imaging field of view to reveal local differences in function. Furthermore, disease progression of many neuromuscular disorders have a distal to proximal nature, and thus requires subsequent studies that quantify muscle contraction along the entire length of the muscle to reveal local differences in contraction patterns related to this disease progression. Therefore, a multi-dimensional imaging modality with a large field of view is needed for a comprehensive mapping of muscle contraction. To increase the field of view, we have applied a transducer with a large footprint of 15 cm (**Chapter 4**) that allowed to image a considerable length of the tibialis anterior muscle in 2D. To extend this approach to 3D, clinical available ultrasound systems scanners (SIEMENS ABVS), that allow to scan large volumes by stacking multiple 2D images, may be used to obtain this information. However, this approach requires repeatable motion to facilitate gated acquisition. In practice, repeatable motions are not feasible or desirable since these may introduce muscle fatigue and also impose practical limitations to the possible activities and patients that can be studied. Although this seems

a cumbersome procedure that prevents widespread clinical use, this might serve as an initial step to demonstrate the value of full 3D strain imaging of muscles.

When studying superficial and small structures, one obvious strategy to increase spatial resolution is to use a high frequency ultrasound system. An increase in frequency decreases wavelength and consequently decreases both beam width (lateral resolution) and pulse duration (axial resolution), at a cost of penetration depth [14]. As a result of increased spatial resolution, a better performance of high frequency ultrasound systems seems evident in strain imaging. However, in **Chapter 2** the high frequency approach was unexpectedly found to be inferior to conventional ultrasound-based measurements. A possible explanation for this phenomenon might be the smaller elevational beam width, which makes the technique more sensitive to out-of-plane motion, resulting in tracking errors. Out-of-plane motion is a fundamental challenge and is the inherent limitation of 2D imaging to evaluate 3D tissue motion. The use of 3D ultrasound (**Chapter 5**) using a real-time 3D matrix array transducer could circumvent this limitation. As discussed, the spatial resolution of this phased array configuration is poor in axial direction (relatively low central frequency) as well as in lateral/elevational direction (lack of phase information, diverging field) and thus the performance of 3D strain imaging remains limited. Additionally, 3D ultrasound imaging comes at the cost of lower temporal resolution which is undesirable when studying fast contracting muscle in highly dynamic tasks such as running or jumping. Nowadays, much effort is put in developments to improve image quality and frame rate. These new techniques are focusing on ultrafast imaging acquisition up to 20.000 Hz, also known as plane-wave imaging, in combination with advanced beam-forming techniques [15]. Furthermore, new transducer technology and materials like capacitive micro-machined ultrasonic transducers (CMUT) [16] will provide large footprint matrix array transducers with a non-diverging field and also the feasibility to perform displacement compounding to improve the lateral/elevational strain estimate in the near future.

The presented studies are explorative studies based on small groups of patients and healthy participants to show the feasibility of the developed techniques or novel applications. In order to get more insight in the reliability and reproducibility, it is important to conduct larger cohort studies. Since the application of ultrasound strain imaging of the musculoskeletal system is relatively new, there is no consensus yet on the data acquisition and analysis that allow researchers and clinicians to evaluate soft tissue deformation in a standardized protocol. Future research should focus on the design of repeatable dynamic exercises in combination with reliable and standardized acquisition protocols. The design of loading devices and the use of force measurements to monitor force variation can help in the repeatability of the dynamic exercises. Additionally, the collection of ground truth data for the cross-validation of the estimated deformation of tissue with other modalities such as MRI or digital image correlation techniques, and the use of *ex vivo* measurements will provide more insight on the reliability of the developed techniques. In addition to

standardization of imaging protocols, future studies should obtain normative values for the parameters derived from dynamic ultrasound imaging. These reference strain values in muscle and other tissue are required to facilitate the discrimination between healthy and pathologic tissue. The collection and sharing of *in vivo* data in a standardized protocol in an open science environment allows researchers and clinicians worldwide to study the musculoskeletal system more effectively with the available tools.

With the collection of standardized data of muscle contraction, models of muscle contraction can be created and used to improve strain estimation techniques. Since the displacement estimations from speckle tracking techniques are prone to errors such as noise, peak-hopping or decorrelation, the final displacement fields need to be regularized to reduce these errors. *A priori* knowledge on tissue motion can be used to regularize the displacement, by fitting the estimated displacements to the expected motion obtained from the muscle contraction model. Consequently, the regularization of displacement estimations may lead to improved tissue tracking and strain estimation.

The application of speckle tracking in neuromuscular patients (**Chapter 3**) and the development of computer aided detection of motion in muscle ultrasound (**Chapter 6**) have shown that quantitative ultrasound techniques are valuable tools that may extend the clinical toolbox for improved diagnosis and disease monitoring of (neuro)muscular diseases. **Chapter 6** showed the potential clinical usefulness of an automated approach to movement analysis in muscle ultrasound videos. The quantitative techniques and additional derived physiologic features of muscle motion will have the potential to improve diagnosis and may lead to fully automatic classification of motions in neuromuscular diseases. Prior to clinical incorporation of these dynamic assessment tools, more clinical experience is needed to gain insight whether specific contraction patterns or fasciculations and other spontaneous muscle movements observed with ultrasound are useful to distinguish between different neuromuscular diseases. Subsequently, these new ultrasound techniques may be used as an extension of the clinical examination toolbox.

A current trend in ultrasound imaging is the development of portable systems that allows us to retrieve functional information of muscles or other soft tissue during daily activities and highly dynamic tasks outside the clinical or scientific setting. This is especially relevant when predicting risks for post-operative loading situations by monitoring the biomechanical status of the tissue with ultrasound techniques. However, these portable systems lack computational power that is required for fast processing of the ultrasound data and retrieve functional information. The trend of increasing processing power and decrease in size and cost of computers will most likely resolve this issue. With deep learning techniques entering the clinical field, complex ultrasound data might be analyzed automatically [17] and provide clinicians or even patients directly, a valuable tool. Especially the combination with ambulant ultrasound systems with 3D acquisition possibilities will boost the applications within the musculoskeletal field that can be applied at the point-of-care or outside the clinic.

In conclusion, ultrasound strain imaging is a valuable tool to study the functional behavior of muscles and ligaments during dynamic loading conditions. This functional information increases our fundamental understanding of muscle function and can be of potential use as a follow up biomarker in (neuro)muscular diseases. Furthermore, this information may be used to obtain reliable biomechanical models that can guide and predict surgical outcomes. Although further research is required towards the collection of ground truth data and thorough validation of *in vivo* tissue deformation, the presented ultrasound techniques are likely to extent the clinical toolbox as they yield pathophysiological insights in the deformation of soft tissue in the musculoskeletal system.

References

1. Englund, E.K., et al., *Combined diffusion and strain tensor MRI reveals a heterogeneous, planar pattern of strain development during isometric muscle contraction*. Am J Physiol Regul Integr Comp Physiol, 2011. **300**(5): p. R1079-90.
2. Hicks, J.L., et al., *Is My Model Good Enough? Best Practices for Verification and Validation of Musculoskeletal Models and Simulations of Movement*. Journal of Biomechanical Engineering, 2015. **137**(2): p. 020905-020905-24.
3. Luo, J. and E.E. Konofagou, *Effects of various parameters on lateral displacement estimation in ultrasound elastography*. Ultrasound Med.Biol., 2009. **35**(8): p. 1352-1366.
4. Hansen, H.H., et al., *Full 2D displacement vector and strain tensor estimation for superficial tissue using beam-steered ultrasound imaging*. Phys Med Biol, 2010. **55**(11): p. 3201-18.
5. Jensen, J.A. and P. Munk, *A new method for estimation of velocity vectors*. IEEE Transactions on Ultrasonics, Ferroelectrics, and Frequency Control, 1998. **45**(3): p. 837-51.
6. Hodges, P.W., et al., *Measurement of muscle contraction with ultrasound imaging*. Muscle Nerve, 2003. **27**(6): p. 682-92.
7. Lopata, R.G., et al., *Dynamic imaging of skeletal muscle contraction in three orthogonal directions*. J Appl Physiol (1985), 2010. **109**(3): p. 906-15.
8. Lieber, R.L., et al., *Skeletal muscle mechanics, energetics and plasticity*. J Neuroeng Rehabil, 2017. **14**(1): p. 108.
9. Marra, M.A., et al., *A subject-specific musculoskeletal modeling framework to predict in vivo mechanics of total knee arthroplasty*. J Biomech Eng, 2015. **137**(2): p. 020904.
10. Lieber, R.L. and J. Friden, *Clinical significance of skeletal muscle architecture*. Clin Orthop Relat Res, 2001(383): p. 140-51.
11. Mohagheghi, A.A., et al., *In vivo gastrocnemius muscle fascicle length in children with and without diplegic cerebral palsy*. Dev Med Child Neurol, 2008. **50**(1): p. 44-50.
12. Li, L., K.Y. Tong, and X. Hu, *The effect of poststroke impairments on brachialis muscle architecture as measured by ultrasound*. Arch Phys Med Rehabil, 2007. **88**(2): p. 243-50.
13. Cortez, C.D., et al., *Ultrasound shear wave velocity in skeletal muscle: A reproducibility study*. Diagn Interv Imaging, 2016. **97**(1): p. 71-9.
14. Shung, K.K., *Ultrasonic Transducers and Arrays*, in *Diagnostic ultrasound : imaging and blood flow measurements*. 2006, CRC Press. p. 39-78.
15. Tanter, M. and M. Fink, *Ultrafast imaging in biomedical ultrasound*. IEEE Trans Ultrason Ferroelectr Freq Control, 2014. **61**(1): p. 102-19.
16. Salim, M.S., et al., *Capacitive Micromachined Ultrasonic Transducers: Technology and Application*. Journal of Medical Ultrasound, 2012. **20**(1): p. 8-31.
17. Cunningham, R.J., P.J. Harding, and I. Loram, *The application of deep convolutional neural networks to ultrasound for modelling of dynamic states within human skeletal muscle*. bioRxiv, 2017.

8

Samenvatting

Samenvatting

Het menselijke spier-skeletstelsel – of bewegingsapparaat – bestaat uit spieren, pezen, ligamenten, botten en kraakbeen. Het is het orgaanstelsel dat ons lichaam steun en vorm geeft maar bovenal ons in staat stelt om te bewegen. Musculoskeletale aandoeningen, zijn klinische problemen die ons bewegingsapparaat treffen. Dit resulteert veelal in pijn, beperking in bewegingsvrijheid, letsel, ziekte en verminderde kwaliteit van leven. Om de diagnose van musculoskeletale aandoeningen te verbeteren, evenals methodologieën om behandelingen en revalidatie te begeleiden, is een fundamenteel en uitgebreid begrip van het functioneren van spieren en andere weefsels zoals ligamenten en pezen belangrijk. Medische beeldvormingstechnieken, waaronder echografie, worden steeds meer gebruikt als aanvullend instrument voor klinisch en elektrofysiologisch onderzoek van het bewegingsapparaat. Echografie is een uitstekende beeldvormingstechniek om de vervorming van zachte weefsels te evalueren, omdat het naast een hoge spatiële resolutie ook beschikt over een hoge temporele resolutie.

Dit proefschrift is gericht op de ontwikkeling en het gebruik van beeldvormingstechnieken op basis van echografie (ultrageluid) om functionele informatie over spieren, pezen en ligamenten in de onderste extremiteiten te verkrijgen. Veelgebruikte technieken in cardiologie zijn ‘speckle tracking’ of ‘strain imaging’, welke gebruikt worden om de vervorming (rek) van het hart gedurende contractie te meten. Echter, de mogelijkheden van deze technieken zijn nog niet volledig onderzocht binnen het domein van musculoskeletale aandoeningen. In dit proefschrift zijn verschillende aspecten onderzocht van het in beeld brengen en meten van vervorming van spieren en ligamenten gedurende bewegingen. Daarnaast is een techniek voor het automatisch detecteren van fasciculaties (spontane spiercontractie in neuromusculaire aandoeningen) en andere spierbewegingen in echografie-opnames ontwikkeld en toegepast op klinische data.

De functionele informatie die deze technieken leveren, vergroot ons fundamentele begrip van het bewegingsapparaat en kan van potentieel nut zijn om neuromusculaire ziektes te detecteren en hun verloop te volgen. Bovendien biedt deze functionele informatie hulp bij de regeneratie, optimalisatie en validatie van biomechanische modellen. Deze modellen kunnen worden gebruikt om ingrepen (bijvoorbeeld chirurgie) en het functionele resultaat van de patiënt te voorspellen en te optimaliseren. Dit hoofdstuk vat de belangrijkste bevindingen van het onderzoek in dit proefschrift samen.

Nauwkeurige en kwantitatieve informatie over de vervorming (rek) van ligamenten is nodig om abnormaliteiten te detecteren en ons begrip over de onderliggende mechanismen van letsel te verbeteren. Clinici kunnen deze informatie gebruiken om de biomechanische status van weefsel te beoordelen en om veranderingen gedurende de aandoening over de tijd te onderzoeken. Vanuit een modellerend perspectief zijn deze gegevens nuttig om patiënt-specifieke modellen te genereren en te valideren. **Hoofdstuk 2** beschrijft de resultaten van rekmetingen met behulp van echografie (ultrasound strain imaging) van

de laterale collaterale ligament (buitenste knieband). Het doel van deze experimenten was om enerzijds de prestaties van echografische bepalingen van de rek in kleine structuren te onderzoeken en daarnaast om de potentiële voordelen van hoogfrequente echografie (> 20 MHz) te onderzoeken in vergelijking met conventionele echografie (~ 7 MHz). Daarom werd een experimentele setup ontworpen die axiale uitrekking van de ligamenten *ex vivo* mogelijk maakte, terwijl echografische- en digitale-beeldgegevens (camera-beelden) gelijktijdig konden worden opgenomen. De ligamenten werden uitgerekt tot 5% rek en echografische bepalingen van de rek werden vergeleken met metingen van de rek aan het oppervlakte van de ligamenten op basis van de camera beelden (digital image correlation; DIC). De resultaten toonden goede correlaties tussen de echografische bepalingen van de rek, en de rek aan de oppervlakte zoals bepaald met behulp van DIC, met R^2 waarden van 0,71 voor hoogfrequente echografie en 0,93 voor conventionele echografie. Deze studie demonstreerde dat rekmetingen met behulp van echografie mogelijk zijn in *ex vivo* laterale collaterale ligamenten, wat relatief kleine structuren zijn. Hoewel verwacht werd dat het gebruik van hoogfrequente echografie gunstig zou zijn bij het bestuderen van deze kleine en oppervlakkige structuren, vanwege de verhoogde spatiële resolutie, toonde deze studie aan dat rekbeoordeling op basis van hoogfrequente echografie inferieur was aan echografie op ultrasound gebaseerde metingen. Een mogelijke verklaring voor dit fenomeen is de smallere bundelbreedte in elevationale richting van hoogfrequente echografie, waardoor deze techniek gevoeliger is voor beweging uit het beeldvlak (out-of-plane motion), wat resulteert in meetfouten. Aangezien deze studie werd uitgevoerd in een goed gecontroleerd *ex vivo* experiment, zijn aanvullende onderzoeken nodig om de prestaties van echografische rekmetingen van de collaterale banden te bepalen.

Na de echografische rekbeoordeling van passief vervormende ligamenten hebben we ons gericht op de vervorming van actief samentrekkende weefsels, de spieren. De manier waarop spieren vervormen gedurende contractie is complex en hangt af van de spier-architectuur en de (pathologische) biomechanische toestand waarin de spier verkeert. Om te bestuderen hoe pathologische spieren samentrekken en kracht doorgeven, hebben we in **Hoofdstuk 3** echografische technieken toegepast om de vervorming van de tibialis anterior spier bij patiënten met fascioscapulohumerale dystrofie (FSHD) te kwantificeren en dit vergeleken met de manier waarop gezonde spieren vervormen. Uit de resultaten bleek dat het vervormingspatroon van spieren met afwijkende echogeniciteit verschilt van die van gezonde of slechts licht aangetaste spieren. Dit is mogelijk gerelateerd aan de verminderde hoeveelheid spierweefsel die beschikbaar is voor contractie en de manier waarop de kracht wordt overgebracht door aangetast weefsel van patiënten. Ernstig aangetaste spieren vertoonden een afname in beweging van de centrale peesplaat in de spier, dit suggereert dat de er minder kracht via deze peesplaat loopt en dus minder kracht kan worden geleverd. De vervormingspatronen, zoals bepaald met echografie, toonden een goede overeenkomst met klinische uitkomstmaten, spier-echogeniciteits-

waarden en maximaal uitgeoefende kracht. Deze dynamische informatie biedt inzicht in de pathofysiologische mechanismen en kan helpen om de verschillende stadia van aangetaste spieren bij FSHD te onderscheiden en de progressie van de ziekte te volgen.

Aangezien de vervorming van een spier afhankelijk is van zijn spierarchitectuur, zoals de oriëntatie van de spiervezels, hebben we in **Hoofdstuk 4** een algoritme ontwikkeld dat het mogelijk maakt om, in 2D, de vervorming van spieren gelijktijdig te analyseren met de spiervezeloriëntatie. Deze methode combineert echografische rekbepaling om spiervervorming (hoofdrekken) te meten, met een techniek die de spiervezelrichting bepaalt aan de hand van lokale Radon-transformaties van de echobeelden. Deze nieuwe methode is getest bij acht gezonde vrijwilligers tijdens een isometrische contractie van de tibialis anterior spier. Gedurende contractie nam de hoofdrekk van de spier toe en de vervorming was heterogeen verdeeld over de spier. De lokale verkortingsrichting van een spier week af van de spiervezelrichting zoals ook eerder werd aangetoond door onderzoeken met behulp van magnetische resonantie (MR). Met behulp van echografie konden we deze relatie gedurende contractie meten en de resultaten toonden aan dat het verschil tussen de verkortingsrichting en de spiervezelrichting groot was ($\sim 45^\circ$) aan het begin van de contractie en convergeerde tot $\sim 30^\circ$ bij grotere vervormingen aan het plateau van de contractiefase. Deze studie ondersteunt de huidige consensus dat de relatie tussen spiervezelrichting en contractierichting complex is. Daarnaast biedt onze methode de mogelijkheid om deze relatie kwantitatief te karakteriseren gedurende contracties.

Om de complexe vervorming van spieren volledig te karakteriseren, zijn rekbepalingen in 3D vereist. Daarom hebben we in **Hoofdstuk 5** een techniek ontwikkeld die de rek in 3D bepaalt op basis van 3D echobeelden. De prestaties van deze 3D-techniek zijn experimenteel gevalideerd in een fantoomstudie en vergeleken met rekbepalingen van de 2D-techniek. Tevens werd de haalbaarheid van 3D rekbepaling *in vivo* onderzocht in de quadriceps-spieren van een gezonde vrijwilliger. De resultaten van de fantoom-studie toonden betere prestaties van de 3D-techniek ten opzichte van de 2D-techniek, doordat de fout ten gevolge van bewegingen uit het beeldvlak verminderde. Hoewel de 3D-techniek een hoge nauwkeurigheid in axiale richting heeft, was de prestatie van de rekbepaling in de laterale- en elevatie-richting beperkt als gevolg van divergerende geluidsbundels in de gebruikte 'matrix array transducer'. De toepassing van de 3D-techniek *in vivo* bleek mogelijk en de methode was in staat de 3D-beweging van het spierweefsel in de 3D-ruimte te volgen. Dit maakte meting van lokale spiervervorming mogelijk, waarbij de verdikking van de spier een goede overeenkomst vertoonde met de geleverde kracht.

Ten slotte presenteerden we in **Hoofdstuk 6** de ontwikkeling en toepassing van een algoritme om, automatisch, spontane bewegingen (bijvoorbeeld fasciculaties) te detecteren in echo-opnames. Hierbij hebben we iteratief leerproces gehanteerd, waarbij alle aanwezige bewegingen automatisch werden gedetecteerd en daarna beoordeeld door klinici. Op basis van hun beoordeling werd de differentiatie van de verschillende bewegingen door het algoritme verder verfijnd op basis van specifieke parameters die de

bewegingen karakteriseerden. Uit de resultaten bleek dat het algoritme in staat was tot betrouwbare detectie van beweging van weefsel in echo-opnames. Met behulp van het algoritme vonden waarnemers meer fasciculaties in vergelijking met subjectieve annotaties, wat een betrouwbare en vroege diagnose van neuromusculaire aandoeningen zou kunnen verbeteren. Er werden ook veel andere soorten bewegingen gedetecteerd, waarvoor we fysiologische kenmerken hebben berekend die als input kunnen dienen voor toekomstige 'machine learning-technieken' om de detectie en classificatie van intramusculaire bewegingen in echo-opnames volledig te automatiseren.

Concluderend is aangetoond dat echografie een waardevol hulpmiddel is om het functionele gedrag van spieren en ligamenten tijdens dynamische belasting te bestuderen. Deze functionele informatie verrijkt onze kennis over spierfunctie en kan van potentieel nut zijn als biomarker bij (neuro) musculoskeletale-aandoeningen. Bovendien kan deze informatie worden gebruikt om meer betrouwbare biomechanische modellen te verkrijgen die chirurgische uitkomsten kunnen sturen en voorspellen. Hoewel verder onderzoek vereist is om de ontwikkelde methoden nauwkeurig *in vivo* te valideren, zullen de gepresenteerde ultrageluid-technieken waarschijnlijk de klinische gereedschapskist uitbreiden en pathofysiologische inzichten leveren in de vervorming van de zachte weefsels in het bewegingsapparaat.

&

List of publications

List of conference presentations

PhD portfolio

Dankwoord

Curriculum Vitae

List of publications

Journal publications

Computer aided detection of fasciculations and other movements in muscle with ultrasound: development and clinical application. *Journal of Clinical Neurophysiology. In press*

Gijsbertse K, Bakker MA, Sprengers AMJ, Wijntjes J, Lassche S, Verdonschot N, de Korte CL and van Alfen N.

Continuous analysis of skeletal muscle strain with respect to fascicle orientation using ultrasound. *Journal of Medical Engineering and Physics. Submitted*

Gijsbertse K, Sprengers AMJ, Bakker MA, Nillesen MM, Heskamp L, de Korte CL and Verdonschot N.

A Noninvasive MRI Based Approach to Estimate the Mechanical properties of Human Knee Ligaments. *Journal of the Mechanical Behavior of Biomedical Materials. Submitted*

Naghbi Beidokhti H, Mazzoli V, **Gijsbertse K**, Hannink G, Sprengers AMJ, Janssen D, Boogaard TM, Verdonschot N.

How useful is muscle ultrasound in the diagnostic workup of neuromuscular diseases? *Curr Opin Neurol.* 2018 Oct; 31(5):568-574

van Alfen N, **Gijsbertse K** and de Korte CL.

Strain imaging of the lateral collateral ligament using high frequency and conventional ultrasound imaging: An ex-vivo comparison. *J Biomech.* 2018 May; 17(73):233-237

Gijsbertse K, Sprengers AMJ, Naghibi Beidokhti H, Nillesen MM, de Korte CL and Verdonschot N.

Tendon displacements during voluntary and involuntary finger movements. *J Biomech* 2018 Jan; 23(67):62-68

van Beek N, **Gijsbertse K**, Selles RW, de Korte CL, Veeger D, Stegeman DF and Maas H.

Ultrasound Imaging of Muscle Contraction of the Tibialis Anterior in Patients with Facioscapulohumeral Dystrophy. *Ultrasound Med Biol.* 2017 Nov;43(11):2537-2545

Gijsbertse K, Goselink RJM, Lassche S, Nillesen MM, Sprengers AMJ, Verdonschot N, van Alfen N and de Korte CL.

Three-dimensional ultrasound strain imaging of skeletal muscles. *Phys Med Biol.* 2017 Jan 21;62(2):596-611

Gijsbertse K, Sprengers AMJ, Nillesen MM, Hansen HHG, Lopata RGP, Verdonschot and de Korte CL.

Book chapters

Introduction to speckle tracking in ultrasound video, *Handbook of Speckle Filtering and Tracking in Cardiovascular Ultrasound Imaging and Video* (p. 241-257); IET 2018; 10.1049/PBHE013E

Hendriks AGM, Fekkes S, **Gijsbertse K** and de Korte CL.

List of conference presentations

European Conference of Radiology 2018, Vienna, Austria.

Ultrasound imaging of muscle contraction of the tibialis anterior in patients with facioscapulohumeral dystrophy. *Oral presentation*

IEEE International Ultrasonics Symposium 2017, Washington, USA.

Ultrasound imaging of muscle contraction of the tibialis anterior in patients with facioscapulohumeral dystrophy. *Poster presentation*

Dutch Bio-Medical Engineering Conference 2017, Egmond aan zee, The Netherlands.

Ultrasound imaging of muscle contraction of the tibialis anterior in patients with facioscapulohumeral dystrophy. *Oral presentation*

International Conference on Ultrasonic Biomedical Microscanning 2016, Klarendijk, Bonaire.

High frequency ultrasound strain imaging in musculoskeletal applications. *Oral presentation*

IEEE International Ultrasonics Symposium 2015, Taipei, Taiwan.

Three-dimensional ultrasound strain imaging of skeletal muscle. *Oral presentation*

The Artimino Conference on Medical Ultrasound Technology 2015, Helsinborg, Sweden.

Frustum conversion in 3D ultrasound strain imaging of skeletal muscles. *Oral presentation*

Dutch Bio-Medical Engineering Conference 2015, Egmond aan zee, The Netherlands.

3D ultrasound imaging of soft tissue deformation in the lower extremity: methods and initial results. *Oral presentation*

International Tissue Elasticity Conference 2014, Chicago, USA.

Three-dimensional strain imaging: phantom validation. *Oral presentation*

PhD portfolio

Institute for Health Sciences
Radboudumc

Name PhD candidate: K Gijsbertse

PhD period: 15-10-2013 – 1-05-2018

Department: Orthopaedic Research Laboratory

Promotors: Prof. N. Verdonschot, Prof. C de Korte.

Research School: Radboud Institute for Health Sciences

Co-promotors: Dr. A Sprengers, Dr. M Nillesen

	Year(s)	ECTS
TRAINING ACTIVITIES		
a) Courses & Workshops		
- Management for PhD students (RU)	2014	2
- The art of presenting science (RU)	2014	1.5
- Academic writing (RU)	2014	3
- Summer school in Advanced Ultrasound imaging (DTU)	2015	2.5
- Scientific Integrity (RIHS)	2016	0.5
b) Seminars & lectures^		
- USART training course	2013	1
- IUS short course on Tissue Elasticity	2014	0.2
- IUS short course on Plane Wave Imaging	2015	0.2
c) (Inter)national Symposia & congresses^		
- IEEE international ultrasonics symposium	2014	0.75
- International tissue elasticity conference*	2014	1.25
- 5 th Dutch conference on Biomedical Engineering*	2015	0.75
- 17 th Artimino Ultrasound Conference*	2015	1
- IEEE international ultrasonics symposium*	2015	1.25
- International conf. on Ultrasonic Biomedical Microscanning*	2016	1.25
- Symposium Echography: New recipe, better than ever!	2016	0.25
- Symposium: Tendon Mechanics and Ultrasound	2016	0.25
- 6 th Dutch conference on Biomedical Engineering*	2017	0.75
- IEEE international ultrasonics symposium#	2017	0.75
- European Conference of Radiology*	2018	1.25
d) Other		
- Journal club ORL	2013-2015	1
- Radiology research meetings	2013-2018	4
- Orthopaedics research meetings and lab lunches	2013-2018	4
- Bi-annual meetings NVMU	2013-2018	2
TEACHING ACTIVITIES		
e) Lecturing		
- Assisting practical assignment KME-2	2014-2017	3.75
- Prepare examination "VWO opfriscursus"	2015	0.4
f) Students		
- Supervision Anniek Driessen (MBRT)	2017	2
TOTAL		37.55

^Indicate oral and poster presentations with a * and # after the name of the activity, respectively.

Dankwoord

23 juli 2018 - Ik schrijf mijn dankwoord met twee prominent aanwezige gevoelens; allereerst is daar de pijn in mijn voeten en spieren van het lopen van de vierdaagse afstandsmarsen, welke mij een nieuw ontzag heeft gegeven voor het menselijk lichaam. Gedurende mijn voorbereiding kreeg ik last van mijn rechterknie, al gauw bleek dat dit kwam doordat mijn rechterbeen een paar millimeter korter is ten gevolge van een oude botbreuk in mijn jeugd. Als remedie kreeg ik een hakverhoging. Dit verhielp de klachten aan mijn knie, maar veroorzaakte weer een nieuw probleem. Doordat mijn hiel nu hoger was, moest mijn voorste scheenbeenspier tijdens het lopen harder en langer werken om mijn voet af te remmen bij het neerzetten, wat resulteerde in onaangename pijn tijdens de vierdaagse. Dit demonstreert hoe wonderlijk en complex ons bewegingsapparaat functioneert. Gelukkig heb ik de vierdaagse met goed gevolg kunnen uitlopen, wat mij brengt bij mijn tweede gevoel. Ik voel mij rijk. Ik ben gezegend met een gezond lichaam en ik word omringd door fantastische mensen die mijn leven enorm plezierig maken. Zo ook gedurende mijn promotieonderzoek, waar ik graag iedereen die een bijdrage hieraan heeft geleverd wil bedanken, waaronder sommigen in het bijzonder.

Allereerst mijn promotor **Nico**, die overal mogelijkheden ziet en in mij het vertrouwen had om met ultrasound het spierskeletstelsel te bestuderen. Bedankt voor deze mooie mogelijkheid en al het advies, met name je kunde om de juiste mensen en mogelijkheden samen te brengen en te enthousiasmeren om het beste resultaat te behalen. Daarnaast heb ik je openheid en eerlijkheid gewaardeerd en wist ik altijd waar ik op kon rekenen. Dit verwachtte je ook van mij en heeft geleid tot doelgericht werken, wat ik als zeer prettig heb ervaren en ervoor heeft gezorgd dat er nu een proefschrift ligt waar ik trots op ben.

Ik was fortuinlijk om een tweede promotor te hebben gedurende mijn onderzoek. **Chris**, je hebt mij niet alleen de benodigde kennis verstrekt over ultrasound en bijbehorende technieken, maar bovenal welkom geheten in de 'MUSIC-familie'. Een zeer waardevolle club waaraan jij met veel positiviteit aan het hoofd staat. Ik heb genoten van onze samenwerking waarin veel ruimte was voor een lolletje, maar waar ik ook altijd op je steun kon rekenen op wat meer kritieke momenten. Je ongebreidelde enthousiasme, optimisme en motivatie zijn een fijne bron van energie voor de gemoedelijke werksfeer binnen jouw team. Bedankt voor alles.

Daarnaast had ik ook twee copromotoren: **Maartje** en **André**. Ogenscheinlijk zijn jullie twee compleet verschillende personen, maar beiden met een ontwapenend en vriendelijk persoonlijkheid waar ik altijd terecht kon voor een inhoudelijk gesprek of kopje koffie. Maartje bedankt voor je hulp op het gebied van ultrasound en je grondige blik op mijn papers. Lange tijd zaten we naast elkaar te werken en wisselde we dit af met afleidende

gesprekjes waar ik weer energie uit haalde. André, jij ook bedankt voor alle goede koppen koffie in het restaurant waar we hebben bijgekleetst, maar natuurlijk ook voor je inhoudelijke kennis en creatieve ideeën voor onze studies. Beiden hebben jullie mij gemotiveerd gedurende mijn promotietraject en afgeleid van de bijbehorende perikelen.

Ik wil de leden van de manuscriptcommissie, prof. van Engelen, prof. Stegeman en prof. D'hooge, bedanken voor de tijd die zij genomen hebben om mijn manuscript te lezen en te beoordelen.

Alle personen die bereid waren om deel te nemen als proefpersoon aan mijn onderzoek wil ik ook hartelijk danken. Het enthousiasme en de inzet van jullie tijdens de metingen werkte aanstekelijk en ik vond het geweldig om met jullie de ultrasound technieken te testen en ontwikkelen.

Al het begin is moeilijk en ik ben mijn dank verschuldigd aan **Rik** en **Richard L.** Jullie hebben mij op weg geholpen met het 3D strain-algoritme en de 'frustum-frustrations'. Bedankt voor de geïnvesteerde tijd en interesse in mijn werk.

Rik jij maakt bovendien deel van de MUSIC-groep en daarom maak ik hier gebruik om het bruggetje te slaan naar mijn dagelijkse collega's. Jij allereerst nogmaals dank voor je bereidheid om altijd met mij mee te denken over inhoudelijke uitdagingen. Jouw scherpe en snelle manier van denken heeft er vaak toe geleid dat ik weer verder kon. **Jan** en **Gert**, bedankt voor jullie technische ondersteuning en interesse in mij en mijn werk. Jullie bezitten en beheren waardevolle kennis in de groep. **Gijs**, bedankt voor de fijne samenwerking op het gebied van 3D-strain en ABVS-metingen. Het is bewonderingswaardig om te zien hoe gecontroleerd jij door jouw promotie-traject heen gaat. **Chuan**, jij hebt vaak een lach op mijn gezicht getoverd met je grapjes en fun-facts over panda's, Xièxiè en blijven zingen. **Anton** bedankt voor al het Russische snoep en het oefenen van ons Spaans. **Leon**, als collega's op spierecho hebben we regelmatig gebrainstormd, bedankt voor de gezellige samenwerking op jouw kantoor en succes met je onderzoek. **Roel**, ons enige congresreisje naar Wenen zal ik niet vergeten; ik heb met (en om) je gelachen en ben blij dat je je vlucht nog hebt gehaald. **Shreya**, thank you for your kindness and good luck with your study on that challenging muscle in 3D. **Thomas**, jouw onuitputtelijke energie is aanstekelijk, daarnaast bedankt voor je hulp in machine learning. **Khalid**, mon ami des cavernes, c'était génial travailler avec toi. Nos conversations en français vont me manquer. Merci et je te souhaite bonne chance. **Sandra** bedankt voor alle secretariële ondersteuning, laten we na mijn promotie een Flugel drinken. **Sonja**, je hebt ons allemaal verwend met je hulp en alle andere attente activiteiten, heel erg bedankt. **Aisha**, bedankt voor al je gezelligheid en de overvloed aan taart (inclusief onze middag spekkoekebakken). **Marinette**, terima kasih! **Han**, **Jeroen** en **Livia** ook bedankt voor de

interesse in mij en mijn werk. Iedereen heel erg bedankt voor de fijne tijd, het was elke dag enorm gezellig in ons volle kantoor, of tijdens een van de vele sociale activiteiten. Jullie zijn toppers.

Anne en Stein, het bleek al snel dat we het goed met elkaar konden vinden en onze eerste congresreis naar Amerika is het fundament van wat ik nu zie als waardevolle vriendschap. In de afgelopen jaren hebben we lief en leed met elkaar gedeeld en het was fantastisch om dit avontuur met jullie tegelijk aan te gaan. Daarnaast mag ik nog regelmatig van jullie en jullie partners, **Willem Jan en Fenneke**, gezelschap genieten. De ondernemingen zijn ondertussen al talloos, maar de wintersport, kookclub, stap-avondjes en jullie bijdrage aan mijn bruiloft zijn voorbeelden van dierbare herinneringen gedurende mijn tijd als promovendus. Het is mij dan ook een genoegen dat jullie mijn paranimfen willen zijn en achter mij staan tijdens mijn verdediging.

Ik had nog een tweede groep fijne collega's van het Orthopedisch Research Lab die ik allen wil bedanken voor de gezellige BBQs, kerstborrels en andere sociale activiteiten! Wanneer ik op het lab langskwam was er altijd tijd voor een praatje of helpende hand voor dringende zaken. Een kei hierin, is **Richard van S.**, die wanneer ik hem verzocht om iets te ontwerpen en hij mij vroeg: "wanneer heb je het nodig?" waarop ik standaard antwoorde: "het liefst nu", hij het altijd tijdig voor elkaar kreeg. Bedankt dus voor al je werk en het plezier dat we hadden gedurende de experimenten. Daarnaast heb ik ook veel lol en steun aan je beleefd tijdens onze 4-daagse. **Sebastiaan**, bedankt voor je hulp bij de voorbereiding van mijn experimenten. Ik heb genoten van je anatomie lessen en de enthousiaste manier waarop jij over de orthopedie spreekt. Helaas is het niet gelukt om de MPFL te meten, maar wie weet wat de toekomst brengt... **Max**, met jou heb ik heel wat uurtjes achter de pc gezeten. Fascinerend hoe snel jij werkende code genereert, wat heeft geleid tot twee mooie verhalen. Bedankt voor deze voorspoedige maar ook gezellige samenwerking. **Ineke en Joke** bedankt voor alle secretariële ondersteuning en de herinnerings-mailtjes, anders had ik veel van de gezelligheid gemist. Mijn bezoeken waren altijd langer dan gepland, want een kleine vraag ontspoorde vaak in gezellige gesprekken over van alles.

I am also grateful for my team members of the BiomechTools-project: **Valentina, Hamid, Marco, Kenan, Hao and Dennis**, working with you on this big and challenging project was enjoyable. Hamid, we spent a looooot of time preparing our specimens for the tensile tests. Exiting via the fire escape in our lab coats, to paint our specimens, always was a fun spectacle. Thanks a lot. Valentina, unfortunately our endeavors to compare your MRI with my ultrasound techniques did not go as planned, but I have enjoyed our time working together. **Kevin**, wil ik hierbij ook betrekken en bedanken voor de inzet om een MRI/US compatibel fantoom te ontwikkelen.

Ik heb de eer gehad om een student te begeleiden met haar afstudeeronderzoek. **Anniek**, samenwerken met jou heeft mij niet alleen veel geleerd maar het heeft ook het fundament gelegd voor een mooi paper. Je was al bekend met de ABVS-scanner en de omgeving wat voor een soepel lopend project zorgde, bedankt. Ook **Linda, Franciska** en **Mark** wil ik hierbij betrekken en bedanken voor de leuke samenwerking.

Het opsporen van de juiste spieren en kleine ligamenten met ultrasound is een moeilijke taak en ik heb veel hulp gekregen van radiologen **Jacky, Marieke** en **Leo** om deze structuren goed in beeld te krijgen. Bedankt voor jullie hands-on uitleg en interesse in mijn werk.

De samenwerking met de collega's van de afdeling klinische neurofysiologie was super interessant en bovendien erg productief. **Nens, Rianne, Saskia, Juerd** en **Jonne**, bedankt voor de fijne samenwerking. Naast jullie klinische ervaring heb ik ook dankbaar gebruik mogen maken van jullie apparatuur en input voor mijn papers. Het doet mij bovendien goed, dat de speckle tracking technieken in veel van jullie werk terug te vinden is.

Naast alle samenwerkingen heb ik veel ontspannende momenten beleefd met alle collega's van de afdeling Radiologie en Nucleaire geneeskunde op bijvoorbeeld het jaarlijkse dagje uit of kerstborrel. Dus aan al mijn collega's: hartelijk dank voor de gezellige werkomgeving!

Uiteraard hebben vrienden en familie mij van de benodigde steun en interesse voorzien. Ik hoop dat na het lezen van mijn proefschrift het wat duidelijker is geworden wat ik heb uitgespookt afgelopen 4,5 jaar. De lijst is te lang om iedereen te noemen, maar ik ben mijn familie, wageningen homies (inclusief jullie betere wederhelften), dispuut XOUN, jongens van de harde-kern, oud-studiegenoten, Brandhoudtjes, Tractus Sanus en alle andere dankbaar voor de interesse en de nodige afleiding. Het is heerlijk om omringd te worden door zoveel leuke mensen.

Ik heb veel geluk met mijn schoonfamilie: **Ina, Herman, Dafne** en **Klaas Jan** waarmee ik altijd heerlijk kan ontspannen in het mooie Twente. De grote BBQ's, plonsjes in het zwembad, wintersport, of een mooie vlucht in Spanje waren fijne afwisselingen van de werkweek. Daarnaast ook bedankt voor de steun en getoonde interesse gedurende mijn promotieonderzoek.

Mijn zusje, **Zoë** en tweelingbroer, **Robbert**. Jullie zijn mij ontzettend dierbaar en ik ben trots op jullie. Jullie staan altijd voor mij klaar met raad en daad en ik kan eindeloos met jullie klieren. Hierbij wil ik ook **Frank, Noa, Gwenn, Kelly** en **Brandon** betrekken; bedankt voor jullie interesse en pret die we samen beleven.

Ik ben fortuinlijk met mijn ouders, die mij alle kansen hebben geboden en mij hebben voorzien van de middelen om mijn doelen te bereiken. **Mam** en **Adrian, Pap** en **Trudy**, bedankt voor de veilige en gezellige thuishaven, jullie steun en vertrouwen!

Maar mijn grootste schat, **Evita**, dat ben jij. Jouw onvoorwaardelijke steun is van onschatbare waarde. Je weet mij altijd te motiveren, maar even belangrijk weet je ook wanneer je mij moet remmen. Je verrijkt mijn leven op zo veel manieren en ik weet dat ik samen met jou alles aankan! Ik prijs mij enorm gelukkig met jou. Ik geniet van ons leventje samen en kijk uit naar de tijd die komen gaat.

Curriculum Vitae



Kaj Gijsbertse was born on June 20th, 1986 in Wageningen, The Netherlands. In 2005 he obtained his high school diploma from the RSG Pantarijn in Wageningen, after which he started studying biomedical engineering at the University of Twente. He obtained his Bachelor's degree in 2010 and subsequently enrolled in the Master program of biomedical engineering. During his masters he performed an internship at the department of Mechanical and Industrial Engineering of the Gadjah Mada University, Yogyakarta, Indonesia. There he improved the design of tibial bone plates with the use of Rontgen data. He graduated in 2013 with his Masters' project on the design of a mechatronic system that automatically scanned a breast-like shape to acquire 3D ultrasound data for the localization of suspected lesions, which was a collaboration between the department of Robotics and Mechatronics, and the department of Biomechanical Engineering of the University of Twente.

In 2013 he started as a PhD candidate at the Radboud university medical center, Nijmegen, The Netherlands. His research project was a collaboration between the department of Orthopedics and the department of Radiology and nuclear medicine, under supervision of Nico Verdonchot and Chris de Korte. His work focused on the development of ultrasound imaging techniques to study and evaluate the biomechanical properties and dynamic behavior of healthy and pathological muscle tissue in the lower extremity. This work involved the design, evaluation and validation of these techniques in the clinical field and is presented in this thesis.

Currently, he applies his knowledge of the interaction between humans and technology at the department of Training and Performance Innovations, TNO, Soesterberg, The Netherlands. This department focuses on innovations to improve human performance in complex and challenging environments.

